BRAIN METABOLISM POST-PROCESSING, A KEY TO UNVEIL PATHOLOGICAL FINGERPRINTS OF CENTRAL NERVOUS SYSTEM DISORDERS

A multimodal neuroimaging approach to investigate clinical trajectories in alpha-synucleinopathies' continuum, autoimmune encephalitis, and brain tumor-related epilepsy.

PhD Candidate: Dr Pietro Mattioli
PhD Tutor: Prof. Dario Arnaldi

PhD programme in Neuroscience
Curriculum: Clinical and Experimental Neuroscience – XXXVIII Cycle

INDEX

PROLOGUE

A journey of a thousand miles begins with a single step[1]

When I decided to work on a clinical and methodological project for my Ph.D., I had no idea how challenging it would be to bring it to completion without ending up with something that sounded like a poorly made Italian soup — the *minestrone*. *Minestrone* is a dish that, like many originally humble recipes such as the French *bouillabaisse*, has become a "must-try" of Italian cuisine. A good result depends on the careful choice of ingredients and their proportions, the right cooking time, and just the right amount of basil pesto. The recipe can be adjusted along the way, but the risk of ending up with a potato soup or a cabbage stew is high. In the same way, I had to approach this project.

The idea was to review and strengthen the application of neuroimaging techniques—particularly Fluorine-18 fluorodeoxyglucose positron emission tomography ([18F]-FDG PET)—from both methodological and clinical perspectives. To do so, I started from the clinical and paraclinical foundations of several conditions, especially sleep disorders and parasomnias, brain tumors, inflammatory diseases of the central nervous system, and epilepsy. These topics often overlapped by definition, as in the case of REM Sleep Behaviour Disorder (RBD, which is both a REM parasomnia and an alpha-synucleinopathy), brain tumor–related epilepsy (BTRE), autoimmune encephalitis–associated epilepsy (AEAE), or amygdala enlargement (AE), a radiological finding with heterogeneous etiologies (inflammatory, neoplastic, dysplastic, or idiopathic) often associated with epilepsy, psychiatric, or sleep disorders.

The journey to create this *minestrone* was long and rather challenging, and the result is presented here.

CHAPTER 1 INTRODUCTION

Brain fluorine-18 fluorodeoxyglucose ([^{18}F]FDG) positron emission tomography (PET) allows the assessment of cerebral glucose consumption.[2] This imaging technique is widely used in the evaluation of numerous neurological and oncological diseases and has a significant impact on patient management.[3] Methodologically, it relies on the injection and tracking of a radioactive tracer, namely [^{18}F]FDG.[2, 4] At the cerebral level, this tracer follows the same metabolic pathway as glucose, thereby enabling the evaluation of brain metabolism. More specifically, [^{18}F]FDG crosses the blood–brain barrier via glucose transporter type 1 (GLUT1) and is taken up primarily by astrocytes, where it is phosphorylated to glucose-6-phosphate by hexokinase and made available for energy production, either for astrocytic metabolism or for transfer to neurons to support cellular processes and synaptic activity.[5, 6] Unlike glucose, however, due to its biochemical structure, [^{18}F]FDG cannot undergo the complete glycolytic pathway and therefore remains "trapped" within the cell, allowing radioactive decay to occur and the signal to be detected by the PET scanner.[5]

These characteristics allow [^{18}F]FDG PET to probe multiple physiological and pathological processes related to brain activity, including synaptic function and dysfunction and, potentially, microglial metabolism and neuroinflammation—more generally, processes associated with altered glucose consumption. Owing to its versatility, [^{18}F]FDG PET has been widely applied in several neurological fields, both in research and clinical settings.[4, 7–11]

Sleep disorders

Brain metabolic imaging is not the technique of choice for the evaluation of sleep or sleep disorders per se. However, it becomes relevant when a sleep disorder represents an early manifestation of an underlying neurodegenerative process, as in the case of Rapid eye movement (REM) sleep behaviour disorder (RBD).

RBD is a parasomnia characterized by dream enactment and loss of physiological muscle atonia during REM sleep.[12, 13] When not associated with overt neurological or psychiatric conditions, it is defined as idiopathic or isolated (iRBD). iRBD is now widely recognized as a prodromal stage of α-synucleinopathies.[14, 15] Indeed, more than 70% of patients with iRBD eventually phenoconvert to an overt α-synucleinopathy within 12 years of diagnosis.[14, 16]

Markers of neurodegeneration, including mild cognitive impairment, altered brain metabolism, and nigrostriatal dysfunction, can already be detected in the isolated form of RBD.[17–19] In 2021, during my work in the laboratories of Prof. Arnaldi and Prof. Nobili, I investigated the value of brain metabolic imaging in iRBD and identified a significant association between dysfunction of posterior parietal regions—particularly the cuneus and precuneus—and the presence of mild cognitive impairment, along with their anatomical and functional correlates.[20] Even relatively simple analytical approaches, such as a two-sample *t*-test implemented in statistical parametric mapping (SPM), allow discrimination between different disease processes at prodromal stages, as we subsequently demonstrated when differentiating mild cognitive impairment related to α-synucleinopathies from that due to Alzheimer's disease.[21]

A particularly relevant aspect of iRBD is that the vast majority of patients exhibit biological evidence of synucleinopathy in skin nerve biopsies and/or cerebrospinal fluid.[22] Consequently, iRBD represents an ideal target population for future disease-modifying trials.[23] The design of such trials requires biomarkers capable of predicting short-term phenoconversion, given the marked interindividual variability in time to clinical conversion, with some patients remaining unconverted for over a decade.[14, 15] Nonetheless, disease-modifying trials are generally expected to have a duration of no more than two years.

In this context, [^{18}F]FDG PET, combined with advanced analytical techniques, may represent a promising biomarker of phenoconversion, as it has already demonstrated predictive value in other neurodegenerative diseases, including Alzheimer's disease.[24–27] The scaled subprofile model with principal component analysis (SSM-PCA) enables the extraction of voxel-wise covariance patterns and has been applied to [^{18}F]FDG PET data to identify disease-specific metabolic signatures in several neurological conditions, including iRBD and Parkinson's disease (PD).[7, 28, 29] The Parkinson's disease–related pattern (PDRP) has been shown to increase with disease progression and to decrease in response to effective therapy.[30–32] However, as PDRP is expressed in PD irrespective of RBD status, a pattern specifically derived from PD patients with RBD may better capture disease progression in this population, as we will describe later in the following chapters[28].

These findings support the role of [^{18}F]FDG PET as a potential biomarker for phenoconversion in prodromal α-synucleinopathies.

Epilepsy

In epilepsy, [^{18}F]FDG PET is an established tool in the presurgical evaluation of patients and plays an increasingly important role in the diagnostic work-up of autoimmune encephalitis and autoimmune encephalitis–associated epilepsy (AEAE). It contributes to seizure focus lateralization in focal epilepsies, characterization of interictal dysfunctional networks, and prognostic stratification, as focal hypometabolism is associated with better surgical outcomes. Compared with structural MRI, [^{18}F]FDG PET provides complementary information on synaptic and network-level dysfunction, supporting the current network-based understanding of epileptogenesis rather than a purely focal lesion model.

[^{18}F]FDG PET is a recognized tool in the presurgical evaluation of patients, but it is of great assistance also in the diagnosis of autoimmune encephalitis (and more broadly for the assessment of autoimmune encephalitis associated epilepsy(AEAE)). Namely, it allows to determine the lateralization in focal epilepsies, to evaluate the ictal and interictal networks, and has a prognostic value as the detection of a localized hypometabolism is related with a better surgical outcome.[3] Overall, when compared with structural neuroimaging like structural MRI, it allows to detect synaptic functioning, providing clues on broader alterations involved by the epileptogenic networks. On the other side, potential limitations of brain [^{18}F]FDG PET imaging in epilepsy are related to its lower spatial resolution and on the use of a radioactive tracer implying exposure of ionizing radiation. Visual analysis is the cornerstone of brain [^{18}F]FDG PET inspection. Accordingly, visual-qualitative interpretation relies on a certain amount of experience and may benefit of post-processing, as, for example, the co-registration to the brain MRI, that allows a better detection of areas of brain relative hypo- and hypermetabolism at individual patient level[33]. Furthermore, a more objective software-based approach can be implemented through a single-subject analysis comparing the patients with age matched controls and providing maps of a statistical significant clusters of relative hypo or hypermetabolism, increasing the specificity[34]. Finally the voxel-based asymmetry index analysis have been implemented also for [^{18}F]FDG PET imaging allowing the comparison between the two hemispheres of the individual brain unveiling subtle asymmetries, increasing the sensitivity of the technique.[35, 36].

Despite international guidelines, the use and interpretation of [^{18}F]FDG PET in epilepsy vary widely across centers. Visual analysis remains the cornerstone of interpretation but is operator-

dependent and benefits from post-processing techniques such as MRI co-registration, single-subject statistical parametric mapping (ssSPM), and hemispheric asymmetry index (AI) analysis, which can improve sensitivity and specificity when appropriately applied.

Within my activity in the Neuroimaging Commission of the Italian League Against Epilepsy (LICE), I coordinated the design and analysis of a national survey investigating the clinical use of [^{18}F]FDG PET in epilepsy. A total of 118 LICE members completed the survey, with balanced representation in terms of age, years of experience, patient population (adult vs pediatric), and clinical workload. Most participants completed the survey independently, without consultation with nuclear medicine physicians.

Presurgical evaluation was the main indication for [^{18}F]FDG PET. In more than half of cases, scans were performed in external centers, and the lack of an in-house nuclear medicine unit emerged as the main barrier to access. While two-thirds of respondents reported PET–MRI co-registration before interpretation, approximately one-third relied solely on visual assessment of standalone PET/CT images. When post-processing was used, AI analysis was the preferred method. PET findings were discussed in multidisciplinary team (MDT) meetings in about 70% of cases; however, nuclear medicine physicians participated in only one-third of these meetings, often due to logistical constraints related to off-site imaging.

Regarding peri-procedural management, sedation was used when required, particularly in pediatric settings, and the sedative agent was usually documented. However, monitoring for interictal or ictal activity during tracer uptake was limited: simultaneous EEG was performed in only a small minority of cases, with most centers relying on clinical history alone. This represents a critical issue, as unrecognized ictal activity during tracer uptake may lead to misleading patterns of hyper- or hypometabolism and false lateralization, particularly in focal epilepsy and AEAE. EEG information is especially relevant in autoimmune encephalitis, where inflammatory hypermetabolism may overlap with seizure-related metabolic changes.

The survey also highlighted heterogeneity in post-processing strategies. While MRI–PET co-registration is considered mandatory, a substantial proportion of centers still rely on visual inspection alone. AI and ssSPM analyses are commonly used and can enhance detection of subtle abnormalities, though each method has inherent limitations in sensitivity, specificity, and availability of normative datasets. Advanced analyses should therefore be interpreted cautiously and integrated with clinical, EEG, and structural imaging data.

Overall, this survey reveals a heterogeneous and sometimes suboptimal use of [^{18}F]FDG PET in epilepsy care in Italy, despite well-established guidelines. While its primary role remains presurgical evaluation, its application in autoimmune encephalitis is expanding. These findings underscore the need for harmonized national protocols, improved access to PET imaging, greater integration of nuclear medicine physicians into MDT discussions, and systematic use of MRI co-registration and EEG-informed interpretation. Strengthening national networks and standardizing practice may allow the full potential of [^{18}F]FDG PET to be realized in epilepsy care.

CHAPTER 2 AIMS

In the following chapters I will provide an excursus of the main projects I participated over the past three years. The projects will be heterogeneous and they will span from sleep disorders, within the continuum of alpha-synucleinopathies, to epilepsy, within the concept of brain tumor related epilepsy (BTRE) and autoimmune associated epilepsy. The methodology however will follow the *fil rouge* of the usefulness of advanced post-processing to disclose significant features of the disease, independently by the disease itself.

The final chapter aims to apply some of these methodologies to a radiological finding that puts together the above disorders: the enlarged amygdala (EA), within the context of limbic encephalitis (LE). EA is a recently described neuroimaging finding that can be associated with several conditions, often epilepsy, but its clinical meaning is not fully understood yet.[37] EA's underlying physiopathology is heterogeneous, including both autoimmune[38] or tumoral-dysplastic processes, with different pathological findings or even with non-lesional cases[39] if advanced post-processing is performed[40]. Literature data also suggest that it might be a consequence of seizures[41]. Hence, biomarkers able to predict the clinical trajectory of EA patients are needed[42]. Recently, a further step was made to better phenotype this condition, finding a specific seizure onset pattern and, possibly, a different outcome compared to other TLE forms.[43] However, the presence of an EA is often associated with alterations of extratemporal regions, resulting in temporal plus epilepsy, often involving stress-mediated limbic network[44] and emotion recognition.[40] The hypothesis leading this last study is that post-processing might disclose clues on the aetiology of such cumbersome neuroradiological finding, possibly guiding to an aetiological hypothesis and therefore a clinical trajectory prediction.

The overall aims of the PhD projects are:

1-provide a *cook-book* analysis for advanced post-processing of mainly [^{18}F]FDG-PET, and MRI, not strictly related to a specific disease

2-provide insights of the application of such methodologies in the following topics:

a) Alpha-synucleinopathies continuum
b) Brain tumor related epilepsy
c) Autoimmune associated epilepsies/limbic encephalitis

3) provide clues from brain metabolism in the topic of epilepsy and enlarged amygdala in temporal lobe epilepsy within the context of temporal lobe epilepsy and limbic encephalitis.

CHAPTER 3 METHODOLOGIES

This chapter is intended to be purely methodological and as detached as possible from specific disease entities. Nevertheless, the choice of advanced post-processing techniques is discussed in relation to their respective advantages and limitations, particularly with regard to their applicability in clinical contexts.

Brain metabolism: why, how, and when?

A practical guide to [^{18}F]FDG PET analysis

Glucose metabolism is a fundamental feature of brain physiology, and its assessment enables the investigation of a wide range of pathological processes.

The concept of functional networks is intrinsic to the evaluation of brain metabolism. When interpreting [^{18}F]FDG PET, the nuclear medicine physician does not merely assess regions of overt metabolic alteration by comparison with normative patterns, but also evaluates interhemispheric asymmetries and potential diaschisis between distant yet highly interconnected brain regions.

Post-processing of raw PET data primarily enhances visual assessment and enables quantitative evaluation of metabolic abnormalities, either relative to a control group (single-subject analysis, SSA), the contralateral hemisphere (voxel-based asymmetry index, AI), or through the assessment of functional connectivity (inter-regional correlation analysis, IRCA). Depending on the study objectives, both group-level and single-subject analyses may be applied. In all cases, a certain degree of preprocessing is required.

Data acquisition and preprocessing

Brain [^{18}F]FDG PET should be performed in accordance with current guidelines, in particular those issued by the European Association of Nuclear Medicine (EANM)[3, 45]. To ensure blood glucose levels below 7.8 mmol/L, patients are required to fast for at least six hours prior to the examination. After verification of blood glucose levels, patients rest for 10 minutes in a quiet, dimly lit room, with eyes closed and ears unplugged. Subsequently, 185–250 MBq of [^{18}F]FDG are injected intravenously via a venous cannula.

Following tracer injection, patients remain in the same resting conditions for 30 minutes before being transferred to the PET scanner. Image acquisition begins 15 minutes later and lasts 10 minutes. Head motion is minimized using a polycarbonate head holder. Images are acquired using a Biograph Hi-Rez PET/CT system (Siemens, Munich, Germany) with a 256 × 256 matrix in three-dimensional mode, a 16.2 cm axial field of view, and an in-plane spatial resolution of 5.8 mm full-width at half-maximum (FWHM). Image reconstruction is performed using an ordered subset expectation maximization (OSEM) algorithm (16 subsets, 6 iterations), resulting in a voxel size of 1.33 × 1.33 × 3.0 mm.

Preprocessing is required to bring all images into a common spatial framework. While single-subject analyses such as AI are performed in the individual subject's native space (as discussed in the following chapter), group-level analyses and comparisons with control datasets require normalization to a standard space. The Montreal Neurological Institute (MNI) space is the most widely used standard space in both research and clinical practice.

Several normalization and smoothing strategies can be adopted for image preparation. A commonly used software for pre- and post-processing is Statistical Parametric Mapping (SPM), which enables spatial normalization followed by smoothing with an 8–10 mm isotropic Gaussian kernel to account for interindividual anatomical variability and improve signal-to-noise ratio.

Group-level analysis

Basic group-level analyses rely on comparisons of single parameters and are particularly useful for research purposes. In the case of multi-group comparisons (e.g., three-group analyses), voxel-wise univariate analysis of variance (ANOVA) is typically performed using SPM. Continuous or categorical variables, such as age, can be included as nuisance covariates. Post hoc two-sample *t*-tests are then conducted to directly compare pairs of groups, with the aim of identifying specific volumes of interest (VOIs) capable of discriminating between groups.

Typically, only clusters comprising at least 100 contiguous voxels are considered. Statistical inference is based on an uncorrected voxel-level threshold (usually ranging from $p < 0.001$ to $p < 0.05$, with false error correction where applicable) and a cluster-level family-wise error (FWE)–corrected threshold of $p < 0.05$.

Uptake values within the identified VOIs are extracted for each subject and normalized to whole-brain uptake (or cerebellar uptake) to obtain relative metabolic measures. To investigate metabolic connectivity between the VOI and the rest of the brain, voxel-wise inter-regional correlation analysis (IRCA) can be performed using multiple regression models in SPM12, with normalized VOI uptake as the independent variable.

Finally, VOI-derived metabolic values can be correlated with clinical or paraclinical variables.

More advanced multiparametric analyses are also available, most commonly based on principal component analysis, allowing the identification of disease-related metabolic patterns. One of the most widely used approaches is the scaled subprofile model–principal component analysis (SSM-PCA), originally described by Spetsieris and Eidelberg. and implemented in MATLAB (version 2020a; MathWorks, Natick, MA). This method derives and combines components that collectively explain more than 50% of the variance within the group of interest.

To assess robustness and generalizability, patterns are typically derived from a subset of the dataset and validated on an independent subset.[7, 46]. Disease-related patterns can subsequently be applied to external datasets to evaluate their discriminative performance. Pattern validation is commonly performed using a leave-one-out cross-validation (LOOCV) approach [76,77]. Individual subject scores—reflecting the expression of both the original and LOOCV-derived patterns—are *z*-transformed relative to a control group to enable comparison.

Bootstrap resampling (typically 1000–2000 iterations) is used to identify the most stable pattern components. Both unthresholded and thresholded voxel maps, defined using the 2.5%–97.5% confidence interval, are generated and overlaid onto a standard T1-weighted MRI template for visualization.

Compared with conventional univariate SPM approaches, this multivariate method offers increased sensitivity for group discrimination. Although currently confined primarily to research settings, its ability to generate a single-subject measure of pattern expression—effectively a metabolic fingerprint—makes it a promising tool for patient classification. However, the method is highly sensitive to artifacts and therefore requires rigorous quality control and cautious interpretation.

Single-subject analysis

The two main post-processing methods applicable in routine clinical practice are single-subject versus control SPM analysis (ssSPM) and voxel-based asymmetry index (AI) analysis.

ssSPM is methodologically similar to group-level SPM analysis. In brief, a single subject's MNI-normalized and smoothed [^{18}F]FDG PET scan is statistically compared with a control group to identify regions or volumes of interest (VOIs/ROIs) showing significant metabolic differences. Although ssSPM is widely used in both research and clinical settings—and is implemented in some CE-certified workstation software—it presents several technical and interpretative limitations. While ssSPM increases specificity, it often reduces sensitivity. Moreover, the requirement for an appropriate healthy control dataset limits its broader clinical applicability.

AI analysis enables the mathematical identification of interhemispheric asymmetries in brain metabolism ([^{18}F]FDG PET) or perfusion (arterial spin labeling, ASL). By providing asymmetry masks and *z*-scored values, AI enhances the sensitivity of the imaging modality to which it is applied. It can be relatively easily implemented using open-access software such as FSL or SWANE [Genovese]. AI is typically calculated following the method described by Boscolo Galazzo et al.[47]

Briefly, ASL/[^{18}F]FDG PET images in native space are affine-registered to the individual high-resolution 3D T1-weighted anatomical images using FLIRT (FSL). T1-weighted images are then non-linearly registered to MNI space (1 mm³ resolution) using FNIRT. Transformation parameters are combined to spatially normalize ASL/[^{18}F]FDG PET maps into MNI space. The normalized maps are smoothed with a 2 × 2 × 2 mm FWHM Gaussian kernel. A voxel-wise asymmetry index is then computed using the formula:

$$\mathbf{AI = 100 \times (Right - Left) / (Right + Left)}$$

The choice between AI and ssSPM depends on clinical requirements: AI should be preferred when higher specificity is required, whereas ssSPM is more suitable when higher sensitivity is desired. Notably, the absence of a control group precludes the use of ssSPM.

MRI: co-registration, segmentation, and beyond

The first and essential step in MRI analysis within a multimodal framework is co-registration. Ideally, a high-resolution, isotropic 3D T1-weighted MRI (1 × 1 × 1 mm³) should be acquired.

All lower-resolution neuroimaging modalities are co-registered to the T1-weighted image to improve spatial accuracy. Subsequent post-processing includes segmentation, three-dimensional reconstruction, and assessment of anatomical connectivity, either using standardized brain atlases or subject-specific data. Specific techniques also allow visualization of small but clinically relevant structures, such as the substantia nigra.

Structural analysis (3D T1-weighted images)

Structural analysis enables segmentation of three-dimensional brain regions, either atlas-based (e.g., FreeSurfer individual segmentation; FreeSurfer v7.1, https://surfer.nmr.mgh.harvard.edu) or manual, particularly in the presence of focal lesions such as brain tumors. For group analyses, voxel-based morphometry (VBM) can be performed. Preprocessing and statistical analyses are conducted using the Computational Anatomy Toolbox (CAT12) or SPM12 on MATLAB.

For group-level analysis, images must be normalized to a standard space such as MNI. T1-weighted images are segmented into gray matter (GM), white matter (WM), and cerebrospinal fluid (CSF), and smoothed using an 8-mm FWHM Gaussian kernel. Smaller structures, including the amygdala, hippocampus, thalamus, and brainstem, can be further parcellated using developmental versions of FreeSurfer.

Brain anatomical connectivity

Brain anatomical connectivity can be assessed using diffusion tensor imaging (DTI) to reconstruct white matter tracts. When DTI data are unavailable, atlas-based approaches may be employed. The Brain Connectivity and Behaviour (BCB) toolkit (http://www.toolkit.bcblab.com) allows characterization of structural connectivity of VOIs/ROIs based on normative diffusion data. As previously described[48], the BCB toolkit is based on whole-brain tractography derived from diffusion-weighted imaging of 35 healthy controls. Prior studies have demonstrated that as few as 10 subjects are sufficient to generate white matter maps explaining over 70% of population variance, and that age does not significantly affect disconnectome reliability in adult and elderly populations.[48]

VOIs/ROIs can be used as seeds for whole-brain tractography within the BCB framework [36]. The toolkit estimates the probability that a white matter tract is disconnected by a lesion affecting the VOI/ROI (typically considering tracts with probabilities >50%) and quantifies the extent of disconnection.[48]

Nigrosome imaging

Multi-echo three-dimensional gradient-echo (GRE) sequences, either visually assessed or post-processed, allow reliable visualization of the substantia nigra. The protocol includes whole-brain acquisitions of magnitude and phase data using a multi-echo 3D GRE sequence with eight echoes ($TE_1/\Delta TE$ = 5.6/5.6 ms; TR = 51 ms; flip angle = 18°; resolution = 1 × 1 × 1 mm^3; matrix = 224 × 224 × 144; GRAPPA = 2; partial Fourier = 6/8 in both phase-encoding directions; bandwidth = 340 Hz/px; acquisition time = 8 min 45 s) [23,24].

Additional structural imaging includes sagittal T1-weighted MPRAGE (TR = 2300 ms; TE = 2.96 ms; TI = 900 ms; flip angle = 9°; resolution = 1 × 1 × 1 mm^3; matrix = 256 × 256; GRAPPA = 2; bandwidth = 240 Hz/px; acquisition time = 5 min 30 s).

For each subject, R2*, quantitative susceptibility mapping (QSM), and susceptibility map–weighted imaging (SMWI) are reconstructed using MATLAB 2019b (MathWorks, USA). R2* maps are computed using the Auto-Regression of Linear Operations (ARLO) method [25] from the MEDI Toolbox. QSM reconstruction follows the RIN network protocol [24] using a pipeline based on the STI Suite. Brain masks are derived using the Brain Extraction Tool (BET) from FSL. Phase unwrapping is performed using Laplacian unwrapping, followed by background field removal with V-SHARP [28], and QSM reconstruction via the iLSQR method.

SMWI images are obtained by combining averaged GRE magnitude images with QSM maps, using parameters Xth = 1 ppm and m = 4. The substantia nigra is segmented using MRICloud's multi-atlas tool for automated segmentation of brain gray matter nuclei and susceptibility quantification. Segmentations are eroded using a 1 mm Gaussian kernel to minimize partial volume effects.

CHAPTER 4 CLINICAL AND RESEARCH APPLICATIONS

Alpha-synucleinopathies continuum

Recently proposed research frameworks for the diagnosis of neuronal alpha synuclein disease are grounded on the identification of the biological substrate of the disease and of the nigro-striatal dopaminergic disfunction and envision the use of biomarkers to stage neuronal alpha-synuclein disease and detect neurodegeneration (**figure 1**, [49, 50]). The biological definition of the disease of such disorder is strictly related to the evaluation of biomarkers able to predict the disease outcome and to accurately stage it. For the analysis of such topic we mainly worked on prodromal phase of the disease, i.e. during the iRBD phase.

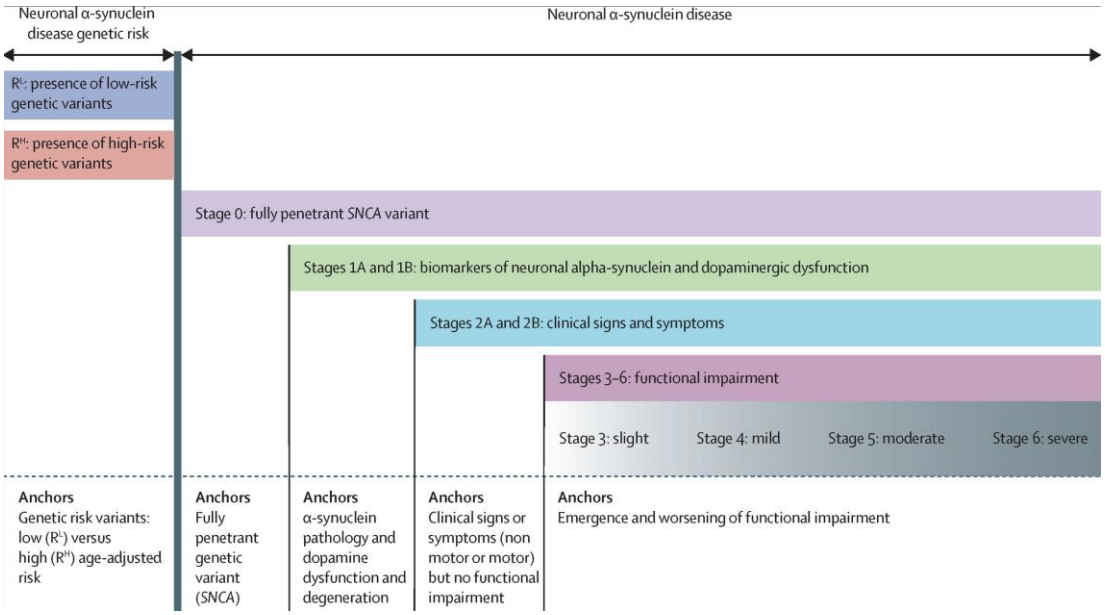

Figure 1: Cumulative framework of the neuronal α-synuclein disease integrated staging system. Adapted from (Simuni et Al 2024 Lancet Neurology)[50]

Brain metabolism, disease related pattern and phenoconversion prediction.

The evaluation of brain metabolism has always been of great importance for the evaluation of neurodegenerative disorders including Alzheimer Disease and alpha-synucleinopathies. A part from its diagnostic power the quantification of brain metabolism allows to better explain diseases' clinical manifestations [20, 21] and help to predict the clinical trajectory, a possibility that is particularly useful for prodromal stages of the disease, like iRBD for alpha-synucleinopathies. As we described in the methodology section there are several ways of quantify brain metabolism, and even if SPM group level analysis are quiet easy and straightforward to be performed, multivariate analysis as SSM-PCA are allows deeper analysis

of the metabolic fingerprint of the disease. For this project using SSM-PCA analysis, we studied [^{18}F]FDG PET imaging data of both iRBD patients who subsequently developed an overt alpha-synucleinopathy and those who did not (i.e., retained the iRBD diagnosis) at follow-up, to gain insight into the phenoconversion-related pattern, and its ability to predict short-term phenoconversion. The study was conducted in two centres, each one used to derive the pattern that was then validated in the other center, thus increasing the stability of the results.
Materials and Methods From two Italian centers, Genoa (GE) and Rome Tor Vergata (RTV), we enrolled 30 iRBD patients (mean age: 73±6, 23 males, follow-up time: 21±14 months) who subsequently phenoconverted to an overt alpha-synucleinopathy (iRBD converters), and 46 iRBD patients (mean age: 69±6, 38 males, follow-up time: 33±19 months) who did not phenoconvert (iRBD non-converters). Moreover, 44 healthy controls (mean age: 70±8.53, 16 males) and 32 de novo PD patients (mean age: 73.12±5.86, 10 males) with RBD were selected from our dataset. Diagnosis of RBD was confirmed in both iRBD and de novo PD patients by polysomnography, according to current criteria. As for de novo PD patients, the diagnosis was performed following current criteria[51] and confirmed by evidence of dopaminergic deficit on [^{123}I]FP-CIT SPECT and by at least two years of follow-up. At baseline, all patients underwent the movement disorder society Unified Parkinson Disease rating scale, motor section (MDS-UPDRS-III) to investigate the presence of parkinsonism, the Mini Mental State Examination (MMSE), as a measure of global cognitive function, as well as a comprehensive neuropsychological assessment, including at least two tests for each of the main cognitive domains (verbal memory, executive functions, attention and working memory, visuospatial abilities and language)[52] to evaluate the presence of mild cognitive impairment (MCI).[52] Patients with dementia and parkinsonism fulfilling criteria for the diagnosis of PD, MSA or DLB at baseline (i.e., they did not have iRBD) were excluded. Clinical conditions (including activities and instrumental activities of daily living assessment, motor and cognitive assessment) were evaluated prospectively every six months from baseline. Pheno-conversion to overt synucleinopathy (i.e., PD, DLB or MSA) was assessed using current criteria.[53–55] All patients gave their written consent to the study. The study protocol met the approval of the local Ethics Committee, and all participants signed an informed consent form in compliance with the Helsinki Declaration of 1975.

[^{18}F]FDG-PET

All patients underwent [^{18}F]FDG-PET to investigate brain glucose metabolism within 12 months from iRBD diagnosis. Brain [^{18}F]FDG-PET scans were acquired according to the

guidelines of the European Association of Nuclear Medicine.[56] GE and RTV acquisition protocols are described in detail in Supplementary Materials. All [^{18}F]FDG-PET images were acquired in static mode and then subjected to affine and nonlinear spatial normalization into Montreal Neurological Institute (MNI) brain space using SPM12 (Wellcome Department of Cognitive Neurology, London, UK). All the default settings of SPM were used and the specific[^{18}F]FDG-PET brain template was used as reference.[57] The spatially normalized set of images was then smoothed with a 10-mm isotropic Gaussian filter to account for individual anatomical variability and to improve the signal-to-noise ratio.

Polysomnographic recording

Patients underwent overnight polysomnography. Sleep scoring was performed following current criteria.[58] PSG derivations were placed according to recommended rules[58] to evaluate sleep features, respiratory, cardiac, and limb events. Patients were asked to withdraw melatonin, hypnotic medications, and antidepressant drugs for two weeks before the recording.

iRBDconvRP derivation and validation among GE and RTV centers

The phenoconversion-related pattern of iRBD (iRBDconvRP) patients was derived using an automated algorithm[59, 60] from the University Medical Center Groningen (UCMG), The Netherlands, based on the SSM-PCA method of Spetsieris and Eidelberg[61] implemented in Matlab (version 2020a; MathWorks, Natick, MA). We first derived independent patterns for the two centres (GE and RTV) as across-centers validation test, since having multiple sites often represents an issue.[62] In brief, SSM-PCA was first applied to a derivation set (GE patients) of 16 converter and 27 non-converter patients. The resulting iRBDconvRP was then applied to a validation set (RTV) of 14 converters and 19 non-converters patients, to confirm its ability to discriminate between converters and non-converters. The same process was repeated for the RTV cohort, obtaining the iRBDconvRP from RTV patients and subsequently calculating subject scores in the GE cohort (see Supplementary Materials for details).

iRBDconvRP derivation and validation on the whole patient group

We pooled the data to identify the iRBDconvRP in the total dataset (30 converters and 46 non-converters). For validation, we performed a leave-one-out cross validation (LOOCV)[30, 63]. Subject scores expressing both the original iRBDconvRP and the LOOCV iRBDconvRP were z-transformed with respect to the non-converter iRBD patients. Considering the known heterogeneity of iRBD patients[64], and to enhance the stability of the results, we performed a

bootstrap resampling (2000 repetitions) to extract the most stable regions in the iRBDconvRP. Unthresholded and thresholded voxels (2.5% - 97.5% CI) were overlaid on a T1-MRI template for visualisation.

DenovoPDRBDRP derivation

32 de novo PD patients with RBD and 44 healthy controls were used to obtain a denovoPDRBDRP, using same methodology described in the previous section. The denovoPDRBDRP was applied to the iRBD group to obtain the subject scores for each patient. Subject scores were z-transformed in the respect to the non-converter iRBD patients.

Statistical analysis

Between-group differences in clinical characteristics and subject's z-scores were assessed using the unpaired t-test for continuous variables and the chi-square test for categorical variables. To determine sensitivity and specificity of the patterns, a receiver operating curve (ROC) was plotted based on z-transformed subject scores. As for the iRBDconvRP, LOOCV z-scores were used in the analysis. The cut-off that gave optimum sensitivity and specificity, calculated with the Youden Index method[65], was chosen as the threshold. Next, Kaplan-Meyer survival analysis was performed to estimate the risk of phenoconversion from iRBD to an overt alpha-synucleinopathy, using pattern expression values, categorised as below or above the threshold previously computed by the Youden Index method. The survival time was set as the interval (expressed in months) between the date of [^{18}F]FDG-PET and the last follow-up visit in non-converter patients, and between the date of [^{18}F]FDG-PET and the date of phenoconversion in converter patients. The hazard ratio (HR) was calculated with a Cox regression, using age, sex and site as covariates. As for the iRBDconvRP, the presence of MCI and the MDS-UPDRS-III score were subsequently added as covariates, in order to explore their possible influence in predicting the phenoconversion. The aforementioned survival analyses were first performed using the subject scores of GE and RTV groups obtained by applying both the RTV-iRBDRP and the GE-iRBDRP on GE and RTV cohort, respectively. Then, the iRBDconvRP was tested by using the subject scores derived from the application of the iRBDconvRP after the LOOCV procedures on the whole group. Subsequently, the denovoPDRBDRP was applied on the whole iRBD group. Finally, the predictive power of the iRBDconvRP and of the denovoPDRBDRP were compared on Cox-regression. Moreover, time-dependent ROC curves were calculated and the AUC of each timepoints were compared (one time point every six months, until month number 48).Partial Pearson's correlation analysis

was performed between i)iRBDconvRP expression and survival time, ii) iRBDconvRP expression and MDS-UPDRS-III score, and iii) denovoPDRBDRP and iRBDconvRP expression, using age as a nuisance variable. Binary logistic regression was applied between iRBDconvRP expression and presence/absence of MCI. Finally, iRBDconvRP expression was compared between iRBD patients with and without MCI.

Statistical threshold was set at .05 and p-values were reported corrected for multiple comparisons using Bonferroni approach.

All analyses were performed using MatLab (version 2020a; MathWorks, Natick, MA) and Stata software (StataCorp. 2013. Stata Statistical Software: Release 13. College Station, TX: StataCorp LP).

Results

Clinical results

As expected, non-converter patients were younger, had higher MMSE, lower MDS-UPDRS-III scores, and were less frequently affected by MCI, when compared with converter patients. RTV patients had a higher MDS-UPDRS-III score when compared with GE patients.

iRBDconvRP derivation and validation

GE-iRBDconvRP significantly predict pheno-conversion in RTV patients (Hazard-ratio, HR=9.29, p=0.004), while RTV-iRBDconvRP showed a lower, but still significant prediction power in GE patients (HR=3.67, p=0.033)

SSM-PCA was then applied to the whole cohort. The first two principal components (PC) explained the top 50% of the total variance. A weighted linear combination of PC 1 and 2 (variance explained: 36.42% and 10.59%, respectively) best discriminated between converters and non-converters in the logistic regression model and was termed the iRBDconvRP. All voxel weights in the iRBDconvRP contributed to the subject scores. Voxels that survived a two-tails confidence interval (CI) threshold of 95% (percentile method) after bootstrapping were overlaid on a T1-MRI template for visualisation and included positive voxel-weights in the cerebellum, brainstem, the anterior cingulate cortex, middle and mesial temporal and postcentral areas, lentiform nucleus, while negative voxel-weights were found in the posterior cingulate, precuneus, middle frontal gyrus and parietal areas. iRBDconvRP subjects LOOCV z-scores were significantly higher in converters than non-converters patients ($p<0.0001$, Figure

4A) as well as in iRBD patients with MCI than iRBD patients without MCI ($p<0.01$). No significant correlation was found between the iRBDconvRP expression and MDS-UPDRS-III score, while iRBDconvRP expression showed a significant direct correlation with the presence of MCI ($p=0.004$).

iRBDconvRP phenoconversion prediction ability

At ROC analysis between converters and non-converters subject LOOCV z-scores, we found an area under the curve (AUC) of 0.85 (sensitivity: 87%, specificity: 72). The prediction model was statistically significant ($p<0.001$).

On Cox-regression analysis, iRBDconvRP significantly predicted phenoconversion (adjusted HR of 7.42, $p<0.001$, C.I.95%: 2.5-21.4).

The iRBDconvRP expression showed a significant inverse correlation with survival time ($r=-0.320$; $p=0.005$).

The model was significant also including MCI and MDS-UPDRS-III as covariates (HR:8.88, $p<0.001$, C.I.95% 2.65-29.79). Besides iRBDconvRP expression, only MDS-UPDRS-III score contributed to the prediction with a HR of 1.21 ($p=0.028$, C.I.95% 1.02-1.44).

To note, after removing the outlier with longer survival time (137 months) the result did not change significantly.

DenovoPDRBDRP derivation, application and comparison with the iRBDconvRP

Brain areas involved in the denovoPDRBDRP are reported in Supplementary Table 6. As expected, these patterns partially overlapped with the iRBDconvRP, with positive voxel-weights in the cerebellum and in the anterior cingulate cortex, as well as negative voxel weights in the precuneus and parietal areas and were significantly and directly correlated (r:0.6, $p<0.001$).

The denovoPDRBDRP showed a good power in discriminating iRBD converters and non-converters, with an AUC of 0.85 (sensitivity 0.93%, specificity 67%) and significantly predicted phenoconversion (HR=3.99, $p=0.001$, C.I.95% 1.81-8.83).

When combining in the Cox-regression the denovoPDRBDRP and the iRBDconvRP, only the latter maintained a statistical significance, (HR=5.72, ($p=0.003$, C.I.95% 1.83-17.85), while the former had a HR of 1.81 ($p=0.168$, C.I.95% 0.78-4.23).

When comparing the time-dependent ROC curves, the AUC were higher in the iRBDconvRP than in the denovoPDRBDRP at the first two years of follow up, whereas the AUC were higher in the denovoPDRBDRP than in the iRBDconvRP at later timepoints.

Discussion

In this study, we derived and validated a brain metabolic pattern reflecting the glucose metabolic changes associated with phenoconversion from iRBD to an overt alpha-synucleinopathy. Our results reveal the existence of a specific phenoconversion-related pattern (iRBDconvRP) found by applying the SSM-PCA to 30 iRBD patients, who phenoconverted to an overt alpha-synucleinopathy (14 PD and 16 DLB), and 46 non-converters. The iRBDconvRP significantly predicted phenoconversion from iRBD to PD or DLB over time, with a high HR.

At first, because the patients were enrolled by two different centers, two independent iRBDconvRP were derived and cross-center validated on each other, so as to obtain a more reliable pattern. The resulting patterns were topographically similar and significantly able to predict the conversion in the validation group (i.e. GE-iRBDconvRP on RTV patients and vice-versa). To notice, the application of RTV-iRBDconvRP to GE patients showed a lower HR when compared with GE-iRBDconvRP. This finding may be explained by the lower number of patients participating in the derivation of the RTV-iRBDconvRP. Nevertheless, the RTV-iRBDconvRP was significantly able to predict conversion in GE patients. This is an intriguing result, considering that no specific harmonization was performed in the [^{18}F]FDG-PET acquisition among the two centers.

The pattern analysis highlights those voxels that either positively or negatively co-vary together. From a pathophysiological standpoint, we could only speculate that the positive and negative components reflect relatively higher and lower metabolism, respectively. Accordingly, the iRBDconvRP includes positive components (relatively higher glucose metabolism) within the cerebellum, brainstem, anterior cingulate cortex, middle and mesial temporal and postcentral areas, lentiform nucleus, while negative components (relatively lower glucose metabolism) were found in the posterior cingulate, precuneus, middle frontal gyrus and parietal areas.

This pattern partially overlaps with the PDRP described in previous studies, which involves positive voxel weights in the putamen/pallidus, thalamus, pons and motor cortex and negative components in the premotor cortex, supplementary motor area, and parietal

association regions[30, 31, 66], but also shows similarities with the brain glucose metabolism pattern typically found in DLB patients.[67]

It is now recognized that neurodegenerative conditions, such as PD[15, 68, 69], DLB[67], and also iRBD[30] are characterised by disease-specific patterns, derived using [^{18}F]FDG-PET data.

In particular, it has been shown that the PDRP is more expressed in iRBD patients when compared with healthy subjects.[70] Moreover, the PDRP in iRBD patients is more expressed at follow-up than at baseline,[62] suggesting that its expression increases over time, paralleling disease progression from prodromal stages to the over neurodegenerative disease. Indeed, it has been suggested that the PDRP reflects a more advanced stage of the RBDRP, given the partially overlapped topography.[66] Interestingly, Kim et al. (2021) found that RBDRP expression decreases, whereas PDRP expression increases over time, along with disease progression.[71] Of note, Holtbernd et al. (2014)[72], studied the increase of PDRP expression in two groups of iRBD patients (10 and 17 patients respectively) followed for an average time of 5 years. They found an increased expression at baseline of the PDRP expression in both groups, especially in iRBD patients that eventually phenoconverted at follow-up.

However, iRBD patients are highly heterogeneous[64], with about half of them phenoconverting to DLB, thus a PD-related pattern may not be the best choice to identify subjects at risk of phenoconversion. Here, unlike the aforementioned studies, we wanted to find a pattern reflecting the overall risk of conversion from iRBD to overt synucleinopathy in the short-to-medium term. In fact, iRBD patients who do not convert reflect a heterogenous group, consisting of late-converters and those who will truly remain stable (i.e. isolated or idiopathic RBD). Thus, the pattern derived in this study most likely reflects the risk of short-to-medium term phenoconversion, being mean time to conversion less than two years in iRBD converters.

Indeed, a recent multicentric study investigated brain metabolism correlates of DLB core features, showing that the presence of RBD is associated with bilateral parieto-occipital cortex, precuneus, and ventrolateral–frontal metabolism[67], thus in agreement with the iRBDconvRP. To note, the iRBDconvRP only partially overlapped with the previously described RBDRP, which includes positive components within the cerebellum, hippocampus, brain stem and sensorimotor cortex, as well as negative components within the occipital, temporal and parietal cortices.[30, 71] Indeed, in the present study, non-converter iRBD

patients rather than healthy controls were used as a reference group to obtain the iRBDconvRP. The reason for this choice was to clean the pattern from the RBDRP components, as to obtain a pattern that reflects the stage of the disease, highlighting the metabolic brain areas related to a short-to medium phenoconversion, instead of the disease itself.

The iRBDconvRP expression was able to significantly predict phenoconversion in our group of patients, with an adjusted HR of 7.42, thus superior to the so far known risk factors. Indeed, the clinical risk factors showed HRs of 2 to 5[15], while presynaptic dopaminergic impairment achieved an HR of 5.71 in a recent multicenter international study.[68] Interestingly, when used as covariate, the MDS-UPDRS-III scores showed a low, but significant power in predicting conversion in iRBD patients. This is not unexpected considering that subtle motor symptoms have been described as predictors of conversion in iRBD[15] and are likely related to a more advanced stage of the disease. Moreover, the iRBDconvRP showed a higher HR in predicting phenoconversion than the denovoPDRBDRP, as previously described and stated to be a better prediction biomarker than the PDRP.[66]

This result, suggests that [^{18}F]FDG-PET may be one among the most accurate biomarkers for short-to-medium term phenoconversion in iRBD patients, thus to be taken into account as a inclusion criteria for future disease-modifying clinical trials. Moreover, the iRBDconvRP expression showed an inverse correlation with survival time (expressed in months and defined as the difference between [^{18}F]FDG-PET acquisition and phenoconversion diagnosis or last outpatient visit), highlighting its possible role as a progression biomarker. However, 70-90% of iRBD patients will eventually phenoconvert to the overt stage of the disease, when the follow up is longer than 10 years follow up[14], thus the “absence of conversion” that distinguishes non-converter from converter patients, is a condition that is expected to change overtime. Therefore, the iRBDconvRP allows to identify those patients who will eventually phenoconvert in a short-medium term, since its specificity will be lower for a longer predictive outcome. Nevertheless, in term of patients’ selection for neuroprotective trials, the discrimination between long and short-to-medium term converters could be a useful tool for researchers and clinicians.

In this study, clinical characteristics of iRBD patients are in line with the literature: iRBD converters were older and had more cognitive and motor impairment compared with non-converters.[15]

Interestingly, RTV patients had more pronounced motor impairments when compared to GE patients. Accordingly, RTV iRBD patients tended to convert more frequently to PD, whereas GE patients tended to convert more frequently to DLB, although this trend did not reach statistical significance. Despite these differences, the iRBDconvRP well discriminated between converters and non-converters in both centres, suggesting that the iRBDconvRP represents a stable and reliable pattern, regardless the phenoconversion diagnosis.

This study had some limitations. First, the relatively small sample size. However, this work is the largest [^{18}F]FDG-PET longitudinal study of iRBD patients so far. Second, given the lack of a validation group in the whole cohort we applied the LOOCV procedure to cross-validate the results, as done in previous studies.[59, 63] Third, we did not investigate specific differences between converters to DLB and converters to PD, because of the limited number of patients and because it was beyond the aim of this study. Fourth, none of the patients developed multiple systemic atrophy, which is frequently preceded by iRBD, but has a far lower incidence than PD and DLB.[73] Fifth, because of the lack of an external cohort, the longitudinal analyses (i.e. Cox-regression and time-dependent ROC) were applied in the same sample used for deriving the iRBDconvRP, therefore there may be a risk for multicollinearity and these results should be validated in different cohorts of patients. Lastly, the lack of homogeneity in [^{18}F]FDG-PET equipment between the two centres. Despite these limitations, finding two similar iRBDconvRP from two different centres, without previous harmonisation of the data, may even strengthen our result, suggesting the solidity of the data. Nevertheless, centre belonging was used as a nuisance within the analysis. Further longitudinal studies are warranted to confirm these results and eventually to differentiate patterns predicting conversion to different alpha-synucleinopathies.

This work was published on movement disorder [Mattioli Orso 2021] and led to many others, mainly carried out by Dr. Orso, co-first author of the aforementioned project and that validated and applied it to many other cohorts, proving such results and providing clues on the usefulness of [^{18}F]FDG-PET to characterize and predict the pheno-conversion in patients with iRBD .[74–76]

Nigrostriatal path way.

Neurodegeneration in alpha-synucleinopathies is typically assessed by evaluating nigrostriatal pathway dysfunction.[77] using single photon emission computed tomography (SPECT) with [^{123}I]-ioflupane (DaT-SPECT) which serves as the gold standard for in vivo evaluation of the nigrostriatal pathway.[54] Less invasive neuroimaging techniques to evaluate nigrostriatal pathway are currently under validation in research settings.[49] For example, iron sensitive MRI can provide with promising markers of neurodegeneration to assess the substantia nigra (SN) with few studies exploring its use in prodromal alpha-synucleinopathies.[78–80] A visually assessable radiological marker of SN pathology is the loss of the physiological dorsal nigral hyperintensity (DNH), which is caused by iron accumulation. DNH is typically evaluated using magnetic resonance susceptibility-weighted imaging (SWI) a technique combining the magnitude and phase images obtained with a gradient echo (GRE) acquisition. In particular, the SWI reconstruction uses the signal phase, reflecting local field inhomogeneities originating from biological tissues' magnetic susceptibility, to enhance the T2*-weighted contrast embedded in the conventional magnitude images. This way, the hypo-intensity of paramagnetic tissues, such as those with increased iron concentration, is emphasized. The normal appearance of the DNH in SWI at the expected anatomical location of Nigrosome 1 (N1) at level of the midbrain level is known as the swallow tail sign.[81, 82] The assessment of the swallow tail sign using SWI in MRI scanners operating at 3T showed excellent sensitivity (94.6%) and specificity (94.4%) in identifying patients with overt PD[77] but only fair sensitivity (63%) and specificity (79%) in identifying DLB.[83] Few studies investigated iron sensitive MRI in the prodromal phases, such as in idiopathic/isolated REM sleep behavior disorder (iRBD), showing abnormal N1 imaging in about 60% of iRBD cases.[78]

One known limitation of SWI is that it directly relies on local field inhomogeneities to emphasize magnetic susceptibility effects: such field inhomogeneities spatially extends beyond the tissues that generate them, therefore the image feature emphasized by SWI do not precisely co-localize with the underlying anatomy. An improved implementation of SWI, namely susceptibility mapping weighted imaging (SMWI), relies on the same acquisition as SWI, but employs a refined reconstruction pipeline including an image processing step to remove the non-local phase perturbations by a deconvolution operation.[83] Therefore, SMWI results in improved susceptibility contrast and reduced "blooming" artifact and has been proved to

provide enhanced N1 anatomical depiction and visibility at 3T when compared to conventional SWI. SMWI has never been tested in prodromal stages of alpha-synucleinopathies and we hypothesized that SMWI would enable neuroradiologists detecting an altered appearance of the substantia nigra not only in the overt forms of alpha-synucleinopathy, but also the prodromal stages.

The aim of the present project was to confirm this hypothesis by visually evaluating the SMWI swallow tail sign representations of patients along the prodromal to overt alpha-synucleinopathy continuum. For comparison, we included a group of healthy subjects (HC) and patients with Alzheimer's disease (AD). Moreover, we assessed the relationship between the SMWI visual evaluation of the swallow tail sign and quantitative susceptibility mapping (QSM) semi-quantification of iron content in the substantia nigra to further validate this imaging marker. Finally, we aimed to compare the SMWI assessment with DaT-SPECT results.

Materials and Methods

Patients

This project is a single center prospective case-control study conducted between November 2020 and February 2024. The main inclusion criteria were the diagnosis of PD, DLB, prodromal DLB (pDLB) or iRBD, determined in accordance with current criteria by a movement specialist for PD, a cognitive specialist for DLB and pDLB, and a sleep specialist for pDLB and iRBD. The diagnoses of PD and DLB were further confirmed through clinical follow-up of at least 12 months. To be consistent with the new concept of the alpha-synucleinopathy continuum[49, 50], PD and DLB patients were classified as having overt alpha-synucleinopathy, while iRBD and pDLB patients were considered prodromal stages of alpha-synucleinopathy. All subjects underwent 3T brain MRI; additionally, patients with overt DLB and all prodromal patients also underwent brain DaT-SPECT.

As healthy controls, we enrolled a group of subjects with no history of neurological, cognitive or psychiatric disorders (including but not limited to depression and anxiety). Moreover, we included a group of pathological controls diagnosed with AD at the MCI or dementia stage, according to current criteria. All AD patients met the criteria for probable AD, with at least intermediate likelihood based on clinical and neuronal injury imaging data (MRI and/or [18F]FDG PET]. Moreover, imaging and clinical data were carefully assessed to exclude the potential misclassification of DLB patients in the AD cohort. Furthermore, 71.4% of them were considered at high likelihood of AD in presence of positive amyloid biomarker according

to PET with specific tracers or cerebral spinal fluid assessment of amyloid isoforms (Aβ42/Aβ40 ratio), also in accordance with the proposed AT(N) research framework.

Exclusion criteria were claustrophobia, or any contraindications to MRI. MRI scans with motion artifact that precluded visual analysis were not included.

Ethics statement. The study protocol was approved by the local Ethics Committee, and an Informed consent form was signed by all participants, in compliance with the Helsinki Declaration of 1975.

Magnetic resonance imaging

MRI Acquisition

All subjects were scanned with a Siemens Prisma 3T MR system equipped with a 64-channel head coil. The protocol included whole-brain acquisitions of magnitude and phase data using a multi-echo 3D gradient echo (GRE) sequence with eight echoes at TE1/ΔTE = 5.6/5.6 ms; TR = 51 ms; flip angle 18°; 1 x 1 x 1 mm3 resolution; 224 x 224 x 144 matrix size; GRAPPA = 2; partial Fourier 6/8 in both Phase-encoding (PE) directions; Bandwidth (BW) = 340 Hz/px; adaptive coil combine with pre-scan normalize on; acquisition time = 8 min 45 s.

Additional structural brain images were acquired in the sagittal plane using a T1-weighted MPRAGE with TR=2300 ms; TE=2.96ms; TI=900; flip angle 9°; 1 x 1 x 1 mm^3 resolution; 256x256 Matrix size; GRAPPA=2; BW=240 Hz/px; acquisition time = 5 min 30 s.

MRI Data Processing

For each patient, R2* map, QSM and SMWI were reconstructed, as detailed below. All image reconstructions were carried out using Matlab 2019b (MathWorks, USA).

R2* maps were calculated via the Auto-Regression of Linear Operations (ARLO) method from the MEDI Toolbox (http://pre.weill.cornell.edu/mri/pages/qsm.html).

QSM maps were reconstructed according to the RIN-network's protocol previously described in detail (24) using a processing pipeline based on STI Suite (https://people.eecs.berkeley.edu/~chunlei.liu/software.html from UC Berkeley, Berkeley, CA, USA). In short, a brain mask was calculated from the T2*-weighted magnitude image averaged across all echoes using the Brain Extraction Tool (BET) from FSL. For each echo, raw phase images were unwrapped using Laplacian phase unwrapping followed by background

field removal using the Variable-kernel Sophisticated Harmonic Artifact Reduction for Phase data (V-SHARP) approach. QSM maps were then calculated using the iLSQR method.

SMWI was obtained by merging each subject's GRE magnitude image averaged across all echoes and QSM according to a previously documented pipeline (15) with parameters $X_{th} = 1$ part per million and m = 4.

The whole SN was segmented via MRICloud with the "multi-atlas tool for automated segmentation of brain grey matter nuclei and quantification of their magnetic susceptibility based on the joint contrast information from the co-registered T1-weighted image and susceptibility map. The SN segmentations were then eroded via a convolution with a 1 mm Gaussian kernel to avoid partial volume effects.

MRI Image scoring

SMWI reconstructions were evaluated to assess the SN at the level of the posterior third part below the red nucleus using a validated scale of preservation of the swallow tail sign (dorso nigral hyperintensity, DNH) corresponding to the anatomical location of N1 based on trilaminar aspect of SN. In detail, the sign received a score ranging from 1 to 4 (1 = present, 2 = probably present, 3 = probably absent, 4 = absent as shown in figure 1) (14). Visual scores were subsequently dichotomized as present (1 and 2) and absent (3 and 4) and this scoring system was applied independently to right and left nigrosome by two expert neuroradiologists (LF, LR), blinded to the diagnosis of the subject. In the case of different scoring, the case was evaluated again, a consensus reached, and the worst side defined in each patient. To note, a present swallow tail sign is thought to reflect a normal SN, while an absent sign is indicative of an abnormal SN.

DaT-SPECT

DaT-SPECT was acquired according to EANM guidelines (32) in the subgroup of patients diagnosed with prodromal alpha-synucleinopathies and in overt DLB patients, within 12 months since MRI. Data were acquired by means of a 2-headed Millennium VG camera (G.E. Healthcare). The reconstructed DaT-SPECT images were processed using the DaTQUANT^{TM} v 2.0 software to obtain specific binding ratios (SBR) for putamen and caudates nuclei.

Putamen's DaT-SPECT z-scores were calculated. The z-scores of the most affected putamen (MAP) were further categorized as below or above the cut-off of –1. We choose the cut-off of –1 at MAP because it was found to be the most accurate in identifying iRBD patients at high

risk of short-term phenoconversion. Accordingly, for the statistical analysis prodromal patients were considered as positive (prodromal positive, PP) or negative (prodromal negative, PN) depending on the MAP Z score (i.e. below/above -1 respectively). In this case, a positive DaT-SPECT reflects an impaired nigro-striatal dopaminergic function, while a negative DaT-SPECT reflects a normal function.

Statistical analysis

Firstly, we performed a descriptive analysis. For normally distributed data, we used analysis of variance (ANOVA), t-tests for continuous variables, and chi-squared statistics for categorical variables. For non-normally distributed data, Kruskal-Wallis and Mann-Whitney test were performed.

We explored the agreement between the two raters by performing a Cohen's Kappa agreement test. Subsequently, we computed the rates of present/absent swallow tail sign at SMWI visual inspection in all enrolled subjects, as well as the sensitivity and specificity of the swallow tail sign in detecting alpha-synucleinopathies. We used the clinical diagnosis as 'ground truth', and considered the positive and negative results of the nigrosome assessment as follows:

- A true positive was considered when the swallow tail sign was rated as absent (abnormal) and the patient had either prodromal or overt (either DLB or PD) alpha-synucleinopathy,

- A true negative was defined as when the swallow tail sign was rated as present (normal) and the patient was diagnosed with either AD or was a healthy control,

- A false positive occurred when the swallow tail sign was rated as absent (abnormal), but the subject was diagnosed with either AD or classified as a healthy control,

- A false negative was identified when the swallow tail sign was rated as present (normal), but the patient had either overt or prodromal alpha-synucleinopathy.

However, prodromal subjects may exhibit either a positive or negative DaT-SPECT, which has relevant prognostic implications. Specifically, patients with iRBD who have a positive DaT-SPECT have a high risk of short-term phenoconversion.[68] To effectively group subjects with and without nigrostriatal impairment, we conducted a secondary analysis, where prodromal patients with a negative DaT-SPECT (i.e. MAP z score above -1) were assigned to the control group, which also included HC and AD patients. Conversely, prodromal patients with an altered DaT-SPECT (i.e. MAP z score below -1) were assigned in the study group, alongside overt PD

and DLB patients. This secondary analysis allowed us to compute the sensitivity and specificity of the SMWI swallow tail sign assessment in identifying alpha-synucleinopathy patients with nigrostriatal dopaminergic dysfunction, compared to subjects with an intact nigrostriatal dopaminergic pathway, namely AD patients, healthy controls and prodromal patients with a negative DaT-SPECT at the time of the evaluation.

To explore whether the visual analysis of the swallow tail sign corresponded with quantifiable changes in the SN, we then compared mean magnetic susceptibility (from QSM) and R2* across the groups defined by visual scores of the swallow tail sign. To achieve this, we applied two general linear models (GLMs) to assess susceptibility/R2* in relation to visual scores, while including age as a confounding factor, with a significance level of 0.05.

Finally, we compared the DaT-SPECT results with the visual scores of the swallow tail sign. For this analysis, DaT-SPECT z-scores were categorized dichotomously (i.e. below or above –1 z-score).

Statistical analysis was performed with R studio implemented in Bluesky statistics (https://www.blueskystatistics.com), and Python (https://www.python.org).

The data used in the present study can be requested upon reasonable request.

Results

Out of 130 subjects that underwent MRI, 15 were excluded by the study because of motion artifacts whereas 115 subjects were enrolled (mean age=70.78±8.50, 48.69% females): i) 34 patients in the prodromal stage of alpha-synucleinopathy (mean age= 72.35±7.25, 32.35% females; 21 iRBD, 13 pDLB), of which 12 with a MAP z-score above –1 (prodromal negative group, PN, mean age= 71.08±7.87, 33.33% females) and 22 with a MAP z-score below –1 (prodromal positive group, PP, mean age= 73.05±6.98, 31.81% females), ii) 27 patients diagnosed with overt alpha-synucleinopathy (mean age=69,07±7.91, 44.44% females, 22 PD, 5 DLB), iii) 26 healthy subjects (mean age=69.89±10,90, 73.07% females), and iv) 28 patients diagnosed with AD (mean age=71,35±7.98, 50% females). Demographic and clinical data of the patients are reported in **table 1**.

	Healthy Controls n = 26	Prodromal aSyn n = 34		Overt aSyn n = 27		AD N = 26
Diagnosis	n/a	RBD n = 21	pDLB n = 13	PD n = 22	DLB n = 5	n/a
Age (mean; SD)	69.88; 11.10	72.35; 7.34		69.07; 7.61		71.36; 7.97
Sex (Females)	19 (73.08%)	11 (32.35%)		12 (44.44%)		14 (53.85%)
Mini Mental State Examination (mean; SD)	n/a	27.32; 3.02		26.00; 4.84		23.72; 3.50
MDS-UPDRS III (mean; SD)	n/a	6.20; 6.76		19.85; 10.84		n/a
Levodopa equivalent daily dose (LEDD) (mean; SD)	n/a	n/a		PD 620.30 mg; 161.49 mg	DLB n/a	n/a

RBD: REM Behavioral Disorder; pDLB: prodromal dementia with Lewy bodies; PD: Parkinson's disease; DLB: Dementia with Lewy bodies; SD: standard deviation.

Inter-rater agreement

The two raters demonstrated substantial agreement (K=0.80, Standard error (SE)=0.03, Confidence interval (CI)=0.75 - 0.85) in scoring the swallow tail sign within one of the four classes provided. More in detail, the rate of disagreement was 22.94% in the whole group of nigrosomes (left+right, 53 out of 230), 16.67% in the control group (18 out of 108, 5.77% in the healthy control group (3 out of 52), 26.79% in the AD group (15 out of 56)), 26.47% in the prodromal group (18 out of 68) and 31.48% (17 out of 54) in the overt group. When considering the dichotomized classes (present/absent) the two raters demonstrated substantial agreement (K=0.82, Standard error (SE)=0.04, Confidence interval (CI)=0.75 - 0.90) and the rate of disagreement decreased as follows: 6.09% (14 out of 230) in the whole group, 9.26% (10 out of 108, 5.77% in the healthy control group (2 out of 52), 14.29% in the AD group (8 out of 56)) in the control group, 5.88% (4 out of 68) in the prodromal group, 0% (0 out of 54) in the overt group. Further analyses were performed based on the consensus of the two neuroradiologists regarding the most affected side.

Presence/absence of the swallow tail sign across groups:

Rates of present/absent swallow tail sign were different among groups ($p<0.001$, **figure 2**). Alpha-synucleinopathies, whether in their prodromal or overt stage, had a higher proportion of absent swallow tail sign and a lower proportion of present swallow tail sign compared to both HC and AD patients.

Notably, prodromal patients with negative DaT-SPECT appear to fall between control subjects and those with overt alpha-synucleinopathy, exhibiting a relatively balanced percentage of swallow tail sign presence/absence scores (42% versus 58%, respectively). In contrast, prodromal patients with positive DaT-SPECT had swallow tail sign ratings comparable to those of overt alpha-synucleinopathy patients, as shown in **figure 2**.

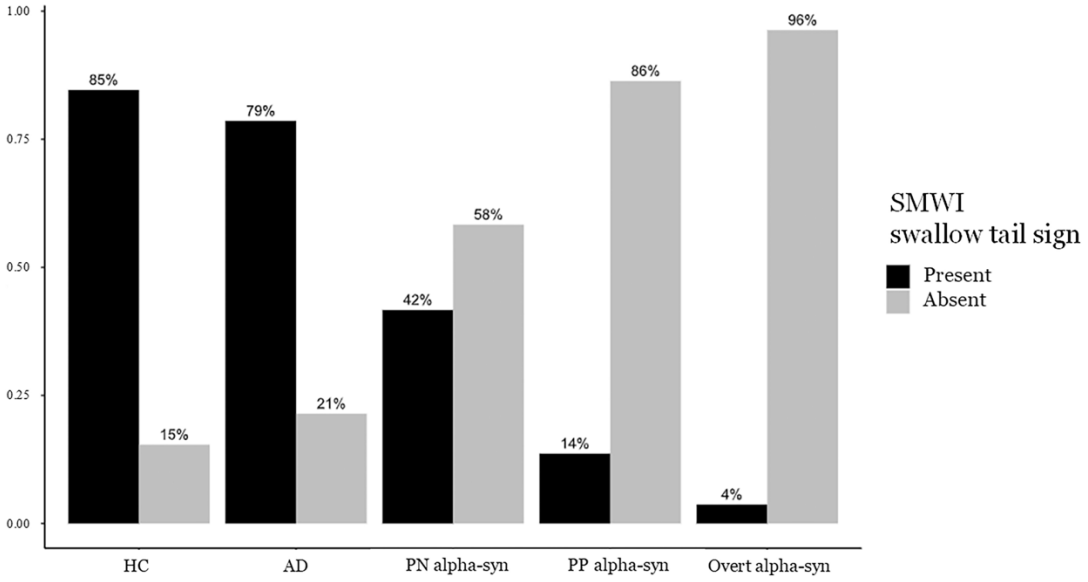

Figure 2. Relative frequencies of the presence and absence of the swallow tail sign in SMWI in the most affected side were analyzed in: healthy controls, patients affected by AD, patients with prodromal alpha-synucleinopathy and overt alpha-synucleinopathy. The prodromal group was further divided based on their most affected putamen z-scores, with one subgroup above the cut-off (prodromal negative PN alpha-syn), and the other below the cut-off (prodromal positive alpha-syn). Chi-squared test results for comparison: HC vs. AD =0.568, HC vs. PN alpha-syn <0.007, HC vs. PP alpha-syn <0.001, HC vs. Overt alpha-syn <0.001, AD vs. PN alpha-syn =0.022, AD vs. PP alpha-syn <0.001, AD vs. Overt alpha-syn <0.001, PN alpha-syn vs. PP alpha-syn =0.066, PN alpha-syn vs. Overt alpha-syn <0.002, PP alpha-syn vs. Overt alpha-syn =0.207. Legend: AD: Alzheimer disease; PN alpha-syn: Prodromal Negative alpha-syn; PP alpha syn: Prodromal Positive alpha-syn.

Sensitivity and specificity assessment

The SMWI visual analysis of the swallow tail sign showed a good sensitivity (0.85) and specificity (0.82) in correctly identifying patients with alpha-synucleinopathy, along with a good accuracy, and positive and negative predictive values (0.83, 0.84, and 0.83, respectively).

In a secondary analysis, where prodromal patients were categorized according to the DaT-SPECT results, the SMWI visual analysis of the swallow tail sign showed an increase in

sensitivity and negative predictive value (both 0.92), a decrease in specificity and positive predictive value (0.74, 0.73, respectively), while accuracy remained nearly unchanged at 0.82.

Quantitative MRI compared to visual scores

GLMs of SN susceptibility and R2* as functions of SMWI visual rating and age were significant, indicating that both predictors significantly impacted susceptibility and R2* ($F = 10.499$, $p < 0.001$; $F = 6.919$, $p < 0.001$, respectively). Even if a certain overlap in terms of confidence interval was observed, post-hoc t-tests between visual ratings revealed significant differences in mean SN susceptibility and R2* based on visual scores, as summarized in Figure 3. Of notice 4 scans (2 HC, 1 AD, 1 RBD) were affected by mild movement artifacts or presented acquisition incompatibility with the analysis, hence were removed from the quantitative analysis.

Comparison between DaT-SPECT and swallow tail sign SMWI visual evaluation in prodromal patients

Thirty-eight patients underwent DaT-SPECT imaging. Among these, 4 patients had overt DLB (mean age=76.40±7.44, 40% females), while 34 patients had prodromal alpha-synucleinopathy (mean age=72.35±7.25, 32.35% females). In this subgroup, the rates of positive and negative findings for the MAP and swallow tail sign were associated, although this association did not reach statistical significance ($p=0.066$). However, when considering DaT-SPECT values as a continuous variable, subjects with the swallow tail sign rated as absent showed significantly lower ($p=0.019$) DaT-SPECT values (-1.857 ± 1.343) compared to those with the swallow tail sign rated as present (-0.385 ± 1.850).

Discussion

Recently proposed research frameworks for the diagnosis of neuronal alpha synuclein disease are grounded on the identification of the biological substrate of the disease and of the nigro-striatal dopaminergic disfunction and envision the use of biomarkers to stage neuronal alpha-synuclein disease and detect neurodegeneration.[49, 50]

Currently, DaT-SPECT is widely used for nigro-striatal pathway assessment. Specifically, the binding ratio in the MAP, adjusted for age and sex, is used to categorize individuals as having or not having a dopamine transporter deficit. Since the new alpha-synucleinopathy research

framework (1,2) allows for the incorporation of emerging measures of dopaminergic dysfunction, in addition to or instead of dopamine transporter loss, the validation of new biomarkers reflecting neurodegeneration specific to neuronal α-synuclein disease remains a current challenge. In this context, susceptibility weighted imaging has emerged as a promising tool for identifying biomarkers of nigrostriatal neurodegeneration.

In this study, we assessed the visual evaluation of the nigrosome using susceptibility map weighted imaging (SMWI) to detect SN impairment in a large and heterogeneous cohort of patients along the continuum from prodromal to overt alpha-synucleinopathy.

SMWI employs a susceptibility weighting mask derived from QSM that enhances the visibility of the swallow tail sign and reduces the "blooming" artifact[84], whose high diagnostic performance in determining nigrostriatal degeneration was demonstrated on different MRI scanners in a recent multi-centric study.[85] In this study, SMWI was reconstructed from the 3D GRE 8-echo acquisition included in the harmonized protocol of the" Italian Neuroscience and Rehabilitation Network" as described in Lancione M et al[86] with an acquisition time of more than eight minutes which could be difficult to implement in the clinical setting. It is worth pointing out that the most recent international recommendations[87] suggest the use of fewer echoes with shorter maximum echo time, which enables shorter acquisition times. Superb SMWI quality can be achieved also with even more efficient acquisition schemes, such as echo-planar imaging, as recently demonstrated in the context of a different neurological application.[88]

Using a visual assessment score on SMWI, we demonstrated that both patient groups in the prodromal and overt stages of the disease exhibit a high rate of absence of the swallow tail sign (96% in overt alpha-synucleinopathies).

When the clinical diagnosis was used as the 'ground truth', the sensitivity and specificity of the SMWI swallow tail sign visual assessment in identifying alpha-synucleinopathy patients were good (above 0.8).

However, when grouping the subjects based on nigrostriatal dopaminergic deficit, both the sensitivity and the negative predictive value improved to excellent (above 0.9), while the specificity and the positive predictive value became acceptable (above 0.7). Additionally, the visual assessment of the SMWI swallow tail sign was associated with quantitative changes in magnetic susceptibility in the SN as measured by QSM, indicating a substantial overlap between visual assessment and semi-quantified approach.

We found that the visual assessment of the SMWI swallow tail sign is highly reproducible, showing a substantial inter-rater agreement (K=0.8). Such results suggest that in the study of neuronal alpha synuclein diseases, SMWI might be potentially useful to detect SN neurodegeneration in fulfillment of recently proposed biological definition of alpha-synucleinopathies,

The prodromal stages of the disease have been less thoroughly investigated using iron-based MRI. Given that SN degeneration has been proposed as a predictor of phenoconversion to overt alpha-synucleinopathy[50], its early recognition is of paramount importance.

Even if some research has been performed in the imaging of iron accumulation and in particular on SWI in PD[77, 89] the literature on the prodromal stages of alpha-synucleinopathies is overall inconsistent. It showed a loss of DNH in 25%[79] to up to 61% of iRBD cases[77, 78], depending on the magnetic field strength and the MRI scan sequences. Our results outperform those of previous studies, showing that in 77% of prodromal patients, the swallow tail sign was scored as absent. Notably, in our sample, approximately 60% of prodromal subjects with a negative DaT-SPECT had the swallow tail sign scored as absent, while in up to 86% of prodromal patients with a positive DaT-SPECT also had the swallow tail sign scored as absent. This finding further strengthened the hypothesis that SMWI may be a reliable biomarker for SN neurodegeneration since prodromal alpha-synucleinopathy stage, with high negative predictive value.

The SMWI visual assessment of the swallow tail sign successfully distinguished the prodromal stages of the disease from healthy subjects, even in the absence of a positive DaT-SPECT. This supports the idea that the loss of DNH reflects the accumulation of iron that occurs in the very early stages of the disease, suggesting that the morphological abnormalities detectable by SMWI at the SN level may manifest before functional presynaptic dopaminergic impairment can be detected by the DaT-SPECT.[90] Conversely, no significant difference was found between overt alpha-synucleinopathies and prodromal patients with positive DaT-SPECT, suggesting that iron deposition in the SN begins in the prodromal phase of the disease and reaches a floor effect in the “late” prodromal/early overt stages, hindering the identification of significant differences. Indeed, while the SMWI swallow tail sign visual assessment and DaT-SPECT were associated, there was not a complete overlap, suggesting that these two metrics reflect different, though connected, aspects of the substantia-nigra dopaminergic system. In

fact, recent evidence suggests that assessing the terminal part of the nigrostriatal pathway does not necessarily reflect the condition of the neuronal cell bodies and/or axons reported the presence of scans without evidence of dopaminergic deficit.[91, 92] This possibility strengthens the hypothesis that visual assessment of the SMWI swallow tail sign could serve as a valuable biomarker for identifying neurodegeneration, even in the prodromal stages of alpha-synucleinopathies, by directly evaluating neuronal body degeneration. Overall, these findings suggest that the SMWI swallow tail sign visual assessment may serve as a valuable biomarker for identifying neurodegeneration, applicable from the prodromal stages of alpha-synucleinopathy, and possibly providing, in a small proportion of patients, non-redundant information compared to DaT-SPECT. Interestingly, 85% of healthy controls showed a present SMWI swallow tail sign (normal), while 79% of AD patients were rated as normal. Although this difference did not reach statistical significance, it may reflect the presence of alpha-synuclein-related co-pathology in a subset of AD patients and might have affected the performances of the neuroimaging techniques. In fact, in a recent study on 240 biologically determined AD patients, a positive αSyn Seed Amplification Assay, suggestive for the presence of co-pathology, was disclosed in 30% of the patients,[93] in agreement with pathological studies.[94]

It is worth pointing out that the AD patients enrolled in the present study did not have any clear sign of parkinsonism, but patients did not undergo systematic motor symptom evaluation. Thus, mild motor symptoms may have been present but unreported. Moreover, it would be particularly interesting to follow the 15% of healthy subjects with an absent SMWI swallow tail sign (abnormal) over time to evaluate whether they might develop signs related to alpha-synucleinopathy. Notably, the healthy subjects did not report dream-enacting behaviors; however, they did not undergo polysomnography, so we cannot exclude the presence of subclinical RBD, as a very early, prodromal, sign of alpha-synucleinopathy. Other, non-specific-motor symptoms commonly seen in the prodromal stages of synucleinopathies, such as hyposmia and constipation, were not formally assessed.

To quantitatively assess the swallow tail sign visual, we employed QSM. This method has not been widely evaluated in iRBD patients[95] (49). However, voxel-wise analysis of QSM revealed increased susceptibility within the SN in both PD and iRBD compared with HC.[96]There is a growing interest in QSM as a progression biomarker in prodromal alpha-synucleinopathies (41). In this study, we found a significant difference in susceptibility and R2* in the SN across the four classes of visual rating. These findings provide a physical basis

for the visual analysis of SMWI nigrosome representation, possibly offering neuroradiologists, after further amelioration and validation of the methodology, an easier-to-use yet accurate tool for assessing nigrosome integrity.

Our results align with the potential association between changes in the swallow tail sign appearance and free water changes in the posterior region of the substantia nigra, but further work is needed to study correlation between DaT-SPECT values, free water values and dopaminergic cell of the nigrostriatal system.

This study had some limitations: i) Not all enrolled subjects underwent DaT-SPECT; only those in the prodromal stage or with overt DLB did. However, all overt PD patients were expected to have nigrostriatal dopaminergic impairment, and PD diagnosis was confirmed after at least 12 months of clinical follow-up. ii) DaT-SPECT and MRI were not acquired simultaneously; DaT-SPECT was performed within six months before or after MRI. However, this period is still below the time resolution of DaT-SPECT, since it usually needs 12 to 18 months to detect reliable nigro-striatal pathway's differences. Nonetheless, prodromal patients were clinically evaluated every six months and remained prodromal at the time of the second imaging technique. iii) The enrolled subjects did not undergo alpha-synuclein seed essay, hence it is possible that within the control group there may be patients with co-occurrence of alpha-synucleinopathy and amyloid disease. Indeed, some of the patients with AD had an absent swallow tail sign. We expect that the statistical significance of the results presented in this study would increase, if patient were grouped based on pathology-proven classification; these considerations warrant future larger multicentric studies with pathological confirmation.

In conclusion, visual analysis of the SMWI swallow tail sign has the potential to become a reliable biomarker for detecting SN neurodegeneration within the continuum of alpha-synucleinopathies, since the prodromal stages of the disease. This approach is applicable at single-subject level, aligning with the new era of biological definitions of alpha-synucleinopathy, and may facilitate earlier diagnosis.

Such project, in which I served as corresponding author, was published in the Journal of Parkinson's Disease in 2025 (first authors Dr. Falcitano and Dr. Calizzano). In my opinion, it fits well within the current framework of the biological definition of α-synucleinopathies, providing a non-invasive alternative to DAT-SPECT. The results of the study were further confirmed by quantitative analyses in a parallel project led by Dr. Kiersnowski and published

in Scientific Reports in 2025, providing evidence of a direct relationship between striatal ^{123}I-FP-CIT SPECT and magnetic susceptibility in the substantia nigra.

Brain tumor related epilepsy

Brain tumor-related epilepsy (BTRE) may present as initial symptom or after brain surgery, where it may signal tumor recurrence.[97, 98] Epilepsy occurs at disease onset in approximately 15–30% of cases and develops postoperatively in about 20%, although the true incidence remains uncertain due to conflicting literature data and the scarcity of robust evidence on clinical and molecular risk factors for seizure occurrence or recurrence after surgery.[99] In primary brain tumors, seizure incidence at onset is inversely related to histological grade, being highest in low-grade gliomas, though epilepsy is also common in high-grade tumors. The mechanisms underlying BTRE are multifactorial and incompletely understood, involving tumor histology, localization and extent, blood–brain barrier (BBB) disruption, peritumoral microenvironmental changes, neurotransmission abnormalities, genetic alterations, and inflammatory processes.[100]

Tumor-related BBB disruption is characterized by reduced transmembrane proteins, tight junction disorganization, and increased vascular endothelial growth factor (VEGF) release.[101, 102] VEGF diffusion in the peritumoral region exacerbates edema and alters tight junction permeability through TGFβ receptor activation, facilitating extracellular potassium accumulation, neuronal depolarization, and epileptogenesis.[103] The peritumoral microenvironment further contributes to seizure generation, as shown by reduced N-acetylaspartate levels on MRI spectroscopy, reflecting neuronal dysfunction that is more pronounced in patients with seizures.[103]

Surgery remains a cornerstone in the management of diffuse gliomas, with the dual goal of improving overall survival and controlling BTRE.[103] While stereotactic biopsy may be used for diagnostic purposes in selected cases, maximal safe resection is preferred. Outcomes improve with increasing extent of resection, ranging from partial to subtotal, gross total, and, more recently, supratotal resection, which includes removal of peritumoral tissue and appears particularly beneficial in low-grade tumors.[104–107] Residual tumor volume is a critical prognostic factor: patients with low residual volumes show significantly better long-term survival compared with those undergoing biopsy alone or with larger residual disease.[108] Importantly, surgical extent also strongly influences seizure outcome, with gross total resection associated with higher rates of postoperative seizure freedom; in low-grade gliomas, seizure control is often achieved with resections of at least 80% of tumor volume.[109] Overall,

surgery plays a fundamental role not only in oncological control but also in the management of epilepsy in glioma patients.

Based on these premises, the present study analyzed a dataset of clinical, histological, and radiological findings from patients with diffuse gliomas, including individuals who developed epilepsy during the disease course, with the aim of identifying predictive factors for BTRE. Analyses were conducted both in the entire cohort and in the subgroup of high-grade diffuse gliomas, exploring associations between demographic variables, tumor characteristics, biomarker status, epilepsy onset, postoperative seizure occurrence, and survival outcomes, including progression-free and overall survival, to better clarify the relationship between glioma biology, treatment, and epilepsy.

Materials and methods

In this retrospective study, we evaluated the clinical, histological, and radiological data of 204 consecutive patients with diffuse gliomas, including 69 with high-grade diffuse glioma, managed by the Neuro-Oncology Disease Management Team (DMT) of the IRCCS San Martino Polyclinic Hospital in Genoa between 2015 and 2024. The Neuro-Oncology DMT is a multidisciplinary team composed of neurologists, oncologists, neurosurgeons, radiotherapists, and pathologists working collaboratively to provide comprehensive care for patients with brain tumors. Patients were included if they had a diagnosis of diffuse glioma according to the 2021 WHO classification and had undergone brain tumor surgery or stereotactic biopsy allowing biomarker analysis. For volumetric analyses, only glioblastoma patients with available pre- and post-surgical brain MRI were selected. Patients lacking a complete evaluation, including clinical assessment, brain MRI, and thorough postoperative pathological investigation, were excluded.

Patients with suspected epileptic events were assessed by neurologists with specific expertise in epilepsy, and seizure diagnosis was established according to the 2025 International League Against Epilepsy criteria; although all patients were evaluated before 2025, seizure semiology was carefully reviewed and the 2025 criteria were retrospectively applied.[110] Tumor diagnosis and classification were based on the 2021 WHO criteria and included assessment of IDH1, IDH2, GFAP, Ki-67, MGMT, synaptophysin, ATRX, and p53. Immunohistochemical markers (ATRX, synaptophysin, p53, and GFAP) were scored as not assessable, negative, or positive, while Ki-67 expression was categorized using predefined cutoffs: 0 (<1%), 1 (1–5%), 2 (5–10%), 3 (10–20%), 4 (20–40%), and 5 (>40%). Somatic mutations in IDH1 (codons 105

and 132) and IDH2 (codons 140 and 172) were analyzed using real-time PCR (EasyPGX ready IDH1/2 CE-IVD kit; sensitivity 0.5–5%) and, when required, PCR followed by capillary sequencing (Genetic Analyzer 3130; sensitivity ~20%). MGMT promoter methylation status was assessed after bisulfite treatment by quantitative analysis of ten CpG islands in the promoter region using the MGMT plus kit IVD on the PyroMark Q96 system (sensitivity ~5%) and/or PCR with automated sequencing (sensitivity ~20%); samples were considered unmethylated below 9% mean methylation and methylated above this threshold. The presence of 1p/19q codeletion was investigated using Vysis 1p36/1q25 and 19q13/19p13 FISH probe kits.

Collected patient variables included demographic data (age, sex, age at diagnosis), lesion localization (hemisphere and lobe), presence of brain tumor–related epilepsy with distinction between seizures at onset and post-surgical seizures, seizure type before and after surgery, seizure frequency at onset and at last follow-up, tumor recurrence, and death. For each patient, progression-free survival was calculated as the time from neurosurgical intervention to recurrence or last follow-up, and overall survival as the time from neurosurgical intervention to death or last follow-up. In the subgroup analysis of high-grade gliomas, additional radiological parameters, including pre- and post-surgical tumor volumes, were also analyzed.

Patients were clinically monitored with follow-up oncological visits and radiologically via MRI every 3-6 months, as it is recommended. In BTRE patients, neurological visits have been scheduled every 6 months to monitor seizures frequency, treatment efficacy and possible side effects.

Magnetic resonance imaging

MRI was performed using 3.0T Magnetom Prisma and 1.5T Magnetom Sola scanners (Siemens Healthineers, Erlangen, Germany) with a standardized acquisition protocol. This included axial T2-weighted Turbo Spin Echo (TSE) sequences, 3D T1-weighted SPACE (Sampling Perfection with Application-optimized Contrast using different flip angle Evolution) TSE sequences, 3D T2 FLAIR TSE sequences, diffusion-weighted imaging (DWI), and susceptibility-weighted imaging (SWI).

The imaging protocol was further completed with a dynamic susceptibility contrast (DSC) perfusion study using a T2*-weighted GRE-EPI sequence (TR: 1500 ms, TE: 32 ms, flip angle: 90°, 60 acquisition volumes, slice thickness: 3 mm), performed during the intravenous administration of a gadolinium-based paramagnetic contrast agent. The total dose of contrast agent was weight-adjusted and administered in two phases: an initial preparatory pre-bolus of

2 mL, followed by the injection of the remaining dose during image acquisition. Cerebral blood volume (CBV) maps were then generated using the Syngo.Via Neurology software (Siemens Healthineers).

Magnetic resonance imaging post-processing

Tumor lesion volumetry, both pre- and post-surgical, was performed using Fenix Software by calculating the product of the antero-posterior (AP), latero-lateral (LL), and cranio-caudal (CC) diameters of the tumor.

Statistical analysis

Statistical analysis was performed using R code implemented in BlueSky Statistics software (BlueSky Statistics LLC, Chicago, IL, USA).

At first, a descriptive analysis of the whole sample's demographic data was carried out, categorizing the data into continuous and categorical variables. Categorical variables were expressed as percentages, while continuous variables were reported as mean, median, and standard deviation.

Then, patients were divided into groups (patients with or without BTRE), and comparisons between groups were conducted using the chi-square test or Fisher's exact test for categorical variables, and the Student's t-test or Mann–Whitney U test for non-parametric data.

A further classification of BTRE patients was performed based on the presence of seizures before and/or after surgical intervention.

Subsequently, a survival analysis was carried out using the Kaplan–Meier method to relate overall survival (OS) in patients with and without BTRE. Survival curves were compared using the log-rank test and alternative methods.

In the second part of the study the smaller sample of high-grade diffuse gliomas (69 patients) was analyzed, adding the possible association between clinical/molecular and radiological characteristics and the occurrence of post-surgery seizures.

It should be noted that all immunohistochemical data concerning tumor lesions (mutations in IDH, ATRX, synaptophysin, GFAP, and MGMT), as well as the presence of pre- or postoperative seizures, tumor recurrence, and residual tumor were converted into categorical

variables. Seizure frequency and Ki-67 were treated as ordinal variables, while initial and residual tumor volume and age were treated as continuous variables.

Statistical significance was set at a p-value ≤ 0.05.

Results

We retrospectively analyzed 204 patients (median age 56.1 ± 13.5, 37.7% females) with a diffuse glioma diagnosis. As is reported in Figure 5, we had 150 patients with glioblastoma, 13 with astrocytoma grade 2, 11 with astrocytoma grade 3, 8 with astrocytoma grade 4, 15 with oligodendroglioma grade 2, 7 with oligodendroglioma grade 3.

BTRE vs no BTRE – whole sample

The confrontation between patients with or without BTRE is displayed, regarding histological diagnosis, localization (hemisphere and lobe) and histological biomarkers did not bring significant results apart from the positivity of p53 status, significantly associated with BTRE.

Survival analysis – whole sample

As it can be observed in **figure 3**, BTRE patients seem to survive longer than non-BTRE patients in a statistically significant manner (p-value 0.0067).

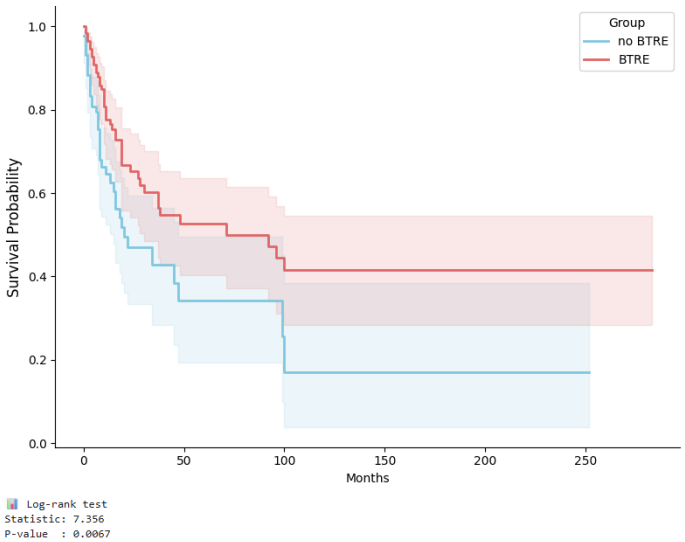

Figure 3. Survival analysis of patients with or without BTRE.

After stratification for BTRE only, patients with seizures before surgery were more likely to survive longer than the other group (p-value = 0.0370, **figure 4**).

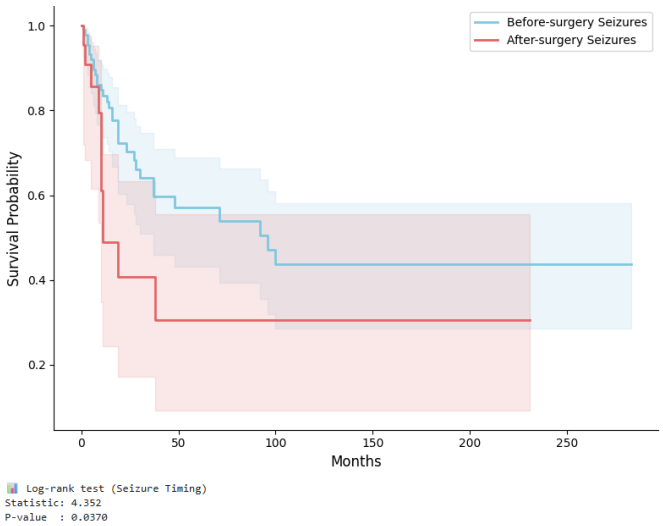

Figure 4. Survival analysis in BTRE patients divided based on seizures onset.

Finally, BTRE with pre-surgery seizures patients survived longer than the other ones (p-value = 0.0018).

Glioblastoma sample

In the second part of the study, only glioblastoma patients (69, median age 61.4 ± 11.2) have been evaluated (**Table 2**).

BTRE vs no BTRE – glioblastoma sample

Through a univariate analysis risk factors for BTRE have been explored (**Table 2**). The demographic and radiological factor that have shown a statistically significant association with BTRE are the male sex, the temporal lobe and the left hemisphere localization. Moreover, a smaller pre-surgery and post-surgery volume has been found more frequently in BTRE patients (**Table 2**).

Charachteristics	**BTRE no (N = 28)**	**BTRE yes (N = 41)**	**P value**
Male Sex	10 (39.3%)	28 (68.3%)	**0.017***
Median Age at Onset	60.9 ± 13.3	61.9 ± 9.6	0.729
Lobe Localization			**0.031***
- **Frontal**	10 (35.7%)	7 (17.1%)	
- **Temporal**	17 (24.6%)	13 (31.7%)	
- **Parietal**	12 (17.4%)	10 (24.4%)	
- **Multilobar**	21 (30.4%)	11 (26.8%)	

- **Multifocal**	2 (2.9%)	0 (0%)	
Left Hemisphere	12 (42.9%)	29 (70.7%)	**0.021***
GFAP (positive)	24 (85.2%)	34 (84.6%)	0.949
Synaptophysin (negative)	8 (28.6%)	9 (22%)	0.531
Ki67%			0.676
- > 40%	5 (18.5%)	7 (17.5%)	
- 20-40%	18 (66.7%)	24 (57.5)	
- 10-20%	4 (14.8%)	7 (17.5%)	
- 5-10%	0 (0%)	2 (5.0%)	
- < 1%	0 (0%)	1 (2.5%)	
ATRX (positive)	18 (66.7%)	27 (67.5%)	0.943
P53 (positive)	17 (60.7%)	24 (58.5%)	0.856
MGMT (methylated)	16 (57.1%)	22 (55%)	0.861
Tumor residue	22 (78.6%)	32 (78%)	0.959
Pre-surgery Volume	101.1 ± 53.1	57.4 ± 61.3	**0.003***
Post-surgery Volume	17.5 ± 20	8.5 ± 9.5	**0.031***
Residual volume %	0.2 ± 0.2	0.2 ± 0.2	0.577
Deceased patients	18 (63.4%)	32 (78%)	0.209
OS	12.4 ± 8.4	17.9 ± 0.4	0.214
Relapse	7 (25%)	19 (46.3%)	0.072
PFS	7.8 ± 6.2	11.4 ± 10.0	0.208

Table 2. Univariate analysis of BTRE and non-BTRE patients regarding clinical, demographic, biomarker data.

At onset seizures vs post-surgery seizures – glioblastoma sample

In the glioblastoma sample, 41 patients suffered from BTRE, with 32 patients who had pre-surgery seizures (typically the symptom that led to diagnosis), while 9 patients presented with post-surgery seizures. Crossing the data, we noticed that 10 patients had before-surgery surgery, but after the surgical treatment they were seizure free .

Then we searched for a correlation between seizure timing and demographic, clinical, radiological and histological variables. In this last analysis we had to remove 4 patients, because of incomplete data.

This univariate analysis shows a statistically significant association between post-surgery seizures and mutated ATRX. Moreover, a higher post-surgery volume and relative percentage were statistically associated with post-surgery seizures. Even though the p value resulted > 0.05, a negative synaptophysin and a higher ki67% value showed some association with post-surgery seizure.

A multivariate regression analysis has clarified the most significant items regarding the risk of post-surgery seizures: synaptophysin has gained statistical significance, while the role of ATRX and post-surgery volume/post-surgery residue as independent predictor of post-surgery seizures is confirmed.

Survival analysis – glioblastoma sample

In high grade glioma, BTRE patients showed a better overall survival (**Figure 5 left side**), especially patients with pre-surgery seizures (**Figure 5 right side**). However, considering only the group of BTRE patients we did not find any significant association between before or after seizures and overall survival

Figure 5. Overall Survival (OS) in BTRE and non-BTRE patients (left) and in BTRE patients with pre-surgery seizures and no BTRE patients (right).

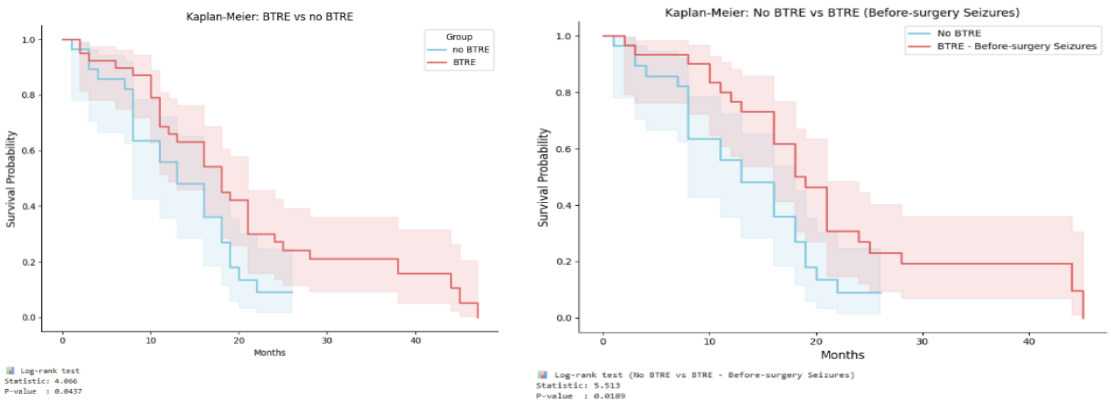

Discussion

The pathophysiology of brain tumor–related epilepsy (BTRE) remains incompletely understood. Multiple factors are thought to contribute, including tumor histology and location, blood–brain barrier disruption and peritumoral microenvironmental changes, as well as alterations in neurotransmitter systems and ionic homeostasis; however, definitive evidence is still lacking.

We analysed a cohort of 204 patients with diffuse gliomas. In line with previous reports,[111] glioblastoma was the most frequent histological subtype (150 patients, 73.5%), most commonly involving the frontal and temporal lobes or presenting with multilobar extension at diagnosis. Approximately 60% of patients experienced seizures during the disease course, consistent with published data,[112] and in most cases (81.9%) seizures represented the presenting symptom leading to tumor diagnosis.

BTRE substantially complicates clinical management, increasing emergency department visits, hospitalizations, and psychosocial burden. Accordingly, this study aimed to identify predictors of epilepsy in glioma patients and to clarify the relationship between BTRE and tumor characteristics, with the goal of supporting more individualized patient management.

In the overall cohort, no significant associations were observed between BTRE and demographic, clinical, or radiological variables, even after stratification by histology or seizure timing. This likely reflects sample heterogeneity and the predominance of glioblastoma. The only significant association identified was between p53 mutation and the presence of seizures. Although the role of p53 in tumor-related epileptogenesis is not fully defined, experimental and clinical evidence suggests that p53 dysregulation may promote neuronal hyperexcitability, possibly through enhanced glutamate release and synaptic network activation.[113, 114]

Survival analyses yielded notable results. Patients with BTRE showed longer overall survival than those without seizures. Within the BTRE group, patients experiencing seizures before surgery—typically as the initial manifestation—had longer survival than those who developed seizures only after surgery. Moreover, pre-surgical seizures were associated with longer survival compared with patients who never developed seizures, whereas post-surgical seizures did not confer a survival advantage. These findings suggest that BTRE, particularly when presenting early, may act as a “protective” factor, possibly by enabling earlier diagnosis and treatment. In addition, BTRE is more frequent in lower-grade gliomas, which are generally associated with a better prognosis. Our results are consistent with previous studies reporting improved survival in glioma patients with preoperative seizures.[112, 115]

Given the predominance of glioblastoma, a subgroup analysis was performed in these patients. As expected, glioblastoma patients were predominantly male, with frontal, temporal, or multilobar tumor localization, and most experienced seizures as the presenting symptom. Seizure frequency was generally low during follow-up, with 74.4% of patients remaining

seizure-free, likely reflecting the effectiveness of surgical treatment and antiseizure medications.

In the glioblastoma subgroup, BTRE was significantly associated with male sex, temporal lobe involvement, and left-hemisphere localization. The association with male sex may reflect epidemiological differences or sex-related neurobiological susceptibility to seizures, although the underlying mechanisms remain unclear.[116, 117] The link with temporal lobe tumors is well established, given the intrinsic epileptogenicity of temporal and adjacent cortical regions.[118, 119] The higher prevalence of left-sided tumors in patients with BTRE is less well documented but may be related to a greater mutational burden in left-hemisphere gliomas, including p53 mutation, PTEN loss, EGFR amplification, and MGMT promoter methylation.[120]

Multivariate analyses identified ATRX mutation as a predictor of BTRE and, specifically, as an independent predictor of post-surgical seizures. Although ATRX alterations have not previously been directly associated with BTRE, their frequent occurrence in lower-grade gliomas[121] suggests that ATRX-mutant glioblastomas may share biological features with more epileptogenic tumors. This observation raises the possibility of using ATRX status to identify patients who may benefit from closer postoperative monitoring or prolonged prophylactic antiseizure therapy.

Tumor volume also appeared to play a role, as patients with smaller pre- and post-surgical tumor volumes were more likely to present with BTRE. Although this finding contrasts with reports linking larger tumor volumes to seizures,[109] it may reflect earlier diagnosis in patients presenting with seizures, when tumors are smaller and more amenable to extensive resection. Consistently, residual tumor volume was associated with post-surgical seizures.

Survival analyses confirmed the protective association of BTRE in both the overall cohort and the glioblastoma subgroup, particularly in patients with seizures at onset. However, in glioblastoma alone, no significant survival difference was observed between pre- and post-surgical seizures, likely reflecting the aggressive biological behavior of the disease and heterogeneity in follow-up duration.

The main limitations of this study include its retrospective design, sample heterogeneity, variable follow-up length, and approximate estimation of tumor volume. Strengths include the relatively large sample size and the comprehensive integration of clinical, histological, and radiological data.

In conclusion, p53 mutation emerged as a predictor of BTRE in diffuse gliomas, while in glioblastoma, male sex, temporal lobe location, and left-hemisphere involvement were associated with epilepsy. ATRX mutation and residual tumor volume were linked to post-surgical seizures, suggesting potential markers for targeted monitoring and prophylactic treatment. Importantly, BTRE—especially when presenting early—appears to be associated with improved survival, supporting its role not only as a complication but also as a potential prognostic indicator. Further prospective studies are warranted to refine predictive models and integrate epileptological considerations into personalized glioma management.

The project underwent several stages of development and contributions from multiple collaborators, including Dr. Costa, who is currently finalizing the final draft, and Dr. Donniaquio. The preliminary results were presented by me as a poster at the International Epilepsy Congress held in Dublin in 2023. Although the study primarily focused on clinical and biological parameters, the inclusion of MRI-based segmentation represented a crucial component of the project, as it enabled a more accurate and unbiased characterization of the study groups and a more robust interpretation of the results.

Autoimmune associated epilepsy and encephalitis

Autoimmune encephalitis are rare and heterogeneous disorders that are relatively difficult to investigate at the group level and are therefore often described through case reports and small case series, with a few notable exceptions such as NMDAR encephalitis and LGI1 encephalitis. Cognitive impairment, sleep disturbances, and seizures are among the most frequent clinical manifestations of these conditions.

On the other hand, autoimmune-associated epilepsy (AAE), also referred to as autoimmune encephalitis–associated epilepsy (AEAE), and acute symptomatic seizures represent distinct but partially overlapping entities within the spectrum of immune-mediated neurological disorders. Acute symptomatic typically occur during the active inflammatory phase of encephalitis and may resolve with adequate immunotherapy and treatment of the underlying cause. In contrast, AAE is characterized by the persistence of unprovoked seizures beyond the acute phase, often reflecting ongoing immune-mediated mechanisms or residual network dysfunction despite apparent clinical stabilization.[122–124]

Differentiating between acute symptomatic seizures and AAE has important diagnostic, therapeutic, and prognostic implications, as the latter is frequently drug-resistant and may

require prolonged or escalated immunomodulatory treatment in addition to antiseizure medications.

Unfortunately, clinical cases are often not so clear-cut, as will be illustrated in the following subchapters. In particular, the decision to continue immunological treatment can be challenging, since, as discussed in the first chapter, clinical presentation may be complex and may overlap with differential diagnoses such as neurodegenerative diseases, which will be addressed in the second and third subchapters. Finally, an important yet particularly challenging issue concerns the monitoring of disease progression—still largely a "far west" in neuroimmunology. Nevertheless, as described in the fourth subchapter of this chapter, advanced brain metabolism post-processing approaches may provide valuable insights into disease activity and evolution.

Ma2 antibody-associated limbic encephalitis: The early etiology treatment may modify the disease clinical trajectory

Paraneoplastic encephalitis includes neurological conditions characterized by autoantibodies directed against neuronal proteins, likely triggered by underlying tumor antigens ([125]). We report two patients with paraneoplastic limbic encephalitis associated with "high-risk-for-cancer" antibodies against the Ma2 antigen and non-typical tumors. These cases allow reflection on the pathogenesis of autoimmune epilepsy, as well as on the importance of early diagnosis and etiological treatment.

The first patient was a 21-year-old man admitted to the Infectious Disease Unit because of confusion, visual hallucinations, and upper-limb myoclonus, following a four-month history of antipyretic-resistant fever, sore throat, and hyperphagia. Cerebrospinal fluid analysis was normal, whereas blood examinations showed pancytopenia. Brain MRI, [^{18}F]FDG-PET, and EEG (**Figure 6 A–D**) suggested central nervous system inflammation involving basal ganglia and mesial temporal lobes. Screening for infectious diseases was negative. Anti-Ma2 antibodies were detected in both serum and CSF using indirect immunofluorescence on primate cerebellum and dot-blot assays.

Treatment with intravenous methylprednisolone (1 g/day for 5 days) and intravenous immunoglobulins (0.4 g/kg/day for 5 days) did not result in clinical improvement. Total body CT, [^{18}F]FDG-PET, pelvic imaging, and testicular ultrasound excluded the presence of overt neoplasms. However, bone marrow analysis performed six months after symptom onset

revealed a clonal population of CD19/CD20^dim/CD21 B lymphocytes, consistent with a mature B-cell indolent lymphoproliferative disorder not requiring immediate treatment. Hospital-acquired sepsis prevented escalation to second-line immunosuppressive therapies and led to death seven months after symptom onset.

The second patient was a 30-year-old man who presented with asthenia, insomnia, mild fever, and daily short-lasting episodes of shivering, horripilation, heart palpitations, and unpleasant taste sensations. Subtle sleep-related involuntary movements were also reported, but no EEG was performed at that time. One month after symptom onset, a right testicular mass was detected and orchiectomy was performed, revealing a post-pubertal teratoma. Two months later, scheduled total-body CT showed enlargement of retroperitoneal lymph nodes, which were completely removed; pathology disclosed a post-pubertal teratoma with an embryonal carcinoma component.

Five months later, the patient experienced a focal-to-bilateral tonic-clonic seizure, prompting initiation of antiseizure medications. Brain MRI and [^{18}F]FDG-PET showed findings consistent with limbic encephalitis, and EEG demonstrated interictal epileptiform discharges in the left temporal lobe (**Figure 6 E–H**). Anti-Ma2 antibodies were detected in both serum and CSF, whereas anti-NMDAR antibodies were absent.

Treatment with intravenous immunoglobulins (0.4 g/kg/day for 5 days) and methylprednisolone (500 mg/day for 3 days), followed by oral prednisone (50 mg/day), led to a reduction in seizure frequency. Intravenous immunoglobulin cycles were repeated six times. Nine months after the first treatment cycle, brain MRI and [^{18}F]FDG-PET showed a reduction in temporal lobe T2 hyperintensities, with persistent mild right mesial temporal hypermetabolism. Due to ongoing focal aware seizures with autonomic symptoms and mild behavioral abnormalities, escalation to rituximab was required. At one-year follow-up, neurobehavioral status improved, with sporadic clusters of focal aware seizures responsive to short courses of oral prednisone. No tumor recurrence was detected in the contralateral testis or other sites.

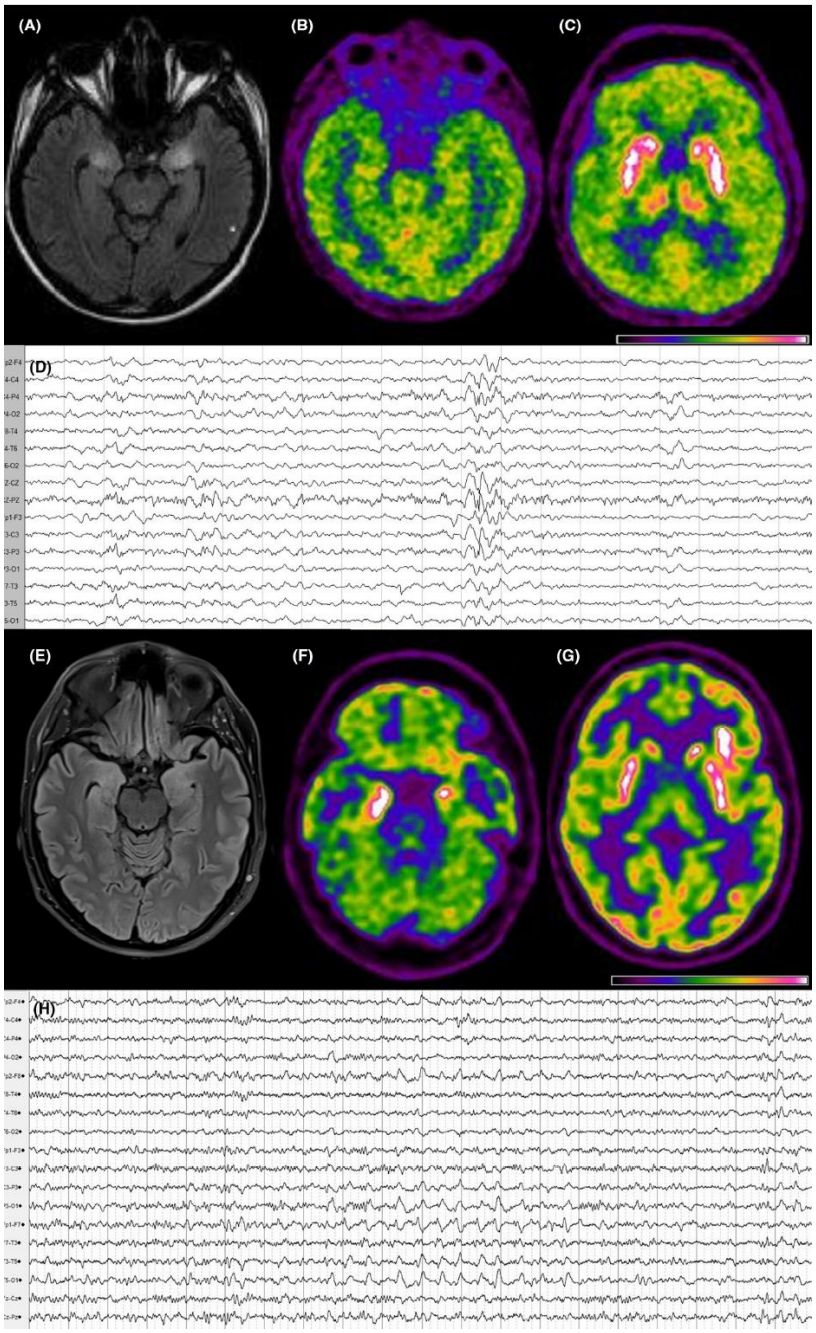

FIGURE 6 Brain MRI, FDG-PET, and EEG of patient 1 (A–D) and patient 2 (E–H). Only pictures of the most significant abnormalities of MRI, FDG-PET, and EEG are shown. As for patient 1, brain MRI revealed T2/FLAIR hyperintensity in mesial temporal lobe, amygdala, and basal ganglia (A). Brain FDG-PET showed a global hypometabolism along with a relative hypermetabolism of basal ganglia (C). EEG showed slowing of background activity, diffuse sequences of irregular theta-delta waves, and isolated sharp waves and spike-and- waves over central-parietal regions bilaterally (D). As for patient 2, brain MRI showed bilateral T2/FLAIR mesial temporal hyperintensities, more pronounced on the right side, along with enlargement of the amygdalae bilaterally (E). Brain FDG-PET disclosed hypermetabolism in bilateral mesial temporal regions, more evident in the right (F) and left frontal, insular and fronto-temporal regions (G). Inter-ictal EEG showed diffuse slowing of background activity in the left hemisphere, with the occurrence of theta-delta activity and sharp waves over the left temporal regions (H).

Discussion

The association of Ma2 antibodies with tumors other than testicular cancer is rare[126–132]. In the first patient, the lymphoproliferative disorder had an insidious presentation, resulting in a six-month diagnostic delay, and was further complicated by hospital-acquired sepsis, which hindered second-line immunosuppressive treatments. In contrast, in the second patient the tumor was treated within one month from symptom onset.

In agreement with existing literature, early immunological treatment combined with prompt tumor eradication likely contributed to a better prognosis.[125, 128] Nevertheless, the persistence of focal aware seizures in the second patient is consistent with recent data showing a high frequency of drug-refractory epilepsy in patients with Ma2 antibodies.[133]

The presence of mild but persistent clinical symptoms (particularly neurobehavioral alterations) and neuroimaging abnormalities, such as residual [^{18}F]FDG-PET hypermetabolism reflecting mesial temporal lobe inflammation, supports the hypothesis that autoimmune epilepsy associated with Ma2 antibodies may be driven by ongoing inflammatory processes rather than by fixed post-encephalitic damage.[122, 123, 133]

These observations support the use of continued immunotherapy to treat persistent seizures, even when a long time has elapsed since seizure onset. Further studies are needed to identify biomarkers of inflammation and to better understand the long-term consequences of sustained immune treatments in this clinical setting.

Such report further confirms that early etiological treatment and continuation of immunotherapy should be considered in patients with paraneoplastic encephalitis. This Clinical Vignette was published in Epileptic Disorders in 2024.[134]

Incident anti-LGI1 autoimmune encephalitis during dementia with Lewy bodies: when Occam's razor is a double-edged sword

Dementia with Lewy bodies (DLB) is the second most common neurodegenerative dementia and is characterized by the accumulation of aggregated α-synuclein in the brain. The disease typically follows a slowly progressive course and is distinguished by marked fluctuations in alertness and arousal, as well as a higher susceptibility to delirium.[54]. Accelerated

cognitive deterioration is uncommon and is associated with reduced survival compared with the usual seven-year disease course day, leading DLB to be included among causes of rapidly progressive dementia.[135] However, treatable conditions may superimpose on DLB and disrupt its typical evolution, resulting in marked clinical worsening that may be overlooked if Occam's razor is applied uncritically. We present a case of anti-leucine-rich glioma-inactivated 1 autoimmune encephalitis (LGI1-AE) superimposed on probable DLB[54]. The patient showed an abrupt clinical shift and EEG abnormalities not typical for DLB, prompting suspicion of a concurrent pathology and leading to targeted treatment with subsequent neurological improvement. We further contextualize this case by reviewing previous reports in which autoimmune encephalitis mimicked neurodegenerative disorders, with particular attention to DLB and overlap syndromes.

Here we presented a 74-year-old man who developed a slowly progressive cognitive impairment characterised by attentional-executive and memory dysfunction, resulting in reduced functional abilities (Clinical Dementia Rating, CDR = 1). Mild parkinsonism with resting tremor of the left upper limb was present, together with a history of REM sleep behavior disorder (RBD), visual hallucinations, fluctuations in alertness, hyposmia, and orthostatic hypotension. Clinical features and reduced dopamine transporter uptake on DaT-SPECT were consistent with probable DLB (McKeith et al., 2017). Additional supportive findings included bilateral parieto-occipital hypometabolism on [^{18}F]FDG-PET and posterior-predominant slowing of EEG background activity. Rivastigmine therapy improved cognition (MMSE from 19/30 to 24/30) and behavioural symptoms, including hallucinations.

Two months later, the patient developed sudden, brief paroxysmal myoclonus-like movements with psychomotor arrest lasting less than 10 seconds, accompanied by rapid cognitive and motor decline leading to complete dependence within weeks. EEG showed severe diffuse theta activity (4 Hz) with focal slowing in the right temporal region, raising suspicion of focal seizures with impaired awareness. Despite treatment with levetiracetam and add-on lacosamide, the patient experienced a generalized tonic-clonic seizure followed by frequent episodes of unilateral or bilateral arm flexion and facial contraction, consistent with faciobrachial dystonic seizures (FBDS). Repeated EEG demonstrated diffuse theta activity without epileptiform discharges, even during FBDS. Laboratory testing revealed mild hyponatremia (128 mEq/L). Brain MRI showed no significant T2/FLAIR or DWI abnormalities. A negative RT-QuIC nasal brushing excluded prion disease, and lumbar puncture was refused. (**figure 7**)

Neuronal surface antibodies were tested in serum using indirect immunofluorescence on transfected EU90 cells (McCracken et al., 2017; Muñoz-Sánchez et al., 2022). Anti-LGI1 antibodies were detected at a serum titer of 1:10, consistent with LGI1-AE (Graus et al., 2016; Van Steenhoven et al., 2023). Whole-body CT excluded malignancy. Treatment with intravenous methylprednisolone (500 mg/day for 5 days with tapering), followed by two cycles of intravenous immunoglobulins (IVIG, 2 g/kg), resulted in rapid resolution of FBDS and allowed reduction of antiseizure medication. Cognitive and motor function returned to baseline, with only occasional hallucinations requiring low-dose atypical antipsychotics.

An abnormal [^{123}I]MIBG cardiac scintigraphy performed three months after immunotherapy further supported the diagnosis of DLB. IVIG maintenance therapy was administered for six cycles every 45 days (Abboud et al., 2021). Over two years of follow-up, no relapses occurred, FBDS progressively diminished, and only mild emotional lability persisted. MMSE at last follow-up was 20/30.

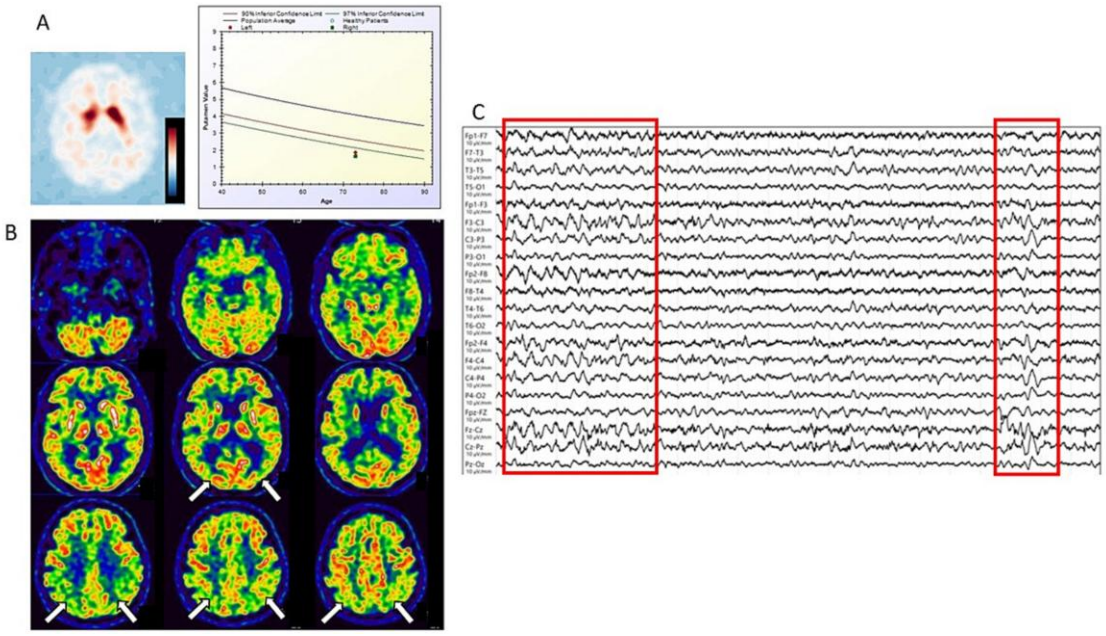

Fig. 7. A (left): Dopamine transporter single-photon emission computed tomography (DaT SPECT) showing bilaterally reduced dopamine transporter uptake in the putamen, more pronounced on the right side. **A (right):** Diagram representing the semi-quantitative analysis of striatal uptake (BasGan software); the left and right putamen are depicted by a red circle and a green square, respectively, and three confidence levels (90%, 95%, and 97%) derived from a reference population of healthy subjects are shown. **B:** [^{18}F]-fluorodeoxyglucose positron emission tomography ([^{18}F]FDG-PET) demonstrating bilateral parieto-occipital hypometabolism (arrows). **C:** EEG recorded four months after the onset of paroxysmal movements, showing diffuse theta activity without epileptiform discharges (highlighted by red boxes)

Discussion

This case illustrates the coexistence of probable DLB and anti-LGI1 autoimmune encephalitis. Neurodegenerative disorders are among the most frequent mimics of autoimmune encephalitis[109], yet in this patient both clinical features and biomarker evidence supported a true overlap.

Seizures occur in approximately 2.5% of DLB cases,[136] likely related to protein aggregation increasing cortical excitability[137]. However, the EEG abnormalities observed here—diffuse theta slowing with focal temporal slowing—deviated from the typical DLB EEG pattern of posterior dominant rhythm slowing with pseudo-periodic activity and were more consistent with autoimmune encephalitis.[138] The subsequent development of FBDS, a hallmark of anti-LGI1-AE[139], further supported this diagnosis.

Although some symptoms overlap between LGI1-AE and DLB, the presence of indicative DLB biomarkers (DaT-SPECT and [^{123}I]MIBG scintigraphy) strongly suggests comorbidity rather than misdiagnosis. Alterations in these biomarkers are rare in autoimmune encephalitis and usually reversible with immunotherapy.[140] In this case, persistent abnormalities after immunotherapy supported underlying DLB pathology.

The coexistence of DLB and LGI1-AE raises questions about shared mechanisms. Neurodegeneration may trigger immune responses[141], facilitated by age-related blood–brain barrier disruption. Similar interactions have been proposed in anti-IgLON5 disease, where immune-mediated inflammation and neurodegeneration coexist.[142]

Conclusions

This case highlights the importance of considering concomitant, treatable conditions in patients with DLB who develop seizures and rapid cognitive decline. Atypical EEG findings and the emergence of FBDS prompted further investigation and appropriate immunotherapy, resulting in clinical improvement. Rigid application of Occam's razor may delay recognition of overlapping pathologies and appropriate treatment.

The aforementioned manuscript, led by Dr. Cerne and Dr. Losa, was subsequently published in the *Journal of Neuroimmunology* in 2024.[143] However, as discussed in the following subchapter, cognitive disturbances are not a feature strictly related to LGI1. In the presence of cognitive disturbances, seizures, and a middle-aged male patient, CASPR2-associated encephalitis should therefore be considered.

CASPR2-related epilepsy: A distinctive and unrecognized form of epilepsy in adult and elderly males

In recent years, several neurological conditions have been associated with antineuronal autoantibodies, involving both the peripheral and central nervous systems. Seizures are a prominent feature of many autoantibody-related encephalopathies and may present with distinctive characteristics that raise specific diagnostic suspicion, such as facio/brachial dystonic seizures in LGI1-related encephalitis or new-onset refractory status epilepticus prompting investigation for NMDA receptor antibodies. Overall, diagnostic criteria for autoantibody-related seizure disorders include subacute onset, high seizure frequency despite anti-seizure medications, and association with other neurological disturbances, particularly cognitive impairment and behavioral abnormalities.[144, 145]

Contactin-associated protein-like 2 (CASPR2) is expressed in presynaptic axonal terminals throughout the nervous system. Antibodies directed against CASPR2 are associated with several clinical syndromes, including limbic encephalitis, peripheral nerve hyperexcitability, Morvan syndrome, and cerebellar ataxia (4,5). Although seizures are a relatively frequent and sometimes early manifestation of CASPR2-IgG-associated disease, their specific clinical phenotype has not been fully elucidated.[146, 147] (6,7).

Here, we describe nine adult and elderly male patients with focal epilepsy associated with CASPR2 autoantibodies, highlighting a distinctive and often unrecognized clinical entity.

Methods

Patients were identified at two epilepsy centers evaluating approximately 800 new epilepsy cases per year. All patients underwent comprehensive clinical assessment, including epileptological history, routine and sleep EEG, brain MRI, biochemical testing, screening for neuronal surface and intracellular autoantibodies, and neuropsychological evaluation. CSF analysis was performed in three patients, and long-term video-EEG monitoring in two. Follow-up ranged from 1 to 6 years.

CASPR2 autoantibodies were detected using commercially available or in-house live cell-based assays. CSF samples were analyzed undiluted, while serum samples were tested starting from dilutions of 1:10 or 1:20.

Results

The cohort included nine male patients aged 56–85 years with seizure onset between 52 and 79 years of age. Seizures were focal with impaired awareness, frequently preceded by epigastric aura, piloerection, olfactory hallucinations, nausea, or dizziness. Tonic–clonic seizures were observed in five patients. Seizure frequency ranged from multi-daily to sporadic.

Cognitive impairment was reported by eight patients, and behavioral or mood disturbances—including agitation, irritability, disinhibition, or depression—were observed in four. One patient reported cramps and fasciculations, suggesting peripheral nervous system involvement.

Interictal EEG revealed unilateral or bilateral temporal epileptiform abnormalities in five patients, while four had unremarkable EEGs. Long-term video-EEG monitoring documented seizures arising from the temporal lobes with bilateral asynchronous onset in two cases.

MRI demonstrated nonspecific white matter T2 hyperintensities suggestive of chronic vascular changes in four patients. In five cases, bilateral amygdalo-hippocampal T2-FLAIR hyperintensities were observed, with unilateral amygdala enlargement in three. FDG-PET, performed in one patient, showed bilateral frontal hypometabolism.

Neuropsychological testing revealed varying degrees of cognitive impairment—ranging from mild to severe deficits in memory, attention, executive function, and visuospatial abilities—in four patients, while two had normal results.

All patients had elevated CASPR2 autoantibody titers in serum, ranging from 1:100 to 1:6400, with higher titers associated with more severe cases. CSF antibodies were detected in three patients. Autoantibodies persisted at low titers in four cases during follow-up. CSF cytochemical examination was unremarkable.

All patients were initially treated with anti-seizure medications. Seizure control was achieved in only two cases, while seven were drug-resistant. These patients received immunotherapy, including high-dose steroids, plasmapheresis, intravenous immunoglobulins, or rituximab, resulting in seizure disappearance and improvement of cognitive function in all cases. No malignancies were detected.

Discussion

Seizures are a common feature of autoimmune encephalitis but may also represent the sole or predominant manifestation for prolonged periods, complicating early diagnosis and differential

classification. The patients described here were adult or elderly males with focal epilepsy, often misdiagnosed as having vascular-related epilepsy due to nonspecific MRI findings. A notable feature was the long delay—averaging six years—between seizure onset and recognition of an autoimmune aetiology.

Interictal EEG findings and the recording of seizures with bilateral asynchronous temporal onset on long-term monitoring strongly supported an autoimmune mechanism. MRI evidence of limbic involvement was present in only half of the cases, and CSF findings were often normal, reinforcing the concept of a chronic autoimmune epilepsy rather than acute symptomatic autoimmune seizures.

The clinical phenotype described here aligns with previous reports of CASPR2-IgG-associated seizures[148], sharing features such as late onset, male predominance, focal seizures with impaired awareness, cognitive impairment, and favourable response to immunotherapy. The absence of inflammatory CSF changes and prolonged disease course further support classification as autoimmune-associated epilepsy rather than classical autoimmune encephalitis.

While caution is warranted to avoid overdiagnosis of autoimmune epilepsy based solely on low-titer antibodies or insidious seizure onset[149], the persistence of CASPR2 autoantibodies in serum and CSF, exclusion of alternative diagnoses, and robust response to immunotherapy strongly support a causal role in these patients. Prior studies have demonstrated that autoimmune epilepsies may present with an insidious onset and chronic course, even in the absence of overt encephalitic features.[150]

CASPR2-IgG testing should be considered in adult and elderly males with recent or long-standing focal seizures with impaired awareness, particularly when associated with progressive memory impairment or behavioral disturbances. In these patients, anti-seizure medications may be ineffective, whereas immunotherapy can result in significant improvement in seizure control and cognitive function. MRI signs of limbic encephalitis may be present but are not mandatory, making early recognition crucial for optimal treatment and prognosis.

The series, led by Prof. Michelucci and Dr. Villani, was published in Epileptic Disorders in 2024.[151]

Longitudinal changes in [^{18}F]FDG PET brain metabolism as a prognostic marker in autoimmune encephalitis

Autoimmune encephalitis (AE) encompasses a group of immune-mediated inflammatory brain disorders characterized by heterogeneous neurological and psychiatric manifestations, including seizures, cognitive decline, movement disorders, and behavioral disturbances.[152–154] Early diagnosis is essential, as timely immunotherapy can lead to substantial recovery in many patients.[155]

The diagnostic criteria proposed by Graus et al. in 2016 emphasize the integration of clinical presentation with MRI, CSF, EEG, and autoantibody testing to ensure early and accurate diagnosis.[124] Despite progress in understanding AE pathophysiology and management, predicting long-term outcomes remains difficult, reflecting the complex interplay between inflammation, synaptic dysfunction, and recovery.

Currently, prognostic evaluation relies mainly on clinical scales. The Clinical Assessment Scale in Autoimmune Encephalitis (CASE) predicts functional outcome and guides escalation to second-line treatment across AE subtypes[156, 157], while the NEOS score is specific to anti-NMDAR encephalitis and incorporates clinical, MRI, and CSF parameters.[158, 159] However, both scales have limitations, as they primarily capture clinical severity and are not designed to reflect ongoing biological activity.

Other proposed prognostic biomarkers, including CSF cytokines and EEG patterns, have shown inconsistent associations with long-term outcome.[160–162] In contrast, [^{18}F]FDG PET has emerged as a powerful diagnostic tool in AE[163], particularly in early or atypical cases where MRI may be normal. Distinct metabolic patterns associated with specific autoantibody subtypes have been described[164–166], and PET abnormalities correlate with disease severity and treatment respons.[124, 167] However, few studies have evaluated the prognostic value of longitudinal PET changes, and evidence remains limited.[167]

This study aimed to assess longitudinal brain [^{18}F]FDG PET changes before and after treatment in a heterogeneous AE cohort, exploring their relationship with clinical recovery, relapse risk, and need for treatment escalation, regardless of antibody subtype.

Methods

Study population

Twenty-two patients fulfilling Graus criteria for definite autoimmune limbic encephalitis, definite anti-NMDAR encephalitis, or probable seronegative AE were retrospectively included between 2013 and 2023. All patients underwent [^{18}F]FDG PET at diagnosis (BS) and after immunotherapy (FU), with a mean interval of 11 months. Clinical follow-up averaged 4 years.

Clinical data included age, sex, antibody status, presenting symptoms, CASE and mRS scores at BS and FU, relapse occurrence, and treatments (first- and second-line).

Autoantibody detection

Neuronal surface and intracellular antibodies were tested in serum and/or CSF using indirect immunofluorescence and line-blot assays following manufacturer protocols.

[^{18}F]FDG PET acquisition and processing

PET acquisition followed EANM guidelines.[3] Images were normalized to MNI space, smoothed, and analyzed using SPM12. Voxel-based analyses compared AE patients with controls at baseline and assessed longitudinal BS–FU changes using paired t-tests, assuming metabolic normalization after treatment.

Statistical analysis

VOIs were defined from significant clusters ($p<0.05$, FWE-corrected, ≥100 voxels). VOI metabolic values were correlated with clinical outcomes using age-adjusted Spearman tests and regression models to assess prognostic value for disability, relapse, and treatment escalation.

Results

At baseline, AE patients showed relative hypermetabolism in limbic and subcortical regions and widespread cortical hypometabolism compared with controls, particularly in fronto-temporal and precuneus/posterior cingulate regions.

Longitudinal analysis identified a hypermetabolic VOI-A (caudate, thalamus, parahippocampal region, right amygdala, anterior cingulate cortex) and hypometabolic VOIs (VOI-B1 and VOI-B2) involving right temporal, fusiform, precuneus, and temporo-parietal regions. At follow-up, VOI metabolic values approximated those of controls, consistent with metabolic normalization after therapy.(**figure h**)

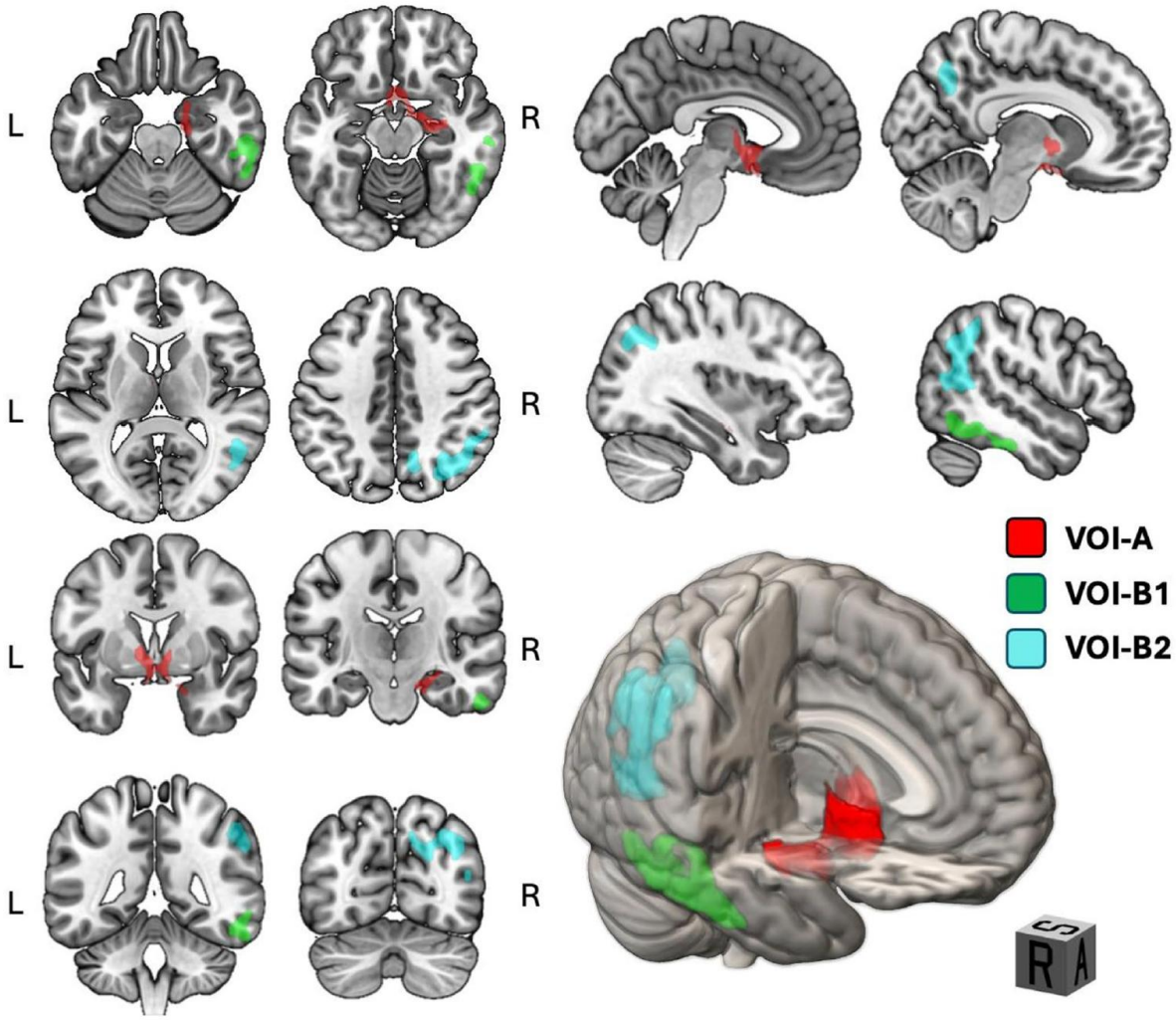

Fig. 8. Two-dimensional representations (axial, coronal, and sagittal slices) and three-dimensional rendering showing VOI-A in red, VOI-B1 in green, and VOI-B2 in light blue, superimposed on the MNI reference atlas (MRIcroGL software; https://www.nitrc.org/projects/mricrogl). In the three-dimensional rendering, midline sagittal and coronal cuts were used to improve visualization of the VOIs. **Abbreviations:** VOI, volume of interest; L, left; R, right; P, posterior; S, superior; A, anterior. Lower baseline metabolism in VOI-B1 correlated with higher CASE scores at follow-up and relapse occurrence. Persistent hypometabolism in VOI-B1 and VOI-B2 at FU was associated with greater long-term disability (mRS>2). Regression analyses confirmed VOI-B1 baseline metabolism as the strongest predictor of relapse and clinical severity, while younger age predicted escalation to second-line therapy.

In the BLM analysis of prediction using BS variables, the best model to predict relapse occurrence included two BS variables (VOI-B1 BS, and VOI-B2 BS), with VOI-B1 BS being the best predictor ($p = 0.032$, AIC = 27.6, BIC = 30.8, $R^2=0.275$). As for the need for escalation therapy, the best BLM model included two variables at BS (age, sex), with age being a significant predictor ($p = 0.020$, AIC = 22.9, BIC = 26.2, $R^2=0.45$).

Discussion

This longitudinal [^{18}F]FDG PET study demonstrates that AE is characterised by dynamic, region-specific metabolic alterations that evolve with treatment and parallel clinical recovery. Hypermetabolism predominated in limbic structures, likely reflecting inflammatory activity, whereas hypometabolism in temporo-parietal and default-mode network regions reflected synaptic dysfunction and network disconnection.[165, 166]

Importantly, baseline hypometabolism in right temporal and precuneus regions predicted relapse and persistent clinical impairment, highlighting hypometabolism as a key prognostic marker. These findings extend previous reports based on cross-sectional PET analyses[168] and support the concept of a shared metabolic trajectory across AE subtypes, including seronegative cases.

The involvement of temporo-parietal and default-mode network regions provides a mechanistic link between metabolic abnormalities and cognitive, behavioural, and psychiatric symptoms observed in AE.[169–175] Persistent metabolic abnormalities at follow-up suggest ongoing pathological processes, supporting the role of PET as a biological tracker of disease activity.

In conclusion, longitudinal [^{18}F]FDG PET reveals region-specific metabolic changes that correlate with recovery, relapse risk, and long-term disability in autoimmune encephalitis. Baseline temporo-parietal hypometabolism, in particular, identifies patients at higher risk of relapse and poorer outcome. These findings support the integration of longitudinal PET into AE management as an objective biomarker to guide prognosis and personalised treatment strategies.

The aforementioned project was published in the *European Journal of Nuclear Medicine and Molecular Imaging*, led by Dr. Cerne and Dr. Massa.[9] The intriguing relationship between brain metabolic differences emerging from this work inspired the final chapter and the *fil rouge* of this thesis, namely the concept of a metabolic fingerprint of autoimmune encephalitis in temporal lobe epilepsy due to amygdala enlargement (chapter 4, subchapter 3).

CHAPTER 5 TRANSLATING METHODOLOGIES

Neuroimaging post-processing, as outlined in the previous paragraphs, is highly versatile. Its strength lies in its disease-agnostic nature, as it is based on mathematical elaborations that can be either hypothesis-driven or data-driven. As described in the methodological section, post-processing approaches can be broadly classified into **single-subject analyses**, which support individualized assessment and clinical decision-making, and **group-level analyses**, which facilitate the identification of disease-related patterns and population-level biomarkers.

In the following two chapters, I present: (i) a project applying the same methodological framework, namely, the **Asymmetry Index**, to two different neuroimaging modalities, Arterial Spin Labeling MRI and [^{18}F]FDG-PET; and (ii) a project focusing on the application of multiple group-level analytical approaches, including Statistical Parametric Mapping (SPM) analysis, interregional correlation analysis, hypothesis-driven region-of-interest analyses, and brain atlas–based white matter connectomes.

Epilepsy- Head to head comparison between Arterial Spin Labelling MRI and [^{18}F]FDG-PET in presurgical evaluation of epilepsy in children: the role of voxel-based Asymmetry Index analysis

Epilepsy is one of the most prevalent neurological disorders[176]. Despite advancements in pharmacological treatments, approximately one-third of individuals with epilepsy continue to suffer from seizures despite optimal medical management. This subgroup of patients experiences substantial morbidity and a reduced quality of life[177, 178]. This is especially important for paediatric patients, who have a longer life expectancy, and an early and effective intervention is crucial, as prolonged seizure activity can lead to adverse neurodevelopmental outcomes[179]. For these patients, surgical intervention offers a potential remedy, particularly when the epileptogenic zone (EZ), the area of the brain responsible for seizure generation, can be precisely identified and resected.

To achieve accurate localisation, a multimodal approach often combines both non-invasive and invasive techniques. Among these modalities, [^{18}F]fluorodeoxyglucose PET ([^{18}F]FDG-PET) can measure metabolic activity in the brain.[180] However, even if it uses very low doses of

ionising radiation, [18F]FDG-PET is considered a minimally invasive procedure and, in paediatric pre-surgical programs, it often requires a further general anaesthesia. For such reasons, arterial spin labelling MRI (ASL) has emerged as a promising tool for the non-invasive assessment of cerebral perfusion.[181–184] Indeed, ASL uses magnetically labelled arterial blood water as an endogenous tracer to measure CBF. This method provides quantitative maps of CBF without the need for exogenous contrast agents or ionising radiation, making it especially appealing for use in children.[185]. In the context of epilepsy, altered perfusion patterns may correlate with the EZ, indicating abnormal neural activity.[186] Despite its potential, the application of ASL in identifying the EZ has been predominantly explored in adults with temporal lobe epilepsy[184, 187], and there have been only a few studies conducted in paediatric populations.[188, 189] Furthermore, there is variability in the approach employed to compare ASL and [^{18}F]FDG-PET[182, 190, 191], and of the way of applying off-station analysis, such as voxel-based asymmetry index analysis (AI)[192].

The purpose of this study was to compare the ability of ASL and [^{18}F]FDG-PET, both before (visual analysis) and after (asymmetry index analysis) AI, to identify the EZ in children undergoing presurgical evaluation for drug-resistant focal epilepsy. We hypothesised that AI enhances the detection of subtle asymmetries in imaging data, which can be particularly useful in identifying the EZ in cases where traditional visual inspection may fall short. By employing this comparative approach, we aimed to determine whether ASL and [^{18}F]FDG-PET have comparable abilities in localising the EZ and to identify the role of asymmetry index analysis.

Material and methods

All patients with unilateral focal epilepsy who underwent presurgical evaluation for epilepsy, including brain [18F]FDG-PET and MR perfusion study, were enrolled. Patients without motion artefact at the MR perfusion study were excluded. Demographic and clinical features were collected for every enrolled patient. Each patient underwent at least a video-EEG, 3T brain MRI, and [^{18}F]FDG-PET in accordance with good clinical practice for presurgical evaluation for epilepsy surgery.

The EZ was determined by the analysis of the anatomo-electro-clinical correlations performed by the multidisciplinary team meeting, and, when feasible, the presence of seizure freedom at post-surgical follow up.

Magnetic resonance imaging acquisition

MRI was performed according to the harmonized neuroimaging of epilepsy structural sequences—HARNESS-MRI protocol[193]. Also, all patients underwent an MRI perfusion study with background-suppressed three-dimensional dimension Pseudo-continuous Arterial Spin Labeling as described in a previous paper from our group[35] and detailed in current guidelines[194].

[^{18}F]fluorodeoxyglucose positron emitting tomography

Brain [^{18}F]FDG-PET was performed in accordance with the European Association of Nuclear Medicine guidelines[195]. Subjects fasted for at least six hours. Before the radiopharmaceutical injection, blood glucose was checked and was <7.8 mmol/L in all cases. After a 10-minute rest in a silent and obscured room with eyes open and ears unplugged, subjects were injected with approximately 200 MBq of [^{18}F]FDG via a venous cannula. They remained in the room for 30 minutes after the injection and then moved to the PET room, where scanning started approximately 45 minutes after the injection and lasted 15 minutes. A polycarbonate head holder was used to reduce head movements during the scan. Images were acquired by means of SIEMENS Biograph 16 PET/CT equipment with a total axial field of view of 15 cm and no interplane gap space. The attenuation correction was based on CT. Images were reconstructed through an ordered subset expectation maximization algorithm, 16 subsets, and 6 iterations, with a reconstructed voxel size of 1.33 × 1.33 × 2.00 mm.

Neuroimaging analysis and post-processing

Firstly, ASL and [^{18}F]FDG-PET, after co-registration in the 3D-T1 high-resolution space, were visually evaluated by an expert neuroradiologist and an expert nuclear medicine physician.

Visual analysis of ASL was performed after defining a standard method of windowing of CBF maps, setting the highest values of the visual windowing within the range of 80-90 ml/100g/min, and the lowest value at 0 ml/100g/min. For visual analysis of [^{18}F]FDG-PET, auto-windowing was a priori based on the striatum considered as a reference region with the greatest [^{18}F]FDG uptake in normal scans.

Hence, a region of interest for altered CBF and for altered brain metabolism were visually identified (ASL visual analysis (V-ASL) and [^{18}F]FDG-PET visual analysis (V-PET), respectively).

Subsequently, AI was calculated for ASL and [^{18}F]FDG-PET according to the method described by Boscolo Galazzo et al.[181] Briefly, ASL and [^{18}F]FDG-PET maps in the native

space were affine-registered to the individual 3D-T1 high-resolution anatomical images by using the FLIRT tool of FSL. Each T1-weighted image was then registered to the Montreal Neurological Institute (MNI) space with 1mm3 resolution using a non-linear method (FNIRT tool in FSL). Finally, transformation parameters were combined to spatially normalize the ASL and [^{18}F]FDG-PET maps in the MNI space. The registered maps were then smoothed with a 2x2x2 mm FWHM Gaussian kernel. Then, a voxel-wise asymmetry index calculation was performed using the following formula: AI = 100 × (Right − Left)/(Right + Left). An expert neuroradiologist and an expert nuclear medicine physician evaluated the obtained maps, coregistered to the individual 3D-T1 high-resolution anatomical images, to identify the clusters of major asymmetry between right and left hemispheres for both techniques (ASL voxel-based asymmetry index analysis, (AI-ASL) and [^{18}F]FDG-PET voxel-based asymmetry index analysis, (AI-PET)).

Regions of altered perfusion/metabolism (V-ASL/V-PET) and clusters of asymmetry (AI-ASL/AI-PET) were classified at a sublobar level, as previously described for other neuroimaging techniques[196]. Of notice, the observers were allowed to identify more than one region/cluster, as it is expected in the clinical practice, and were blind to the surgical outcome and the other neuroimaging technique, but not to the EEG and the structural MRI data.

For each patient, a degree of concordance of V-ASL/V-PET and the AI-ASL/AI-PET with the EZ, was determined. The degree of concordance with the EZ was defined at sublobar level and as follows:

i) no concordance (no overlap between regions/clusters and the EZ),

ii) partial concordance (the EZ is included between the regions/clusters identified, but either one region/cluster is not part of the EZ, or part of the EZ is not included in the regions/clusters identified),

iii) complete concordance (complete overlap between regions/clusters and the EZ, at sublobar level)

Neuroimaging analysis and comparisons are schematically represented in **Figure 9**.

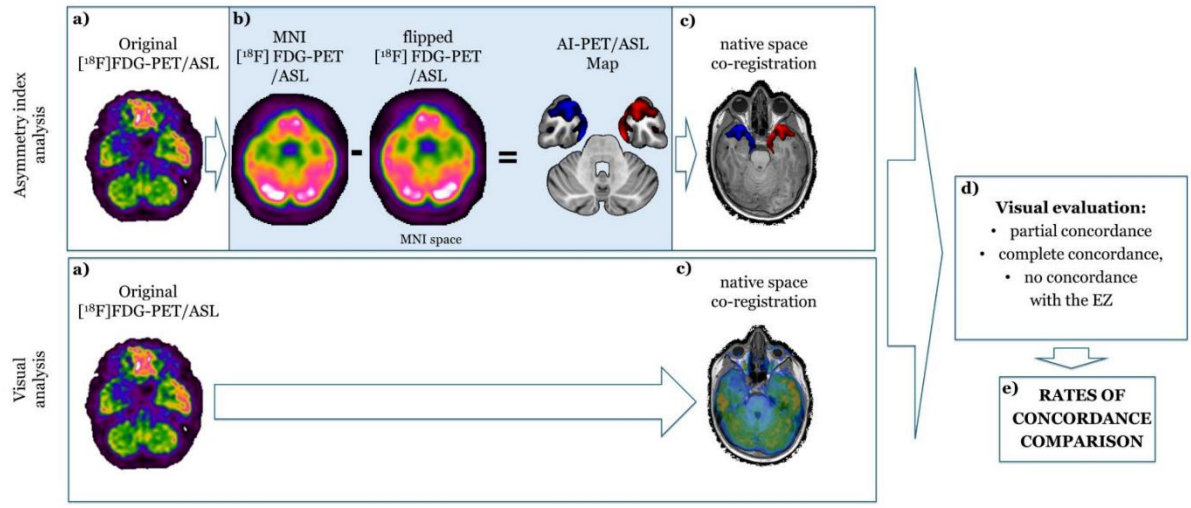

Figure 9. Workflow of analysis. The workflow of the performed analysis is briefly documented. In the top row, the asymmetry index analysis is reported: after acquisition of the raw [^{18}F]FDG-PET/ASL-MRI image (**a**), asymmetry index analysis is performed to obtain an AI-PET/AI-ASL map (**b**), that is visually evaluated after co-registration in the 3D-T1 native space (**c**). In the bottom row, the visual analysis (V-PET/V-ASL) is reported: the original data is directly co-registered in the 3D-T1 native space (**c**). Finally, resulted images are visually evaluated to attribute a rate of concordance (partial, complete, no concordance) with the EZ (**d**) to be compared between each other (**e**).

Statistical analysis

As a first descriptive analysis, clinical, instrumental data and the outcomes of enrolled patients were explored. Then, the performances of V-ASL, AI-ASL, V-PET and AI-PET were compared.

The proportions of concordance of the neuroimaging technique were compared before and after dichotomization of the degree of concordance into two classes: “concordance” and “no concordance” by merging the “partial” and “complete” concordance classes. We considered such dichotomization important from the clinical perspective in the setting of a multimodal neuroimaging approach to presurgical evaluation for epilepsy.

Since neuroimaging technique and post-processing were dependent, categorical variables, Mc Nemar-Bowker test for marginal homogeneity or Mc Nemar test with continuity correction (dichotomous variables) was used to compare the proportion of concordance with the EZ.

The same analysis was repeated in the subgroup of patients in which the EZ defined by anatomo-electroclinical correlation was removed and the patients resulted to be seizure free after a follow up of at least 12 months (true EZ).

The statistical analysis was performed in "r" implemented in BlueSky statistics, p-values below 0.05 were considered statistically significant.

Results

Twenty-eight patients (15 females, 10.07±4.6 years) that underwent presurgical evaluation for epilepsy were enrolled. Twenty-two patients underwent epilepsy surgery, of these 17 had the EZ completely removed, and 14 were seizure free at follow up. Of notice, in one patient the EZ was not completely removed, but the outcome resulted in seizure freedom at follow up. Therefore, 13 out of 17 patients (76.47%) in which the EZ was considered as completely removed were free from seizures at follow up.

Clinical, instrumental and outcome data of the whole group and the subgroup of patients that underwent epilepsy surgery are reported in **Table 3** and **Table 4**, respectively.

Table 3: Patients demographic, clinical and instrumental features. Data are reported as average and standard deviation (in brackets) for continuous variables or absolute number and percentage (in brackets) for categorical variables.

	Overall (N=28)
Age (at ASL, years)	10.07 (4.64)
Sex (females)	15 (53.6%)
Age of seizures' onset	5.39 (4.771)
Epilepsy surgery (performed)	22 (78.6%)
Months between ASL and [^{18}F]FDG-PET	7.68 (10.85)
Extra temporal lobe EZ (presence)	18 (64.29%)
Sedation during ASL (presence)	13 (46.4%)
Sedation during [^{18}F]FDG-PET (presence)	13 (46.4%)
Seizures 48 hours before ASL (presence)	8 (28.6%)
Seizures 48 hours before [^{18}F]FDG-PET (presence)	9 (32.1%)

Legend: ASL: arterial spin labelling MRI; EZ; epileptogenic zone; [^{18}F]FDG-PET: [^{18}F]fluoro-deoxiglucose PET

Table 4: Demographic, clinical and instrumental features of patients who underwent epilepsy surgery. Data are reported as average and standard deviation (in brackets) for continuous variables or absolute number and percentage (in brackets) for categorical variables.

	Overall (N=22)
Age (at ASL, years)	9.87 (4.76)
Sex (females)	12 (54.5%)
Age of seizures' onset	5.000 (4.46)
Follow up time (months)	29.14 (14.23)
Engel	
- Ia	14 (63.6%)

- IIa	2 (9.1%)
- IIb	2 (9.1%)
- IIIa	4 (18.2%)
- IV	0 (0%)
Seizure freedom (presence)	14 (63.6%)
Focal cortical dysplasia (presence)	14 (66.7%)
Gross EZ resection (presence)	16 (72.7%)
Months between ASL and [^{18}F]FDG-PET	7.00 (11.37)
Sedation during ASL (presence)	11 (50.0%)
Seizures 48 hours before ASL (presence)	6 (27.3%)
Sedation during [^{18}F]FDG-PET (presence)	11 (50.0%)
Seizures 48 hours before [^{18}F]FDG-PET (presence)	7 (31.8%)

Legend: ASL: arterial spin labelling MRI; EZ; epileptogenic zone; [^{18}F]FDG-PET: [^{18}F]fluorodeoxiglucose PET

When comparing proportion of concordance of each neuroimaging techniques with the EZ, no significant differences were found between AI-ASL, V-PET and AI-PET, whereas V-ASL showed a significant lower rate of concordance, when compared with AI-ASL, V-PET, and AI-PET (**Table 5**). An explanatory example of one case is documented in **figure 10**

Table 5. Rates of agreement with the epileptic zone (anatomo-electroclinical-correlation) through neuroimaging techniques before and after voxel-based asymmetry index post-processing. Significant results are reported in **bold** (p values).

	Neuroimaging concordance proportion				*Comparisons*					
	V-ASL	*AI-ASL*	*V-PET*	*AI-PET*	V-ASL vs AI-ASL	V-ASL vs AI-PET	V-ASL vs V-PET	AI-ASL vs V-PET	AI-ASL vs AI-PET	V-PET vs AI-PET
Agreement*					**0.005**	**0.012**	**0.005**	0.842	0.584	0.485
No concordance	16 (57.14%)	2 (7.14%)	3 (10.71%)	4 (14.29%)						
Partial concordance	5 (17.86%)	9 (32.14%)	11 (39.29%)	11(39.29%)						
Complete concordance	7 (25.00%)	17 (60.71%)	14 (50.00%)	13 (46.43%)						
Dichotomized#					**0.001**	**0.006**	**0.001**	0.9	0.683	0.9
No concordance	16 (57.14%)	2 (7.14%)	3 (10.71%)	4 (14.29%)						
Concordance	12 (42.86%)	26 (92.86%)	25 (89.29%)	24 (85.71%)						

Legend: AI-ASL: arterial spin labelling MRI voxel-based asymmetry index analysis; AI-PET: [^{18}F]fluorodeoxyglucose PET voxel-based asymmetry index analysis; V-ASL: arterial spin labelling MRI visual analysis; V-PET: [^{18}F]fluoro-deoxiglucose-PET visual analysis.
* Mc Nemar-Bowker for marginal homogenety
# Mc Nemar test with continuity correction

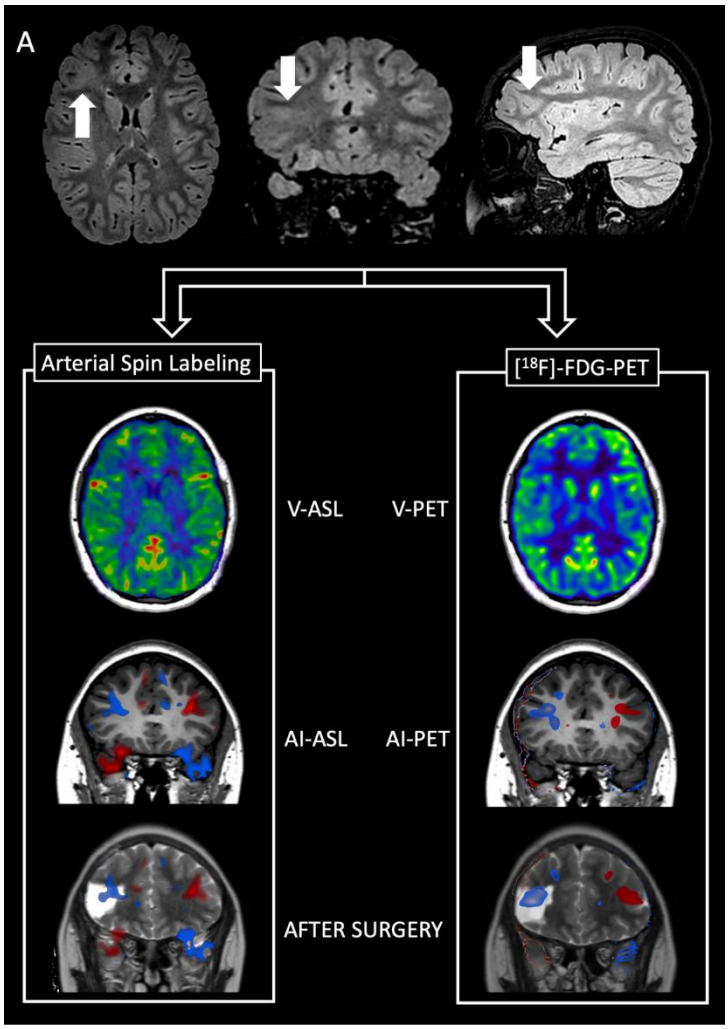

Supplementary Figure 10. MR images of Engel class I patient with focal right frontal epilepsy undergoing surgery. 3D-FLAIR images (A) show right frontal focal cortical dysplasia (white arrows). Qualitative analysis of the ASL-CBF map (V-ASL) revealed faint changes of CBF and [^{18}F]FDG-PET map (V-PET) identified a slight reduction of CBF and SUV in the right frontal region. Quantitative voxel-based analysis of the Asymmetry Index of both ASL (AI-ASL) and PET (AI-PET) confirmed a region of asymmetry in the frontal lobes with reduced perfusion/metabolism in the right side. Coronal T2-weighted image acquired after surgery shows a resected area in the right frontal lobe. AI-ASL and AI-PET maps overlaid on post-surgery T2-weighted image show correspondence of the cluster of significant results with the area of resected lesion.

Finally, when considering the subgroup of 13 patients in which the EZ was considered as completely removed and that were seizure free at follow up, the V-ASL was confirmed to have a lower rate of agreement with the "true" EZ as compared with AI-ASL, V-PET and AI-PET, without reaching statistical significance, likely because of the smaller sample size.

Discussion

In this study we compared the rate of concordance of [^{18}F]FDG-PET and ASL before and after the application of asymmetry index analysis with the epileptogenic zone in a cohort of paediatric patients affected by focal epilepsy who underwent presurgical evaluation at a tertiary epilepsy centre. We found that after voxel based asymmetry index analysis, ASL achieved a performance in determining the EZ comparable to that of [^{18}F]FDG-PET.

An increased or a decreased function of a brain region is usually coupled with a higher or lower brain perfusion and metabolism[186]. Indeed, the function of a brain region directly depends

on glucose metabolism and therefore on its perfusion.[181] Hence, it is expected from neuroimaging techniques that evaluate brain perfusion, such as ASL, or brain metabolism, such as [^{18}F]FDG-PET, to return similar results. In the field of focal epilepsy, literature about the performance of ASL is growing, but data on extratemporal epilepsy, paediatric patients and the effect of post-processing are still lacking.[35, 192, 197, 198] In particular Khalaf and colleagues found that ASL and [^{18}F]FDG-PET had substantial agreement in a cohort of adult patients and that the combination of ASL with [^{18}F]FDG-PET may increase sensibility and specificity so to detect the epileptogenic zone in temporal lobe epilepsy[188]. Shang et al on the other hand found that ASL and [^{18}F]FDG-PET after asymmetry index analysis did not differed significantly in their performances in detecting the EZ in a group of adult patients with temporal and extratemporal epilepsy.[199] Moreover, there is increasing evidence that the integration of ASL within the presurgical evaluation for epilepsy in the multimodal scene may increase the diagnostic accuracy.[200] Finally, ASL performs well even in children with poorly defined focal epilepsy, showing a concordance with [^{18}F]FDG-PET in 75% of cases.[189] In their project, Lam and colleagues evaluated the ASL visually and after post-processing, by applying a more strict, yet elegant, classification of the asymmetry index, based on z-scores and cluster cutoff percentage (of 1.5 and 5%, respectively).[189] In this study, we confirmed these findings in an independent cohort of paediatric patients, employing a more subjective approach. While we acknowledge that the absence of a strict classification by z-scores and cluster size introduces potential biases due to the final subjective decision, our aim was to allow for some level of interpretation by the observer, thereby better reflecting clinical practice.

Nonetheless, several post-processing techniques were applied to ASL.[183, 190] Among these, voxel based asymmetry index analysis showed promising results.[35, 181, 191, 197, 201] In our study we found a significant effect of AI on ASL, in agreement with the literature.[181, 183] Interestingly, however, the application of AI did not have significant effects on [^{18}F]FDG-PET. This is an unexpected finding, since it has been previously described how AI increases the diagnostic accuracy of visual analysis of [^{18}F]FDG-PET.[202, 203] The literature on the topic, however, is still lacking and needs further research.[36] A possible explanation may reside in the classification method that we used, that is the agreement with the EZ either in a dichotomic or semi quantitative classification. Moreover, to mimic the clinical practice, we provided to the raters the EEG and morphological MRI data of the patients, that probably increased their ability to visually interpret the neuroimaging. Therefore, it is possible that the very good performance of V-PET is related to a roof effect that hid the benefits of voxel-based

asymmetry index. Even if this may be considered as an interpretative bias, the same effect was not detectable in V-ASL that had performances significantly lower, underlying the importance of post-processing in this specific neuroimaging technique.

The EZ has been commonly defined as the region of the brain whose removal leads to a complete seizure freedom and, even with stereo-EEG is difficult to determine without an adequate post-surgical follow up.[204] For this reason, to increase the statistical significance of the study, we decided to evaluate the performances of V-ASL, AI-ASL, V-PET, AI-FDG also in the subgroup of patients undergoing epilepsy surgery, with the EZ being removed, and with a follow up time longer than 12 months. The results of such analysis were similar to the whole group analysis but without reaching a statistical significance, likely because of the smaller sample size. Nevertheless, V-ASL was confirmed to have a tendency to a lower agreement with the EZ as compared to V-PET, AI-PET and particularly, AI-ASL.

This study has some limitations, that need some discussion. Firstly, patients' heterogeneity, having one third of them an aetiology different than focal cortical dysplasia, while 63.6% achieved seizure freedom, however, such heterogeneity reflect the design of the study, that is observational and retrospective. Moreover, the most homogenous subgroup of 13 patients with a complete removal of the EZ obtained similar, albeit not significant, results, advocating the need for further, larger studies. Secondly, the sample size is relatively small, yet, to our knowledge, very few studies compared the concordance of ASL and [^{18}F]-FDG-PET in the paediatric population, being the study of Lam and colleagues[189], the largest. Present study is not the first study comparing ASL-MRI with other neuroimaging techniques, indeed, in a very similar fashion, Lam and colleagues evaluated the power of ASL-MRI to identify the EZ and compared such results with other neuroimaging techniques, including [^{18}F]-FDG-PET. The results of our study confirm that ASL allows to help in the identification of the EZ. However, it stresses how necessary is the use of AI to obtain such results. Moreover, MRI and [^{18}F]-FDG-PET were not acquired simultaneously, and in four cases more than one year apart. This is a possible bias in the interpretation of the results since the functional networks in paediatric patients can change relatively quickly and being drug-resistant patients, the different antiseizure medications may have influenced the results. However, such bias does not impact the comparison of the techniques before and after asymmetry analysis. Finally, sedation was necessary in a half of the patient. The effect of sedation is a well-known modifier of brain metabolism[205], hence it may have affected the results of brain [^{18}F]-FDG-PET (and probably

of ASL-MRI), however, the very same patients underwent sedation in both techniques and the effect of the sedation did not affect the comparison of the same technique before and after AI.

Conclusion

Asymmetry index analysis increased the ability of ASL to identify the EZ, achieving performance levels comparable to those of [^{18}F]FDG-PET. In our view, ASL-MRI cannot yet replace [^{18}F]FDG-PET, as its interpretation relies heavily on the use of "off-station" analyses, such as AI. Nonetheless, if the findings of this and previous studies are validated through larger multicentre projects, ASL could potentially emerge as a non-invasive alternative to [^{18}F]FDG-PET in the future. This would offer several advantages for children, including eliminating exposure to ionizing radiation and reducing the number of diagnostic tests required during presurgical evaluations.

The aforementioned project, in which I had a leading role, is currently under revision at **Neurological Sciences** and represents a clear example of the usefulness of the asymmetry index. This approach allows single-subject analyses without the need for a healthy control group, a feature that is particularly valuable when studying fragile populations, such as paediatric patients.

Epilepsy networks in temporal lobe epilepsy: a multimodal approach to deep phenotype the clinical trajectory of enlarged amygdala

"Enlarged amygdala" (EA) is a recently described neuroimaging finding that can be associated with several conditions, often epilepsy, but its clinical meaning is not fully understood yet.[37] EA's underlying physiopathology is heterogeneous, including both autoimmune[38] or dysplastic processes, with different pathological findings or even with non-lesional cases[39] if advanced post-processing is performed[40]. Literature data also suggest that it might be a consequence of seizures[41]. Hence, biomarkers able to predict the clinical trajectory of EA patients are needed[42]. Recently, a further step was made to better phenotype this condition, finding a specific seizure onset pattern and, possibly, a different outcome compared to other TLE forms.[43] However, the presence of an EA is often associated with alterations of extratemporal regions, resulting in temporal plus epilepsy, often involving stress-mediated limbic network[44] and emotion recognition.[40] Even if some network-based project is being carried on, multimodal approach to the condition, taking into account such networks, are still lacking and may help in the diagnosis and prediction of the clinical trajectory of the several aetiologies of EA.

The clinical assessment of patients with temporal lobe epilepsy, in particular if an EA is present, already requires complete investigations such as electroencephalography (EEG), high density EEG, MRI, [^{18}F]-FDG-PET, and neuropsychological evaluation. Such investigations are used in the clinical practice to build the "multimodal scene" that allows to integrate the clinical hypothesis with the results of several diagnostic techniques with the aim of obtaining a more precise diagnosis and eventually decide a treatment. Our hypothesis is that an enlargement of the amygdala in temporal lobe epilepsy may be associated to specific electroencephalographic, metabolic, neuropsychological and clinical features, depending on the EA's aetiology. Advanced multimodal analysis of structural and functional neuroimaging data may unveil such features and the involved networks helping to determine the prognosis of the patient. Such findings will be of great help in the clinical management of patients with temporal lobe epilepsy and enlarged amygdala.

This project, led to a poster presentation at the international league against epilepsy conference in 2025 entitled: "**Metabolic heterogeneity of mesial Temporal Lobe Epilepsy and functional correlates. Preliminary data**." In detai, we investigated cerebral glucose

metabolism with [^{18}F]FDG-PET in patients with mesial temporal lobe epilepsy (mTLE) as compared with patients with limbic encephalitis and neurologically normal controls. Between 2019 and 2024, 15 patients (37±11 years; 8 females; 7 with hippocampal sclerosis, 4 with enlarged amygdala, 4 cryptogenic) and 14 healthy controls (35±10 years; 8 females) were enrolled. Diagnosis was based on anatomo-electro-clinical correlation and, when available, surgical outcome. 2016 Graus criteria were used for diagnosis of patients with limbic encephalitis. PET scans were side-flipped to align the affected hemisphere and compared with controls using SPM12, yielding a region of interest (mTLE-ROI) encompassing the left hippocampus, fusiform gyrus, and basal/polar temporal lobe ($p<0.001$). Normalized uptake within the ROI was reduced in patients with hippocampal sclerosis and enlarged amygdala ($p<0.01$), but not in cryptogenic cases ($p=0.09$). Interregional correlation analysis and atlas-based tractography showed that, in controls, ROI metabolism was functionally and anatomically connected with homologous ipsilateral and contralateral regions. In contrast, patients displayed stronger ipsilateral correlations ($p<0.001$) with loss of contralateral connectivity. These findings highlight the metabolic heterogeneity of mTLE according to aetiology and reveal disrupted interhemispheric functional connectivity (**figure 11**).

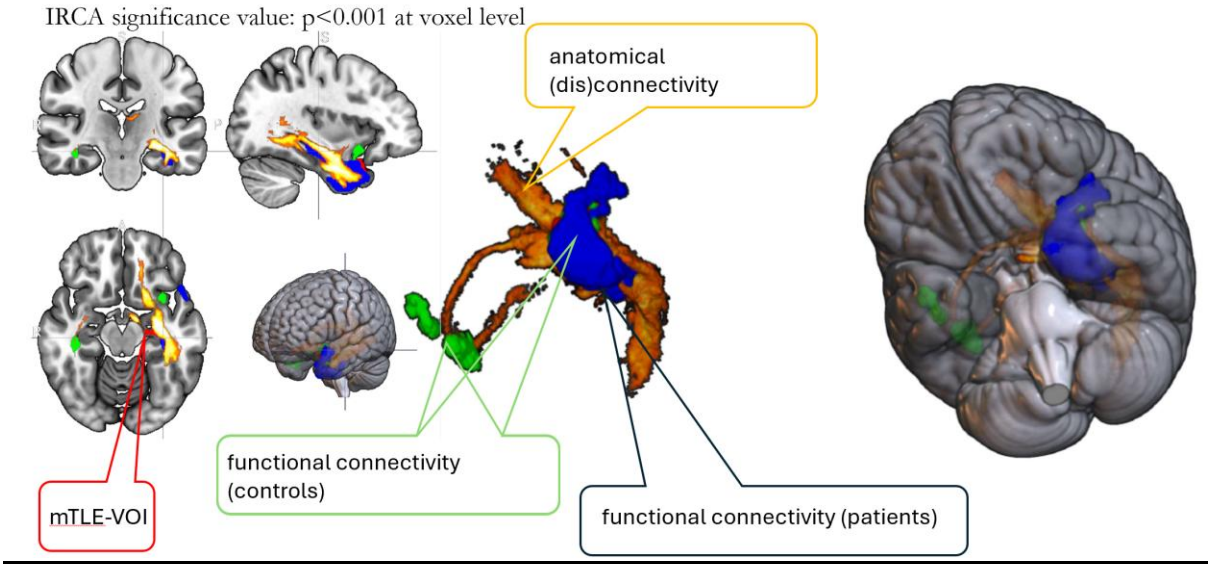

Figure 11: the volume of interest related to mesial temporal lobe epilepsy (mTLE-VOI) is represented along with the clusters of functional connectivity in controls (green) and patients (blue). The clusters are connected by white matter tracks, as expected.

Subsequently, we evaluated 14 patients with limbic encephalitis, 13 of which with an FDG-PET follow up and we enrolled a total of 18 patients with amygdala enlargement. Firstly, we compared baseline FDG-PET with controls, finding a region of interest involving both

temporal mesial regions where a relative hypermetabolism was disclosed, and had its maxima in the amygdala (**figure 12**)

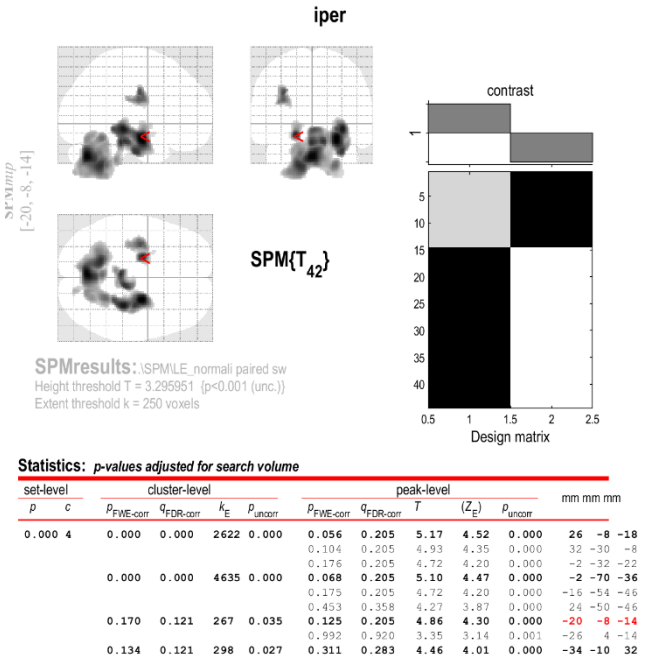

set-level		cluster-level				peak-level					mm mm mm		
p	c	$p_{FWE-corr}$	$q_{FDR-corr}$	k_E	p_{uncorr}	$p_{FWE-corr}$	$q_{FDR-corr}$	T	(Z_E)	p_{uncorr}			
0.000	4	0.000	0.000	2622	0.000	0.056	0.205	5.17	4.52	0.000	26	-8	-18
						0.104	0.205	4.93	4.35	0.000	32	-30	-8
						0.176	0.205	4.72	4.20	0.000	-2	-32	-22
		0.000	0.000	4635	0.000	0.068	0.205	5.10	4.47	0.000	-2	-70	-36
						0.175	0.205	4.72	4.20	0.000	-16	-54	-46
						0.453	0.358	4.27	3.87	0.000	24	-50	-46
		0.170	0.121	267	0.035	0.125	0.205	4.86	4.30	0.000	-20	-8	-14
						0.992	0.920	3.35	3.14	0.001	-26	4	-14
		0.134	0.121	298	0.027	0.311	0.283	4.46	4.01	0.000	-34	-10	32

Figure 12. single parameter limbic encephalitis related pattern. By comparing controls and patients affected by limbic encephalitis via two-sample t-tes, three clusters of relative hypermetabolism are disclosed: right and left mesial temporal lobes (including amygdala and hippocampus) and cerebellum. P value at voxel level<0.001, at P-FEW corrected at cluster level <0.05).

Hence we defined a temporal region of interest and we compared the regional uptake between all the groups to disclose significant differences (right mTLE is disclosed (all patients were flipped to obtain the pathological side on the right(**figure 13**)).

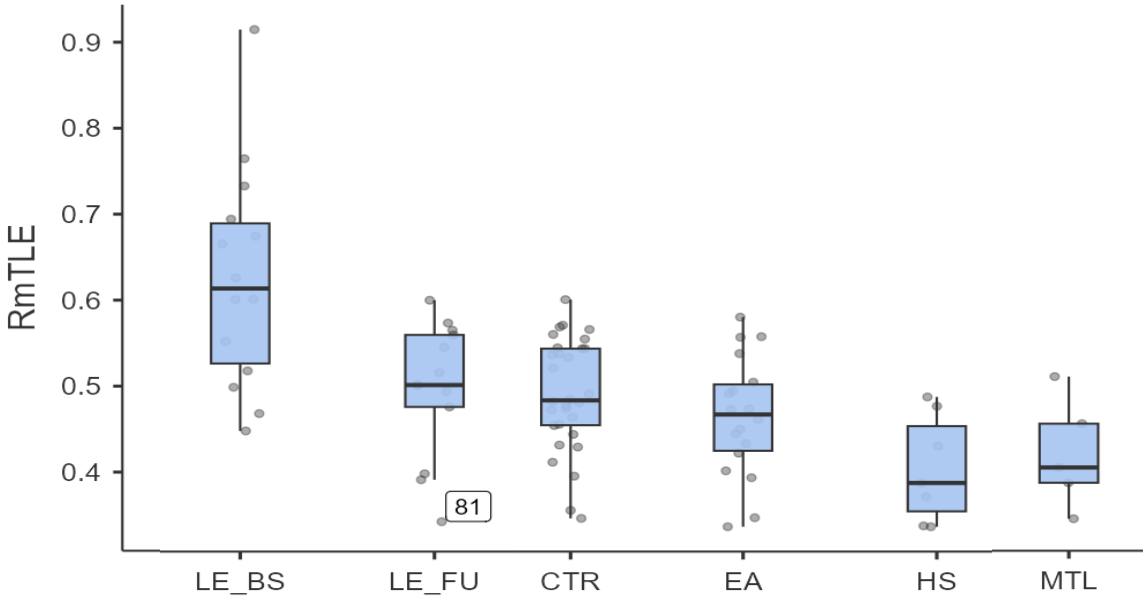

Figure 7. FDG uptake trough groups is represented. On the y axis, RmTLE-ROI (defined a priori and including amygdala, hippocampus and parahippocampus of right hemisphere) uptake, normalized to whole brain, is reported. On x axis, groups are represented including patients with limbic encephalitis at baseline (LE_BS) and follow up (LE_FU), controls,

patients with amygdala enlargement (EA), hippocampal sclerosis (HS) and mesial temporal lobe epilepsy of unknown aetiology (MTL).

Encouraged by such results, we decided to go further in the analysis and included more patients with EA and LE, excluding patients with HS and unknown aetiology mTLE and proceeded with the following analysis:

Regional metabolism

Regional metabolic activity was assessed using standardized uptake value ratios (SUVR). Specific regions were calculated from the AAL brain atlas and metabolic uptake was calculated and normalized to whole brain. A right mesial temporal macroregion was defined *a priori* by averaging SUVR values from the right hippocampus, parahippocampal gyrus, and amygdala, in order to derive a robust composite marker of mesial temporal metabolism and reduce regional variability.

Analyses were restricted to groups with adequate sample size to ensure statistical robustness, including controls (CTR), limbic encephalitis at baseline (LE_BS), limbic encephalitis (LE), limbic encephalitis at follow-up (LE_FU), and Enlarged amygdala patients (EA). Groups with fewer subjects (hippocampal sclerosis [HS] and mTLE) were excluded from inferential analyses due to limited sample size. Of notice, all scans with pathology on the left were images were left–right flipped voxel-wise to align the epileptogenic side across subjects prior to spatial smoothing and voxel-wise statistical analysis.

Statistical analysis

Group differences were assessed using pairwise Mann–Whitney U tests, given the non-normal distribution of SUVR values and unequal group sizes. All pairwise comparisons among the included groups were performed. To account for multiple testing, false discovery rate (FDR) correction was applied using the Benjamini–Hochberg procedure or Dunn test. Comparisons surviving FDR correction were considered statistically robust, while uncorrected results were reported as exploratory. Comparisons were corrected for age and sex.

Finally, individual z-scores relative to the control group were computed to visualize inter-individual variability and subgroup heterogeneity.

Results

A total of 92 subjects were included in the analysis (CTR n = 30; LE n = 18; LE_BS n = 13; LE_FU n = 13; EA n = 18, **table 6**). Groups with smaller sample sizes (HS and mTLE) were excluded from statistical comparisons.

Group	N	Female / Male	Age, years (mean ± SD)	Post-hoc age comparisons (Dunn test, FDR)
CTR	30	20 / 10	47.9 ± 14.8	CTR < LE (**q = 0.004**); CTR < LE_BS (**q = 0.021**)
EA	18	6 / 12	41.2 ± 14.1	EA < LE (**q = 0.015**)
LE_BS	12	5 / 7	57.8 ± 21.2	LE_BS > CTR (**q = 0.021**)
LE	13	7 / 6	66.9 ± 23.2	LE > CTR (**q = 0.004**); LE > EA (**q = 0.015**)
LE_FU	11	6 / 5	57.3 ± 21.6	n.s. vs CTR, EA, LE, LE_BS
HS*	7	5 / 2	35.6 ± 9.4	Descriptive only
MTL*	5	3 / 2	45.4 ± 20.8	Descriptive only

The right mesial temporal macroregion demonstrated a clear group effect. Patients with limbic encephalitis at baseline (LE_BS) exhibited the highest SUVR values, followed by patients with LE and LE_FU ($p<0.001$). When limiting the analysis to the right amygdala region revealed significant group differences: compared with controls, both LE and LE_BS showed significantly higher SUVR values, surviving FDR correction. LE_BS also differed significantly from EA. Differences between baseline groups and follow-up LE_FU were significant at the uncorrected level only, suggesting partial metabolic normalization over time (**Figure 14**).

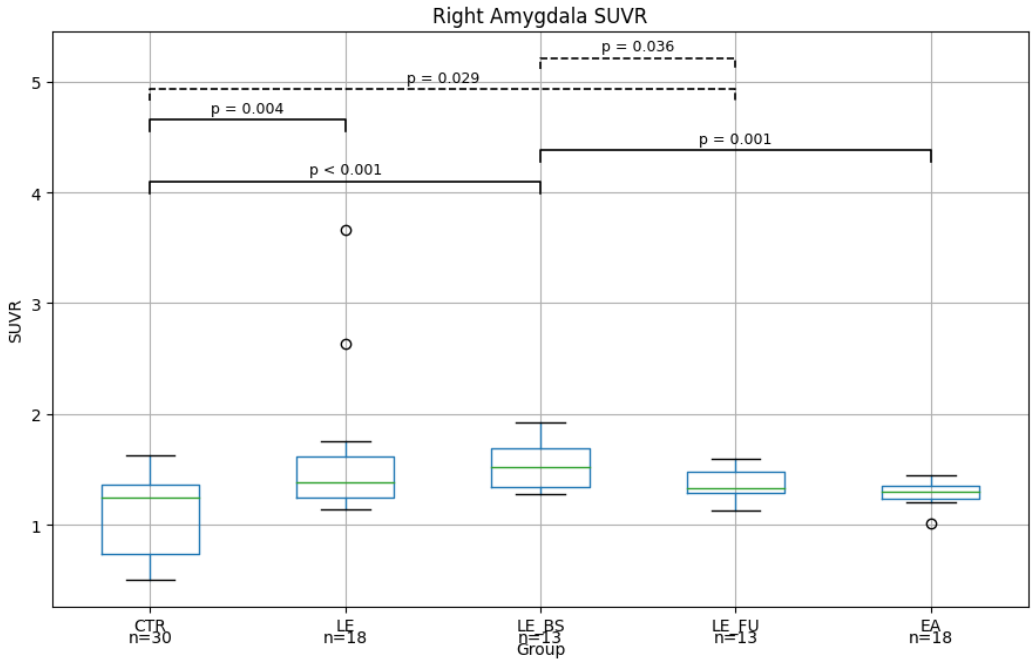

Figure 14. Right amygdala SUVR across groups. Box plot showing standardized uptake value ratios (SUVR) in the right amygdala for controls (CTR), limbic encephalitis (LE), limbic encephalitis at baseline (LE_BS), limbic encephalitis at follow-up (LE_FU), and epilepsy of unknown aetiology (EA). Boxes represent median and interquartile range; whiskers indicate data dispersion. Pairwise comparisons were performed using the Mann–Whitney U test. Solid lines indicate comparisons surviving false discovery rate (FDR) correction, whereas dashed lines indicate comparisons significant at the uncorrected level only. Sample size for each group is reported below the x-axis.

The same analysis was repeated after age correction leading to similar, albeit less significant results as shown in **figure 15.**

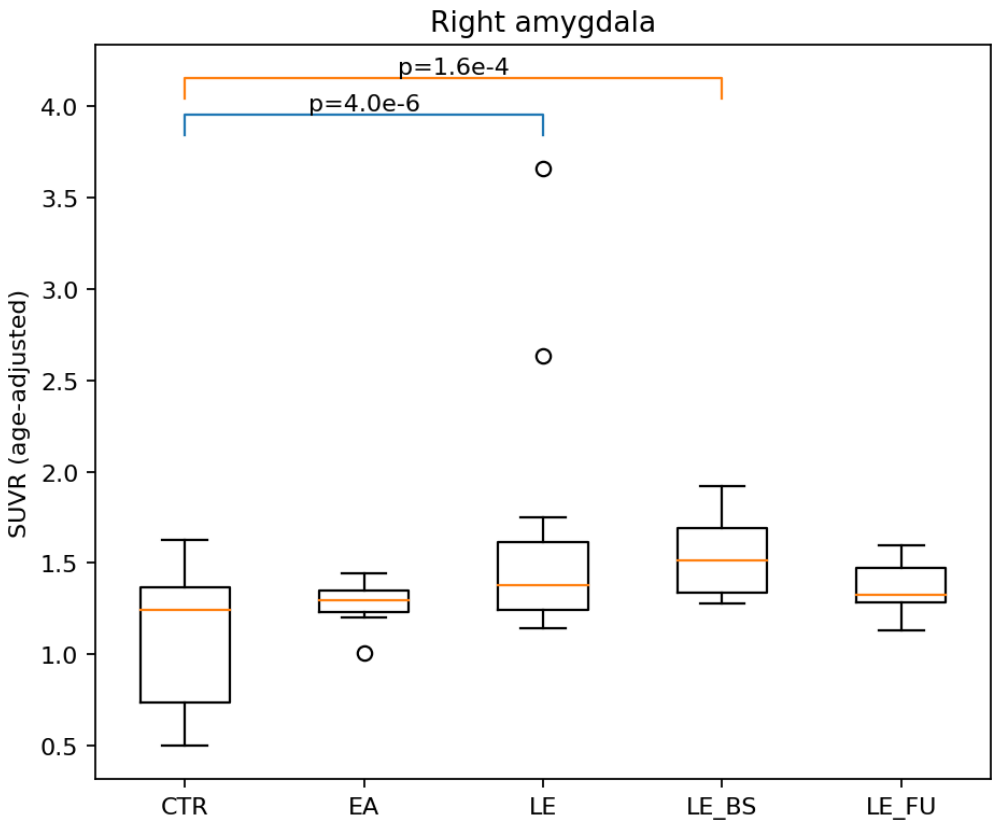

Figure 15. Right amygdala metabolism across groups. Box plots illustrating age-adjusted SUVR values in the right amygdala across groups (CTR, EA, LE, LE_BS, LE_FU). Group effects were tested using ANCOVA including age as covariate, with missing age values replaced by the group mean. A significant group effect was detected ($F = 7.59$, $p = 2.74 \times 10^{-5}$). Post-hoc analysis demonstrated significantly increased amygdala metabolism in LE and LE_BS compared with controls, with all contrasts surviving FDR correction. No significant differences were found between EA or LE_FU and controls. Boxes represent the interquartile range, center lines indicate the median, and whiskers denote 1.5×IQR.

Right amygdala Z-score analysis showed that CTR subjects clustered around zero, whereas LE_BS patients consistently exhibited positive deviations, indicating marked amygdala hypermetabolism. EA and LE_FU groups displayed intermediate values, while the LE group showed substantial inter-individual dispersion, consistent with biological heterogeneity and the presence of distinct metabolic sub-phenotypes within this cohort.

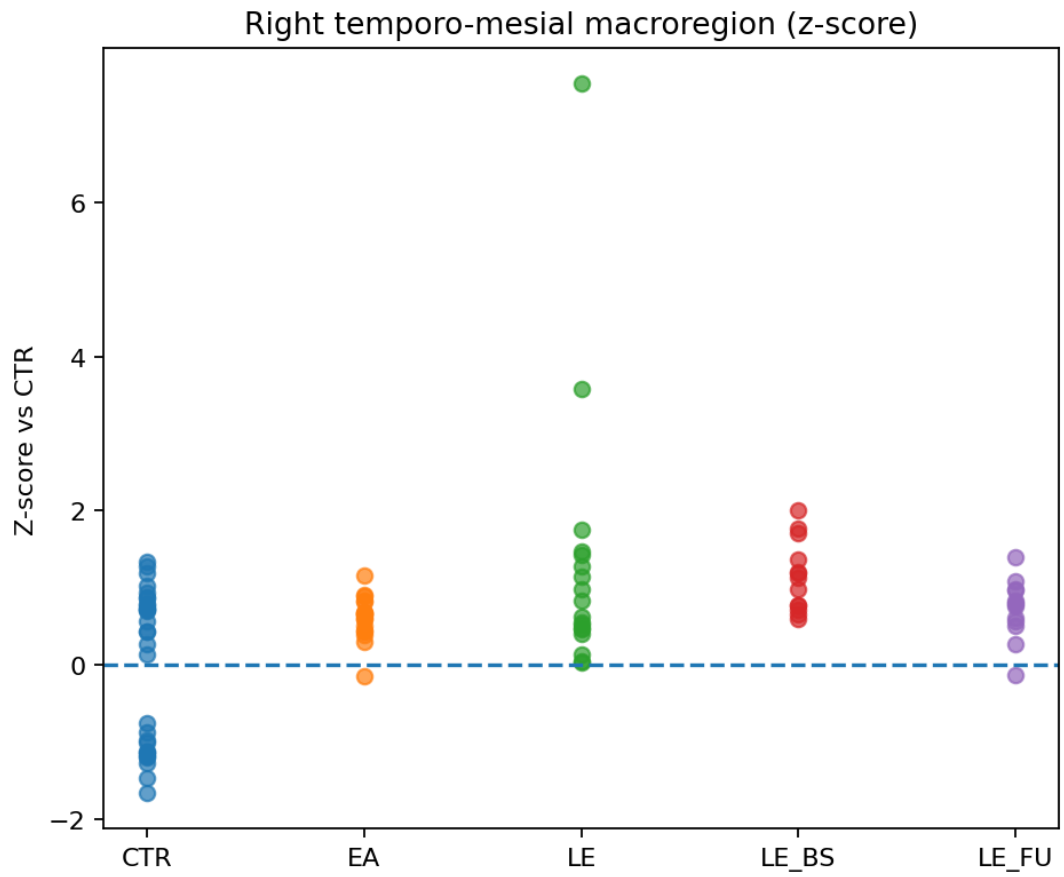

Right amygdala metabolism across diseases. Scatter plot showing individual z-scores of right amygdala SUVR relative to controls (CTR). The dashed horizontal line represents the control mean (z = 0). Patients with limbic encephalitis at baseline (LE_BS) show a consistent upward shift, indicating increased amygdala metabolism, while enlarged amygdala (EA) and limbic encephalitis at follow-up (LE_FU) exhibit intermediate values. The limbic encephalitis (LE) group demonstrates marked inter-individual variability. Statistical analysis revealed a significant overall group effect (ANCOVA) and a highly significant ordinal trend across disease stages, supporting a stage-dependent increase in right amygdala metabolism.

Discussion. This preliminary results support the concept that amygdala enlargement (EA) in temporal lobe epilepsy is not a single-pathology entity but an heterogeneous condition partially overlapping with LE, partially with non-inflammatory temporal lobe epilepsy. It is possible that EA might be a dynamic biological marker, reflecting different disease mechanisms/stages.

Indeed, regional [^{18}F]FDG-PET results demonstrate a metabolic gradient across groups, with limbic encephalitis at baseline showing the highest mesial temporal and amygdala metabolism, followed by LE at later stages and EA, and with controls at the lowest end. It is particularly interesting to notice that while mesial temporal metabolism reach its lower point in EA patients as compared with LE and CTR groups, when viewing amygdala metabolism only,

counterintuitively, the lower point is reached by CTR groups and patients with enlarged amygdala tends (not significantly) to be higher. This pattern suggests that active inflammatory or immune-mediated processes drive early hypermetabolism, particularly within the amygdala, while partial normalization at follow-up might reflect disease modulation over time. The intermediate metabolic profile observed in EA patients supports the hypothesis that EA may represent a chronic or less active limbic condition or early and not yet active inflammatory stage. To date no final conclusion are possible to be obtained and further analysis eventually in multicentric studies are needed.

LIMITATIONS

Most of the studies described in this thesis are exploratory or proof-of-concept, particularly those involving brain tumour-related epilepsy, autoimmune encephalitis, and epilepsy. Larger cohorts and multicentre studies are necessary to confirm the generalisability of identified biomarkers. The integration of multimodal approaches, including neuroimaging, electrophysiology, and molecular markers, within standardised and harmonised pipelines would significantly enhance reproducibility, enable cross-centre comparisons, and speed up clinical translation. As demonstrated for the alpha synucleinopathies continuum, for brain tumour-related epilepsy, autoimmune encephalitis, and epilepsy projects, external validation cohorts and longitudinal designs are essential to strengthen the robustness of findings and improve their generalisability. Currently, several analyses remain exploratory, mainly due to limited sample sizes and cohort heterogeneity, which may obscure subtle yet clinically relevant effects and reduce statistical power, though they are promising for further research and projects.

CONCLUSION

This PhD thesis had the aim to provide an overview of the most frequently applied post-processing neuroimaging techniques, mainly, but not limited to the field of brain metabolism.

Overall, this project demonstrates that deep phenotyping through advanced neuroimaging post-processing and quantitative metabolic analysis is both feasible and clinically relevant for several central nervous system disorders encompassing sleep disorders and alpha-synucleinopathy continuum, brain tumor related epilepsy and autoimmune associated epilepsy, as well as autoimmune and paraneoplastic encephalitis themselves. Integrating structural findings with functional imaging allows a more nuanced interpretation of the results, with potential implications for diagnosis, prognosis, and therapeutic decision-making. Future studies with larger cohorts and longitudinal designs will be essential to translate neuro-imaging post-processing signatures into reliable tools for personalized management of patients with disorders of central nervous system.

REFERENCES

1. Tolkien JRR (1937) The hobbit, or, there and back again
2. Hoh CK (2007) Clinical use of FDG PET. Nucl Med Biol 34:737–742. https://doi.org/10.1016/J.NUCMEDBIO.2007.07.001
3. Guedj E, Varrone A, Boellaard R, et al (2022) EANM procedure guidelines for brain PET imaging using [18F]FDG, version 3. Eur J Nucl Med Mol Imaging 49:632. https://doi.org/10.1007/S00259-021-05603-W
4. Rahman WT, Wale DJ, Viglianti BL, et al (2019) The impact of infection and inflammation in oncologic 18F-FDG PET/CT imaging. Biomed Pharmacother 117:. https://doi.org/10.1016/j.biopha.2019.109168
5. Tyler CW, Likova LT, Nicholas SC (2015) Analysis of neural-BOLD coupling through four models of the neural metabolic demand. Front Neurosci 9:96237. https://doi.org/10.3389/FNINS.2015.00419/BIBTEX
6. Chassoux F, Artiges E, Semah F, et al (2016) Determinants of brain metabolism changes in mesial temporal lobe epilepsy. Epilepsia 57:907–919. https://doi.org/10.1111/epi.13377
7. Meles SK, Tang CC, Teune LK, et al (2015) Abnormal metabolic pattern associated with cognitive impairment in Parkinson ' s disease : a validation study. J Cereb Blood Flow & Metab 35:1478–1484. https://doi.org/10.1038/jcbfm.2015.112
8. Yao Y, Wang X, Zhao B, et al (2024) Hypometabolic patterns are related to post-surgical seizure outcomes in focal cortical dysplasia: A semi-quantitative study. Epilepsia Open. https://doi.org/10.1002/epi4.12903
9. Cerne D, Raffa S, Benvenuto G, et al (2025) Longitudinal changes in [18F]FDG PET brain metabolism as a prognostic marker in autoimmune encephalitis. Eur J Nucl Med Mol Imaging. https://doi.org/10.1007/S00259-025-07526-2
10. Biassoni E, Kreshpa W, Massa F, et al (2023) Right posterior hypometabolism in Pisa syndrome of Parkinson's disease: A key to explain body schema perception deficit? Parkinsonism Relat Disord 110:. https://doi.org/10.1016/J.PARKRELDIS.2023.105371
11. Raffa S, Sofia L, Girtler N, et al (2024) Metabolic and dopaminergic correlates of intellectual enrichment in de-novo Parkinson's disease patients. Q J Nucl Med Mol imaging Off Publ Ital Assoc Nucl Med [and] Int Assoc Radiopharmacol (IAR), [and] Sect Soc of. 68:187–193. https://doi.org/10.23736/S1824-4785.24.03585-4,
12. Schenck CH (2019) The spectrum of disorders causing violence during sleep. Sleep Sci Pract 2019 31 3:1–14. https://doi.org/10.1186/S41606-019-0034-6
13. Ferini-Strambi L (2011) Does idiopathic REM sleep behavior disorder (iRBD) really exist? What are the potential markers of neurodegeneration in iRBD? Sleep Med 12:S43-9
14. Galbiati A, Verga L, Giora E, et al (2019) The risk of neurodegeneration in REM sleep behavior disorder: A systematic review and meta-analysis of longitudinal studies. Sleep Med Rev 43:37–46. https://doi.org/10.1016/J.SMRV.2018.09.008
15. Postuma RB, Iranzo A, Hu M, et al (2019) Risk and predictors of dementia and parkinsonism in idiopathic REM sleep behaviour disorder: a multicentre study. Brain 142:744–759. https://doi.org/10.1093/BRAIN/AWZ030

16. Bedard MA, Aghourian M, Legault-Denis C, et al (2019) Brain cholinergic alterations in idiopathic REM sleep behaviour disorder: a PET imaging study with 18 F-FEOBV. Sleep Med 58:35–41. https://doi.org/10.1016/j.sleep.2018.12.020

17. Rahayel S, Postuma RB, Montplaisir J, et al (2018) Cortical and subcortical gray matter bases of cognitive deficits in REM sleep behavior disorder. Neurology 90:e1759. https://doi.org/10.1212/WNL.0000000000005523

18. Gagnon JF, Vendette M, Postuma RB, et al (2009) Mild cognitive impairment in rapid eye movement sleep behavior disorder and Parkinson's disease. Ann Neurol 66:39–47

19. Miglis MG, Adler CH, Antelmi E, et al (2021) Biomarkers of conversion to α-synucleinopathy in isolated rapid-eye-movement sleep behaviour disorder. Lancet Neurol 20:671–684. https://doi.org/10.1016/S1474-4422(21)00176-9

20. Mattioli P, Pardini M, Famà F, et al (2021) Cuneus/precuneus as a central hub for brain functional connectivity of mild cognitive impairment in idiopathic REM sleep behavior patients. Eur J Nucl Med Mol Imaging 1–12. https://doi.org/10.1007/s00259-021-05205-6

21. Mattioli P, Pardini M, Girtler N, et al (2022) Cognitive and Brain Metabolism Profiles of Mild Cognitive Impairment in Prodromal Alpha-Synucleinopathy. J Alzheimers Dis 90:433–444. https://doi.org/10.3233/JAD-220653

22. Antelmi E, Pizza F, Donadio V, et al (2019) Biomarkers for REM sleep behavior disorder in idiopathic and narcoleptic patients. Ann Clin Transl Neurol 6:1872–1876. https://doi.org/10.1002/acn3.50833

23. Arnaldi D, Famà F, Girtler N, et al (2021) Rapid eye movement sleep behavior disorder: A proof-of-concept neuroprotection study for prodromal synucleinopathies. Eur J Neurol 28:1210–1217. https://doi.org/10.1111/ENE.14664

24. Caminiti SP, Sala A, Iaccarino L, et al (2019) Brain glucose metabolism in Lewy body dementia: Implications for diagnostic criteria. Alzheimer's Res Ther 11:. https://doi.org/10.1186/s13195-019-0473-4

25. Morbelli S, Drzezga A, Perneczky R, et al (2012) Resting metabolic connectivity in prodromal Alzheimer's disease. A European Alzheimer Disease Consortium (EADC) project. Neurobiol Aging 33:2533–2550. https://doi.org/10.1016/j.neurobiolaging.2012.01.005

26. Nobili F, Arbizu J, Bouwman F, et al (2018) European Association of Nuclear Medicine and European Academy of Neurology recommendations for the use of brain 18 F-fluorodeoxyglucose positron emission tomography in neurodegenerative cognitive impairment and dementia: Delphi consensus. Eur J Neurol 25:1201–1217. https://doi.org/10.1111/ene.13728

27. Ashraf A, Fan Z, Brooks DJ, Edison P (2015) Cortical hypermetabolism in MCI subjects: a compensatory mechanism? Eur J Nucl Med Mol Imaging 42:447–458

28. Mattioli P, Orso B, Liguori C, et al (2023) Derivation and Validation of a Phenoconversion-Related Pattern in Idiopathic Rapid Eye Movement Behavior Disorder. Mov Disord 38:57–67. https://doi.org/10.1002/MDS.29236

29. Blazhenets G, Ma Y, Sörensen A, et al (2019) Principal Components Analysis of Brain Metabolism Predicts Development of Alzheimer Dementia. J Nucl Med 60:837–843. https://doi.org/10.2967/JNUMED.118.219097

30. Meles SK, Renken RJ, Janzen A, et al (2018) The Metabolic Pattern of Idiopathic REM Sleep Behavior Disorder Reflects Early-Stage Parkinson Disease. J Nucl Med 59:1437–1444

31. Meles SK, Tang CC, Teune LK, et al (2015) Abnormal metabolic pattern associated with

cognitive impairment in Parkinson's disease: a validation study. J Cereb Blood Flow Metab 35:1478–1484. https://doi.org/10.1038/jcbfm.2015.112

32. Kogan R V, Meles SK, Leenders KL, et al (2019) Brain imaging in RBD. In: Rapid-eye-movement sleep behavior disorder. Springer, pp 403–445

33. Desarnaud S, Mellerio C, Semah F, et al (2018) 18F-FDG PET in drug-resistant epilepsy due to focal cortical dysplasia type 2: additional value of electroclinical data and coregistration with MRI. Eur J Nucl Med Mol Imaging 45:1449–1460. https://doi.org/10.1007/S00259-018-3994-3,

34. Kumar A, Juhász C, Asano E, et al (2010) Objective detection of epileptic foci by18F-FDG PET in children undergoing epilepsy surgery. J Nucl Med 51:1901–1907. https://doi.org/10.2967/jnumed.110.075390

35. Tortora D, Cataldi M, Severino M, et al (2022) Comparison of Qualitative and Quantitative Analyses of MR-Arterial Spin Labeling Perfusion Data for the Assessment of Pediatric Patients with Focal Epilepsies. Diagnostics (Basel, Switzerland) 12:. https://doi.org/10.3390/DIAGNOSTICS12040811

36. Aslam S, Damodaran N, Rajeshkannan R, et al (2022) Asymmetry index in anatomically symmetrized FDG-PET for improved epileptogenic focus detection in pharmacoresistant epilepsy. J Neurosurg 138:828–836. https://doi.org/10.3171/2022.6.JNS22717

37. Beh SMJ, Cook MJ, D'Souza WJ (2016) Isolated amygdala enlargement in temporal lobe epilepsy: A systematic review. Epilepsy Behav 60:33–41. https://doi.org/10.1016/j.yebeh.2016.04.015

38. Chakravarty K, Ray S, Kharbanda PS, et al (2021) Temporal lobe epilepsy with amygdala enlargement: A systematic review. Acta Neurol Scand 144:236–250. https://doi.org/10.1111/ANE.13455,

39. Capizzano AA, Kawasaki H, Sainju RK, et al (2019) Amygdala enlargement in mesial temporal lobe epilepsy: an alternative imaging presentation of limbic epilepsy. Neuroradiology 61:119–127. https://doi.org/10.1007/S00234-018-2109-Y/FIGURES/5

40. Kuchukhidze G, Unterberger I, Schmid E, et al (2022) Emotional Recognition in Patients With Mesial Temporal Epilepsy Associated With Enlarged Amygdala. Front Neurol 12:803787. https://doi.org/10.3389/FNEUR.2021.803787/BIBTEX

41. Shakhatreh L, Sinclair B, McLean C, et al (2024) Amygdala enlargement in temporal lobe epilepsy: Histopathology and surgical outcomes. Epilepsia 65:1709–1719. https://doi.org/10.1111/EPI.17968,

42. Jiang Y, Li W, Li J, et al (2024) Identification of four biotypes in temporal lobe epilepsy via machine learning on brain images. Nat Commun 2024 151 15:1–12. https://doi.org/10.1038/s41467-024-46629-6

43. Feng T, Yang Y, Wang Y, et al (2024) Delineating structural and metabolic abnormalities in amygdala and hippocampal subfields for different seizure-onset patterns via stereotactic electroencephalography. CNS Neurosci Ther 30:. https://doi.org/10.1111/CNS.14905,

44. Makhalova J, Le Troter A, Aubert-Conil S, et al (2022) Epileptogenic networks in drug-resistant epilepsy with amygdala enlargement: Assessment with stereo-EEG and 7 T MRI. Clin Neurophysiol 133:94–103. https://doi.org/10.1016/j.clinph.2021.10.012

45. Morbelli S, Esposito G, Arbizu J, et al (2020) EANM practice guideline/SNMMI procedure standard for dopaminergic imaging in Parkinsonian syndromes 1.0. Eur J Nucl Med Mol Imaging 47:1885–1912. https://doi.org/10.1007/s00259-020-04817-8

46. Spetsieris P, Ma Y, Peng S, et al (2013) Identification of disease-related spatial covariance patterns using neuroimaging data. J Vis Exp. https://doi.org/10.3791/50319

47. Genovese M, Arcasensa A, Morbelli S, et al (2024) SWANe: Standardized workflow for advanced neuroimaging in epilepsy. SoftwareX 26:101703. https://doi.org/10.1016/J.SOFTX.2024.101703

48. Foulon C, Cerliani L, Kinkingnéhun S, et al (2018) Advanced lesion symptom mapping analyses and implementation as BCBtoolkit. Gigascience 7:1–17. https://doi.org/10.1093/gigascience/giy004

49. Höglinger GU, Adler CH, Berg D, et al (2024) A biological classification of Parkinson's disease: the SynNeurGe research diagnostic criteria. Lancet Neurol 23:191–204. https://doi.org/10.1016/S1474-4422(23)00404-0

50. Simuni T, Chahine LM, Poston K, et al (2024) A biological definition of neuronal α-synuclein disease: towards an integrated staging system for research. Lancet Neurol 23:178–190. https://doi.org/10.1016/S1474-4422(23)00405-2

51. Gelb DJ, Oliver E, Gilman S, et al (1999) Diagnostic Criteria for Parkinson Disease. Arch Neurol 56:33. https://doi.org/10.1001/archneur.56.1.33

52. Litvan I, Goldman JG, Tröster AI, et al (2012) Diagnostic criteria for mild cognitive impairment in Parkinson's disease: Movement Disorder Society Task Force guidelines. Mov Disord 27:349–356. https://doi.org/10.1002/mds.24893

53. Postuma RB, Berg D, Stern M, et al (2015) MDS clinical diagnostic criteria for Parkinson's disease. Mov Disord 30:1591–1601. https://doi.org/10.1002/mds.26424

54. McKeith IG, Boeve BF, Dickson DW, et al (2017) Diagnosis and management of dementia with Lewy bodies: Fourth consensus report of the DLB Consortium. Neurology 89:88–100

55. Gilman S, Wenning GK, Low PA, et al (2008) Second consensus statement on the diagnosis of multiple system atrophy. Neurology 71:670–676. https://doi.org/10.1212/01.wnl.0000324625.00404.15

56. Varrone A, Asenbaum S, Vander Borght T, et al (2009) EANM procedure guidelines for PET brain imaging using [18 F] FDG, version 2. Eur J Nucl Med Mol Imaging 36:2103

57. Della Rosa PA, Cerami C, Gallivanone F, et al (2014) A standardized [18 F]-FDG-PET template for spatial normalization in statistical parametric mapping of dementia. Neuroinformatics 12:575–593

58. The AASM Manual for the Scoring of Sleep and Associated Events

59. Teune LK, Renken RJ, Mudali D, et al (2013) Validation of parkinsonian disease-related metabolic brain patterns. Mov Disord 28:547–551

60. Meles SK, Kok JG, Renken RJ, Leenders KL (2021) From Positron to Pattern: A Conceptual and Practical Overview of 18 F-FDG PET Imaging and Spatial Covariance Analysis. PET SPECT Neurol 73–104

61. Spetsieris PG, Ko JH, Tang CC, et al (2015) Metabolic resting-state brain networks in health and disease. Proc Natl Acad Sci 112:2563–2568

62. Kogan R V, Janzen A, Meles SK, et al (2021) Four-year follow-up of [18F] Fluorodeoxyglucose positron emission tomography–based Parkinson's disease–related pattern expression in 20 patients with isolated rapid eye movement sleep behavior disorder shows prodromal progression. Mov Disord 36:230–235

63. Meles SK, Kok JG, De Jong BM, et al (2018) The cerebral metabolic topography of

spinocerebellar ataxia type 3. NeuroImage Clin 19:90–97

64. Arnaldi D, Meles SK, Giuliani A, et al (2019) Brain glucose metabolism heterogeneity in idiopathic REM sleep behavior disorder and in Parkinson's disease. J Parkinsons Dis 9:229–239

65. Fluss R, Faraggi D, Reiser B (2005) Estimation of the Youden Index and its associated cutoff point. Biometrical J J Math Methods Biosci 47:458–472

66. Shin JH, Lee J-Y, Kim Y-K, et al (2021) Parkinson disease-related brain metabolic patterns and neurodegeneration in isolated REM sleep behavior disorder. Neurology 97:e378–e388

67. Morbelli S, Chincarini A, Brendel M, et al (2019) Metabolic patterns across core features in dementia with lewy bodies. Ann Neurol 85:715–725

68. Arnaldi D, Chincarini A, Hu MT, et al (2021) Dopaminergic imaging and clinical predictors for phenoconversion of REM sleep behaviour disorder. Brain 144:278–287. https://doi.org/10.1093/brain/awaa365

69. Zhang H, Iranzo A, Högl B, et al (2022) Risk factors for phenoconversion in REM sleep behavior disorder. Ann Neurol

70. Meles SK, Vadasz D, Renken RJ, et al (2017) FDG PET, dopamine transporter SPECT, and olfaction: Combining biomarkers in REM sleep behavior disorder. Mov Disord 32:1482–1486. https://doi.org/10.1002/mds.27094

71. Kim R, Lee J, Kim YK, et al (2021) Longitudinal Changes in Isolated Rapid Eye Movement Sleep Behavior Disorder-Related Metabolic Pattern Expression. Mov Disord 36:1889–1898

72. Holtbernd F, Gagnon J, Postuma R, et al (2014) Abnormal metabolic network activity in REM sleep behavior disorder. Neurology 82:620–627. https://doi.org/10.1212/WNL.0000000000000130

73. Vanacore N, Bonifati V, Fabbrini G, et al (2001) Epidemiology of multiple system atrophy. Neurol Sci 22:97–99

74. Orso B, Mattioli P, Famà F, et al (2025) Uncovering Clinical and Functional Neuroimaging Characteristics of Overt Stage Phenotypes Within the α-Synucleinopathy Spectrum. Neurology 105:. https://doi.org/10.1212/WNL.0000000000214253

75. Orso B, Mattioli P, Yoon EJ, et al (2024) Progression trajectories from prodromal to overt synucleinopathies: a longitudinal, multicentric brain [18F]FDG-PET study. NPJ Park Dis 10:. https://doi.org/10.1038/S41531-024-00813-Z

76. Orso B, Mattioli P, Yoon EJ, et al (2023) Validation of the REM behaviour disorder phenoconversion-related pattern in an independent cohort. Neurol Sci 44:3161–3168. https://doi.org/10.1007/S10072-023-06829-2

77. Bae YJ, Kim JM, Sohn CH, et al (2021) Imaging the Substantia Nigra in Parkinson Disease and Other Parkinsonian Syndromes. https://doi.org/101148/radiol2021203341 300:260–278. https://doi.org/10.1148/RADIOL.2021203341

78. Frosini D, Cosottini M, Donatelli G, et al (2017) Seven tesla MRI of the substantia nigra in patients with rapid eye movement sleep behavior disorder. Park Relat Disord 43:105–109. https://doi.org/10.1016/j.parkreldis.2017.08.002

79. Barber TR, Griffanti L, Bradley KM, et al (2019) Nigrosome 1 imaging in REM sleep behavior disorder and its association with dopaminergic decline. Ann Clin Transl Neurol 7:26. https://doi.org/10.1002/ACN3.50962

80. Bae YJ, Kim JM, Kim KJ, et al (2018) Loss of Substantia Nigra Hyperintensity at 3.0-T MR Imaging in Idiopathic REM Sleep Behavior Disorder: Comparison with 123I-FP-CIT SPECT.

Radiology 287:285–293. https://doi.org/10.1148/RADIOL.2017162486

81. Oustwani CS, Korutz AW, Lester MS, et al (2017) Can loss of the swallow tail sign help distinguish between Parkinson Disease and the Parkinson-Plus syndromes? Clin Imaging 44:66–69. https://doi.org/10.1016/J.CLINIMAG.2017.04.005

82. Cosottini M, Frosini D, Pesaresi I, et al (2014) MR imaging of the substantia nigra at 7 T enables diagnosis of Parkinson disease. Radiology 271:831–838. https://doi.org/10.1148/RADIOL.14131448

83. Shams S, Fällmar D, Schwarz S, et al (2017) MRI of the Swallow Tail Sign: A Useful Marker in the Diagnosis of Lewy Body Dementia? AJNR Am J Neuroradiol 38:1737–1741. https://doi.org/10.3174/AJNR.A5274

84. Nam Y, Gho SM, Kim DH, et al (2017) Imaging of nigrosome 1 in substantia nigra at 3T using multiecho susceptibility map-weighted imaging (SMWI). J Magn Reson Imaging 46:528–536. https://doi.org/10.1002/JMRI.25553

85. Sung YH, Kim JS, Yoo SW, et al (2022) A prospective multi-centre study of susceptibility map-weighted MRI for the diagnosis of neurodegenerative parkinsonism. Eur Radiol 32:3597–3608. https://doi.org/10.1007/S00330-021-08454-Z

86. Lancione M, Donatelli G, Del Prete E, et al (2022) Evaluation of iron overload in nigrosome 1 via quantitative susceptibility mapping as a progression biomarker in prodromal stages of synucleinopathies. Neuroimage 260:. https://doi.org/10.1016/j.neuroimage.2022.119454

87. Langkammer C, Schweser F, Krebs N, et al (2012) Quantitative susceptibility mapping (QSM) as a means to measure brain iron? A post mortem validation study. Neuroimage 62:1593–1599. https://doi.org/10.1016/j.neuroimage.2012.05.049

88. Bilgic B, Costagli M, Chan KS, et al (2024) Recommended implementation of quantitative susceptibility mapping for clinical research in the brain: A consensus of the ISMRM electro-magnetic tissue properties study group. Magn Reson Med 91:1834–1862. https://doi.org/10.1002/MRM.30006

89. Chau MT, Todd G, Wilcox R, et al (2020) Diagnostic accuracy of the appearance of Nigrosome-1 on magnetic resonance imaging in Parkinson's disease: A systematic review and meta-analysis. Parkinsonism Relat Disord 78:12–20. https://doi.org/10.1016/J.PARKRELDIS.2020.07.002

90. De Marzi R, Seppi K, Högl B, et al (2016) Loss of dorsolateral nigral hyperintensity on 3.0 tesla susceptibility-weighted imaging in idiopathic rapid eye movement sleep behavior disorder. Ann Neurol 79:1026–1030. https://doi.org/10.1002/ANA.24646

91. Honkanen EA, Saari L, Orte K, et al (2019) No link between striatal dopaminergic axons and dopamine transporter imaging in Parkinson's disease. Mov Disord 34:1562–1566. https://doi.org/10.1002/MDS.27777

92. Saari L, Kivinen K, Gardberg M, et al (2017) Dopamine transporter imaging does not predict the number of nigral neurons in Parkinson disease. Neurology 88:1461–1467. https://doi.org/10.1212/WNL.0000000000003810

93. Bellomo G, Toja A, Paolini Paoletti F, et al (2024) Investigating alpha-synuclein co-pathology in Alzheimer's disease by means of cerebrospinal fluid alpha-synuclein seed amplification assay. Alzheimers Dement 20:2444–2452. https://doi.org/10.1002/ALZ.13658

94. Deture MA, Dickson DW (2019) The neuropathological diagnosis of Alzheimer's disease. Mol Neurodegener 14:. https://doi.org/10.1186/S13024-019-0333-5

95. Alushaj E, Kuurstra A, Menon RS, et al (2025) Midbrain and pallidal iron changes identify

patients with REM sleep behaviour disorder and Parkinson's disease. npj Park Dis 2025 111 11:84-. https://doi.org/10.1038/s41531-025-00916-1

96. Varga Z, Keller J, Robinson SD, et al (2024) Whole brain pattern of iron accumulation in REM sleep behavior disorder. Hum Brain Mapp 45:. https://doi.org/10.1002/HBM.26675

97. Pesce A, Armocida D, Paglia F, et al (2022) IDH Wild-type Glioblastoma Presenting with Seizure: Clinical Specificity, and Oncologic and Surgical Outcomes. J Neurol Surgery, Part A Cent Eur Neurosurg 83:351–360. https://doi.org/10.1055/S-0041-1735515/ID/JR202906OA-49

98. Avila EK, Tobochnik S, Inati SK, et al (2024) Brain tumor-related epilepsy management: A Society for Neuro-oncology (SNO) consensus review on current management. Neuro Oncol 26:7–24. https://doi.org/10.1093/NEUONC/NOAD154

99. Maschio M, Newton HB (2015) Brain Tumor-Related Epilepsy: Introduction and Overview. Elsevier Inc.

100. Michelucci R, Pauletto G, Silvani A, et al (2025) Tumor-related epilepsy in glioma: A multidisciplinary overview. Epilepsia 66:3621–3641. https://doi.org/10.1111/EPI.18523

101. Persidsky Y, Ramirez SH, Haorah J, Kanmogne GD (2006) Blood-brain barrier: structural components and function under physiologic and pathologic conditions. J Neuroimmune Pharmacol 1:223–236. https://doi.org/10.1007/S11481-006-9025-3

102. Beaumont A, Whittle IR (2000) The pathogenesis of tumour associated epilepsy. Acta Neurochir (Wien) 142:1–15. https://doi.org/10.1007/S007010050001

103. Ivens S, Kaufer D, Flores LP, et al (2007) TGF-beta receptor-mediated albumin uptake into astrocytes is involved in neocortical epileptogenesis. Brain 130:535–547. https://doi.org/10.1093/BRAIN/AWL317

104. Verly G, Delfino T, Bresciani L, et al (2024) Supratotal Resection Versus Gross Total Resection for Isocitrate Dehydrogenase-Wildtype Glioblastoma and Grade 4 Isocitrate Dehydrogenase-Mutant Astrocytoma: Meta-Analysis of Individual Patient Data. Oper Neurosurg (Hagerstown, Md) 29:198–208. https://doi.org/10.1227/ONS.0000000000001434

105. Kreatsoulas D, Damante M, Gruber M, et al (2023) Supratotal Surgical Resection for Low-Grade Glioma: A Systematic Review. Cancers (Basel) 15:. https://doi.org/10.3390/CANCERS15092493

106. Han Q, Liang H, Cheng P, et al (2020) Gross Total vs. Subtotal Resection on Survival Outcomes in Elderly Patients With High-Grade Glioma: A Systematic Review and Meta-Analysis. Front Oncol 10:. https://doi.org/10.3389/FONC.2020.00151

107. Karschnia P, Vogelbaum MA, van den Bent M, et al (2021) Evidence-based recommendations on categories for extent of resection in diffuse glioma. Eur J Cancer 149:23–33. https://doi.org/10.1016/j.ejca.2021.03.002

108. Roelz R, Strohmaier D, Jabbarli R, et al (2016) Residual Tumor Volume as Best Outcome Predictor in Low Grade Glioma - A Nine-Years Near-Randomized Survey of Surgery vs. Biopsy. Sci Rep 6:. https://doi.org/10.1038/SREP32286

109. Bonney PA, Boettcher LB, Burks JD, et al (2017) Rates of Seizure Freedom After Surgical Resection of Diffuse Low-Grade Gliomas. World Neurosurg 106:750–756. https://doi.org/10.1016/j.wneu.2017.06.144

110. Beniczky S, Trinka E, Wirrell E, et al (2025) Updated classification of epileptic seizures: Position paper of the International League Against Epilepsy. Epilepsia 66:1804–1823. https://doi.org/10.1111/EPI.18338

111. Louis DN, Perry A, Reifenberger G, et al (2016) The 2016 World Health Organization

Classification of Tumors of the Central Nervous System: a summary. Acta Neuropathol 131:803–820. https://doi.org/10.1007/s00401-016-1545-1

112. Fan X, Li Y, Shan X, et al (2018) Seizures at presentation are correlated with better survival outcomes in adult diffuse glioma: A systematic review and meta-analysis. Seizure 59:16–23. https://doi.org/10.1016/j.seizure.2018.04.018

113. Xiang H, Hochman DW, Saya H, et al (1996) Evidence for p53-mediated modulation of neuronal viability. J Neurosci 16:6753–6765. https://doi.org/10.1523/JNEUROSCI.16-21-06753.1996

114. Engel T, Tanaka K, Jimenez-Mateos EM, et al (2010) Loss of p53 results in protracted electrographic seizures and development of an aggravated epileptic phenotype following status epilepticus. Cell Death Dis 1:1–8. https://doi.org/10.1038/cddis.2010.55

115. Lu VM, Jue TR, Phan K, McDonald KL (2018) Quantifying the prognostic significance in glioblastoma of seizure history at initial presentation: A systematic review and meta-analysis. Clin Neurol Neurosurg 164:75–80. https://doi.org/10.1016/J.CLINEURO.2017.11.015

116. Ippolito JE, Yim AKY, Luo J, et al (2017) Sexual dimorphism in glioma glycolysis underlies sex differences in survival. JCI insight 2:. https://doi.org/10.1172/JCI.INSIGHT.92142

117. Reddy DS, Thompson W, Calderara G (2021) Molecular mechanisms of sex differences in epilepsy and seizure susceptibility in chemical, genetic and acquired epileptogenesis. Neurosci Lett 750:. https://doi.org/10.1016/j.neulet.2021.135753

118. Su X, Chen HL, Wang ZY, Lan Q (2015) Relationship between tumour location and preoperative seizure incidence in patients with gliomas: a systematic review and meta-analysis. Epileptic Disord 17:397–408. https://doi.org/10.1684/EPD.2015.0788

119. Zhang X, Zheng L, Duan J, et al (2020) Clinical characteristics of brain tumor-related epilepsy and factors influencing the identification of epilepsy-associated tumors. Acta Epileptol 2020 21 2:25-. https://doi.org/10.1186/S42494-020-00034-W

120. Cini NT, Pennisi M, Genc S, et al (2024) Glioma lateralization: Focus on the anatomical localization and the distribution of molecular alterations (Review). Oncol Rep 52:. https://doi.org/10.3892/OR.2024.8798

121. Liu XY, Gerges N, Korshunov A, et al (2012) Frequent ATRX mutations and loss of expression in adult diffuse astrocytic tumors carrying IDH1/IDH2 and TP53 mutations. Acta Neuropathol 124:615–625. https://doi.org/10.1007/S00401-012-1031-3

122. Rada A, Bien CG (2023) What is autoimmune encephalitis-associated epilepsy? Proposal of a practical definition. Epilepsia 64:2249–2255. https://doi.org/10.1111/epi.17699

123. Steriade C, Bauer J, Bien CG (2025) Autoimmune encephalitis-associated epilepsy. Nat Rev Neurol 21:312–326. https://doi.org/10.1038/S41582-025-01089-4;SUBJMETA

124. Graus F, Titulaer MJ, Balu R, et al (2016) A clinical approach to diagnosis of autoimmune encephalitis. Lancet Neurol 15:391. https://doi.org/10.1016/S1474-4422(15)00401-9

125. Graus F, Vogrig A, Muñiz-Castrillo S, et al (2021) Updated Diagnostic Criteria for Paraneoplastic Neurologic Syndromes. Neurol Neuroimmunol neuroinflammation 8:e1014. https://doi.org/10.1212/NXI.0000000000001014

126. Dalmau J, Graus F, Villarejo A, et al (2004) Clinical analysis of anti-Ma2-associated encephalitis. Brain 127:1831–1844. https://doi.org/10.1093/brain/awh203

127. Kimura M, Onozawa M, Fujisaki A, et al (2008) Anti-Ma2 paraneoplastic encephalitis associated with testicular germ cell tumor treated by carboplatin, etoposide and bleomycin. Int J Urol 15:942–943. https://doi.org/10.1111/j.1442-2042.2008.02119.x

128. Mathew RM, Vandenberghe R, Garcia-Merino A, et al (2007) Orchiectomy for suspected microscopic tumor in patients with anti-Ma2-associated encephalitis. Neurology 68:900–905. https://doi.org/10.1212/01.WNL.0000252379.81933.80

129. Inui R, Saito K, Shimomura Y, et al (2020) Anti-Ma-associated paraneoplastic cerebellar degeneration in a patient with nodular lymphocyte-predominant Hodgkin lymphoma : a case report. BMC Neurol 20:355

130. Ju W, Qi B, Wang X, Yang Y (2017) Anti-Ma2-associated limbic encephalitis with coexisting chronic inflammatory demyelinating polyneuropathy in a patient with non-Hodgkin lymphoma: A case report. Med (United States) 96:1–5. https://doi.org/10.1097/MD.0000000000008228

131. Kraemer M, Berlit P (2007) Anti-Ma2 antibodies in B-cell primary CNS lymphoma. J Neurol 254:1286–1287. https://doi.org/10.1007/s00415-006-0494-3

132. Rizek P, Kumar N, Mandar SJ (2017) Anti-Ma2-Associated Encephalitis Secondary to Hodgkin's Lymphoma. Can J Neurol Sci 44:752–753. https://doi.org/https://doi.org/10.1017/cjn.2017.227

133. Smith KM, Britton JW, Thakolwiboon S, et al (2023) Seizure characteristics and outcomes in patients with neurological conditions related to high-risk paraneoplastic antibodies. Epilepsia 64:. https://doi.org/10.1111/EPI.17695

134. Mattioli P, Grisanti S, Massa F, et al (2024) Ma2 antibody-associated limbic encephalitis: The early etiology treatment may modify the disease clinical trajectory. Epileptic Disord 26:407–411. https://doi.org/10.1002/EPD2.20225

135. Day GS (2022) Rapidly Progressive Dementia. Contin Lifelong Learn Neurol 28:901–936. https://doi.org/10.1212/CON.0000000000001089;REQUESTEDJOURNAL:JOURNAL:CON;ISSUE:ISSUE:DOI

136. Arnaldi D, Donniaquio A, Mattioli P, et al (2020) Epilepsy in Neurodegenerative Dementias: A Clinical, Epidemiological, and EEG Study. J Alzheimers Dis 74:865–874. https://doi.org/10.3233/JAD-191315

137. Bastiaansen AEM, Van Steenhoven RW, De Bruijn MAAM, et al (2021) Autoimmune Encephalitis Resembling Dementia Syndromes. Neurol Neuroimmunol NeuroInflammation 8:e1039. https://doi.org/10.1212/NXI.0000000000001039;WGROUP:STRING:PUBLICATION

138. Morano A, Cerulli Irelli E, Salamone EM, et al (2022) Late-onset seizures and epilepsy: Electroclinical features suggestive of autoimmune etiology. Front Neurol 13:. https://doi.org/10.3389/FNEUR.2022.924859

139. Van Sonderen A, Thijs RD, Coenders EC, et al (2016) Anti-LGI1 encephalitis. Neurology 87:1449–1456. https://doi.org/10.1212/WNL.0000000000003173;REQUESTEDJOURNAL:JOURNAL:WNL;JOURNAL:JOURNAL:WNL;WGROUP:STRING:PUBLICATION

140. Abe K, Chiba Y (2019) A case of treatable dementia with Lewy bodies remarkably improved by immunotherapy. J Neuroimmunol 330:35–37. https://doi.org/10.1016/j.jneuroim.2019.02.003

141. Amin J, Erskine D, Donaghy PC, et al (2022) Inflammation in dementia with Lewy bodies. Neurobiol Dis 168:105698. https://doi.org/10.1016/J.NBD.2022.105698

142. Madetko N, Marzec W, Kowalska A, et al (2022) Anti-IgLON5 Disease - The Current State of Knowledge and Further Perspectives. Front Immunol 13:. https://doi.org/10.3389/FIMMU.2022.852215

143. Cerne D, Losa M, Mattioli P, et al (2024) Incident anti-LGI1 autoimmune encephalitis during dementia with Lewy bodies: when Occam razor is a double-edged sword. J Neuroimmunol 387:. https://doi.org/10.1016/j.jneuroim.2024.578291

144. Matricardi S, Casciato S, Bozzetti S, et al (2022) Epileptic phenotypes in autoimmune encephalitis: from acute symptomatic seizures to autoimmune-associated epilepsy. J Neurol Neurosurg Psychiatry 93:1194–1201. https://doi.org/10.1136/JNNP-2022-329195

145. Dubey D, Singh J, Britton JW, et al (2017) Predictive models in the diagnosis and treatment of autoimmune epilepsy. Epilepsia 58:1181–1189. https://doi.org/10.1111/EPI.13797;PAGE:STRING:ARTICLE/CHAPTER

146. Van Sonderen A, Ariño H, Petit-Pedrol M, et al (2016) The clinical spectrum of Caspr2 antibody-associated disease. Neurology 87:521–528. https://doi.org/10.1212/WNL.0000000000002917;JOURNAL:JOURNAL:WNL;WGROUP:STRING:PUBLICATION

147. Boyko M, Au KLK, Casault C, et al (2020) Systematic review of the clinical spectrum of CASPR2 antibody syndrome. J Neurol 2020 2674 267:1137–1146. https://doi.org/10.1007/S00415-019-09686-2

148. Garrido Sanabria ER, Zahid A, Britton J, et al (2022) CASPR2-IgG-associated autoimmune seizures. Epilepsia 63:709–722. https://doi.org/10.1111/EPI.17164;ISSUE:ISSUE:DOI

149. Elisak M, Krysl D, Hanzalova J, et al (2018) The prevalence of neural antibodies in temporal lobe epilepsy and the clinical characteristics of seropositive patients. Seizure 63:1–6. https://doi.org/10.1016/J.SEIZURE.2018.09.009

150. Bien CG (2018) Overinterpretation and overtreatment of low-titer antibodies against contactin-associated protein-2. Front Immunol 9:370898. https://doi.org/10.3389/FIMMU.2018.00703/BIBTEX

151. Michelucci R, Pasini E, Riguzzi P, et al (2024) CASPR2-related epilepsy: A distinctive and unrecognized form of epilepsy in adult and elderly males. Epileptic Disord 753–760. https://doi.org/10.1002/epd2.20269

152. Abboud H, Probasco JC, Irani S, et al (2021) Autoimmune encephalitis: proposed recommendations for symptomatic and long-term management. J Neurol Neurosurg Psychiatry 92:897–907. https://doi.org/10.1136/JNNP-2020-325302

153. Uy CE, Binks S, Irani SR (2021) Autoimmune encephalitis: clinical spectrum and management. Pract Neurol 21:412–423. https://doi.org/10.1136/PRACTNEUROL-2020-002567

154. Heine J, Duchow A, Rust R, et al (2022) Autoimmunenzephalitis – ein Update. Der Nervenarzt 2022 946 94:525–537. https://doi.org/10.1007/S00115-022-01411-1

155. Titulaer MJ, McCracken L, Gabilondo I, et al (2013) Treatment and prognostic factors for long-term outcome in patients with anti-NMDA receptor encephalitis: An observational cohort study. Lancet Neurol 12:157–165. https://doi.org/10.1016/S1474-4422(12)70310-1

156. Cai MT, Lai QL, Zheng Y, et al (2021) Validation of the Clinical Assessment Scale for Autoimmune Encephalitis: A Multicenter Study. Neurol Ther 2021 102 10:985–1000. https://doi.org/10.1007/S40120-021-00278-9

157. Lim JA, Lee ST, Moon J, et al (2019) Development of the clinical assessment scale in autoimmune encephalitis. Ann Neurol 85:352–358. https://doi.org/10.1002/ANA.25421;WEBSITE:WEBSITE:PERICLES;ISSUE:ISSUE:DOI

158. Balu R, Mccracken L, Lancaster E, et al (2019) A score that predicts 1-year functional status in patients with anti-NMDA receptor encephalitis. Neurology 92:E244–E252.

https://doi.org/10.1212/WNL.0000000000006783;CTYPE:STRING:JOURNAL

159. Peng Y, Dai F, Liu L, et al (2020) Validation of the NEOS score in Chinese patients with anti-NMDAR encephalitis. Neurol Neuroimmunol neuroinflammation 7:e860. https://doi.org/10.1212/NXI.0000000000000860;REQUESTEDJOURNAL:JOURNAL:NXI;PAGE:STRING:ARTICLE/CHAPTER

160. Wesselingh R, Broadley J, Buzzard K, et al (2022) Electroclinical biomarkers of autoimmune encephalitis. Epilepsy Behav 128:. https://doi.org/10.1016/j.yebeh.2022.108571

161. Ciano-Petersen NL, Cabezudo-García P, Muñiz-Castrillo S, et al (2021) Current Status of Biomarkers in Anti-N-Methyl-D-Aspartate Receptor Encephalitis. Int J Mol Sci 2021, Vol 22, Page 13127 22:13127. https://doi.org/10.3390/IJMS222313127

162. Liba Z, Kayserova J, Elisak M, et al (2016) Anti-N-methyl-D-aspartate receptor encephalitis: the clinical course in light of the chemokine and cytokine levels in cerebrospinal fluid. J Neuroinflammation 2016 131 13:55-. https://doi.org/10.1186/S12974-016-0507-9

163. Morbelli S, Djekidel M, Hesse S, et al (2016) Role of 18F-FDG-PET imaging in the diagnosis of autoimmune encephalitis. Lancet Neurol 15:1009–1010. https://doi.org/10.1016/S1474-4422(16)30140-5

164. Ances BM, Vitaliani R, Taylor RA, et al (2005) Treatment-responsive limbic encephalitis identified by neuropil antibodies: MRI and PET correlates. Brain 128:1764–1777. https://doi.org/10.1093/BRAIN/AWH526

165. Baumgartner A, Rauer S, Mader I, Meyer PT (2013) Cerebral FDG-PET and MRI findings in autoimmune limbic encephalitis: correlation with autoantibody types. J Neurol 2013 26011 260:2744–2753. https://doi.org/10.1007/S00415-013-7048-2

166. Bordonne M, Chawki MB, Doyen M, et al (2021) Brain 18F-FDG PET for the diagnosis of autoimmune encephalitis: a systematic review and a meta-analysis. Eur J Nucl Med Mol Imaging 48:3847–3858. https://doi.org/10.1007/s00259-021-05299-y

167. Trevino-Peinado C, Arbizu J, Irimia P, et al (2015) Monitoring the Effect of Immunotherapy in Autoimmune Limbic Encephalitis Using 18F-FDG PET. Clin Nucl Med 40:e441–e443. https://doi.org/10.1097/RLU.0000000000000839

168. Dai Y, Zhu Z, Tang Y, et al (2024) The clinical and predictive value of 18F-FDG PET/CT metabolic patterns in a clinical Chinese cohort with autoimmune encephalitis. CNS Neurosci Ther 30:. https://doi.org/10.1111/CNS.14821

169. Heine J, Prüss H, Kopp UA, et al (2018) Beyond the limbic system: disruption and functional compensation of large-scale brain networks in patients with anti-LGI1 encephalitis. J Neurol Neurosurg Psychiatry 89:1191–1199. https://doi.org/10.1136/JNNP-2017-317780

170. Kvam KA, Stahl JP, Chow FC, et al (2024) Outcome and Sequelae of Autoimmune Encephalitis. J Clin Neurol 20:3–22. https://doi.org/10.3988/JCN.2023.0242

171. Rissanen E, Carter K, Cicero S, et al (2022) Cortical and Subcortical Dysmetabolism Are Dynamic Markers of Clinical Disability and Course in Anti-LGI1 Encephalitis. Neurol Neuroimmunol NeuroInflammation 9:e1136. https://doi.org/10.1212/NXI.0000000000001136;WGROUP:STRING:PUBLICATION

172. Uddin LQ, Yeo BTT, Spreng RN (2019) Towards a Universal Taxonomy of Macro-scale Functional Human Brain Networks. Brain Topogr 2019 326 32:926–942. https://doi.org/10.1007/S10548-019-00744-6

173. Xu J, Wang J, Fan L, et al (2015) Tractography-based Parcellation of the Human Middle Temporal Gyrus. Sci Reports 2015 51 5:18883-. https://doi.org/10.1038/srep18883

174. Chang EF, Raygor KP, Berger MS (2015) Contemporary model of language organization: an overview for neurosurgeons. J Neurosurg 122:250–261. https://doi.org/10.3171/2014.10.JNS132647

175. Palejwala AH, O'Connor KP, Milton CK, et al (2020) Anatomy and white matter connections of the fusiform gyrus. Sci Reports 2020 101 10:13489-. https://doi.org/10.1038/s41598-020-70410-6

176. Perucca P, Scheffer IE, Kiley M (2018) The management of epilepsy in children and adults. Med J Aust 208:226–233. https://doi.org/10.5694/MJA17.00951

177. Birbeck GL, Hays RD, Cui X, Vickrey BG (2002) Seizure reduction and quality of life improvements in people with epilepsy. Epilepsia 43:535–538. https://doi.org/10.1046/J.1528-1157.2002.32201.X

178. Kwan P, Arzimanoglou A, Berg AT, et al (2010) Definition of drug resistant epilepsy: consensus proposal by the ad hoc Task Force of the ILAE Commission on Therapeutic Strategies. Epilepsia 51:1069–1077. https://doi.org/10.1111/J.1528-1167.2009.02397.X

179. Pelliccia V, Deleo F, Gozzo F, et al (2022) Early epilepsy surgery for non drug-resistant patients. Epilepsy Behav Reports 19:100542. https://doi.org/10.1016/J.EBR.2022.100542

180. Steinbrenner M, Duncan JS, Dickson J, et al (2022) Utility of 18F-fluorodeoxyglucose positron emission tomography in presurgical evaluation of patients with epilepsy: A multicenter study. Epilepsia 63:1238–1252

181. Boscolo Galazzo I, Mattoli MV, Pizzini FB, et al (2016) Cerebral metabolism and perfusion in MR-negative individuals with refractory focal epilepsy assessed by simultaneous acquisition of (18)F-FDG PET and arterial spin labeling. NeuroImage Clin 11:648–657. https://doi.org/10.1016/J.NICL.2016.04.005

182. Sierra-Marcos A, Carreño M, Setoain X, et al (2016) Accuracy of arterial spin labeling magnetic resonance imaging (MRI) perfusion in detecting the epileptogenic zone in patients with drug-resistant neocortical epilepsy: comparison with electrophysiological data, structural MRI, SISCOM and FDG-PET. Eur J Neurol 23:160–167. https://doi.org/10.1111/ENE.12826

183. Kojan M, Gajdoš M, Říha P, et al (2021) Arterial Spin Labeling is a Useful MRI Method for Presurgical Evaluation in MRI-Negative Focal Epilepsy. Brain Topogr 34:504–510. https://doi.org/10.1007/s10548-021-00833-5

184. Rahimzadeh H, Kamkar H, Hoseini-Tabatabaei N, et al (2023) Alteration of intracranial blood perfusion in temporal lobe epilepsy, an arterial spin labeling study. Heliyon 9:. https://doi.org/10.1016/J.HELIYON.2023.E14854

185. Detre JA, Wang J (2002) Technical aspects and utility of fMRI using BOLD and ASL. Clin Neurophysiol 113:621–634. https://doi.org/10.1016/S1388-2457(02)00038-X

186. Zijlmans M, Zweiphenning W, van Klink N (2019) Changing concepts in presurgical assessment for epilepsy surgery. Nat Rev Neurol 15:594–606. https://doi.org/10.1038/S41582-019-0224-Y

187. Lim YM, Cho YW, Shamim S, et al (2008) Usefulness of Pulsed Arterial Spin Labeling MR Imaging in Mesial Temporal Lobe Epilepsy. Epilepsy Res 82:183. https://doi.org/10.1016/J.EPLEPSYRES.2008.08.001

188. Khalaf AM, Nadel HR, Dahmoush HM (2022) Simultaneously Acquired MRI Arterial Spin-Labeling and Interictal FDG-PET Improves Diagnosis of Pediatric Temporal Lobe Epilepsy. AJNR Am J Neuroradiol 43:468–473. https://doi.org/10.3174/AJNR.A7421

189. Lam J, Tomaszewski P, Gilbert G, et al (2020) The utility of arterial spin labeling in the presurgical evaluation of poorly defined focal epilepsy in children. J Neurosurg Pediatr 27:243–

252. https://doi.org/10.3171/2020.7.PEDS20397

190. Gaxiola-Valdez I, Singh S, Perera T, et al (2017) Seizure onset zone localization using postictal hypoperfusion detected by arterial spin labelling MRI. Brain 140:2895–2911. https://doi.org/10.1093/BRAIN/AWX241

191. Boscolo Galazzo I, Storti SF, Barnes A, et al (2019) Arterial spin labeling reveals disrupted brain networks and functional connectivity in drug-resistant temporal epilepsy. Front Neuroinform 12:416841. https://doi.org/10.3389/FNINF.2018.00101/BIBTEX

192. Blauwblomme T, Boddaert N, Chémaly N, et al (2014) Arterial Spin Labeling MRI: a step forward in non-invasive delineation of focal cortical dysplasia in children. Epilepsy Res 108:1932–1939. https://doi.org/10.1016/J.EPLEPSYRES.2014.09.029

193. Bernasconi A, Cendes F, Theodore WH, et al (2019) Recommendations for the use of structural magnetic resonance imaging in the care of patients with epilepsy: A consensus report from the International League Against Epilepsy Neuroimaging Task Force. Epilepsia 60:1054–1068

194. Lindner T, Bolar DS, Achten E, et al (2023) Current state and guidance on arterial spin labeling perfusion MRI in clinical neuroimaging. Magn Reson Med 89:2024–2047. https://doi.org/10.1002/MRM.29572

195. Traub-Weidinger T, Arbizu J, Barthel H, et al (2024) EANM practice guidelines for an appropriate use of PET and SPECT for patients with epilepsy. Eur J Nucl Med Mol Imaging 51:1891–1908. https://doi.org/10.1007/S00259-024-06656-3

196. Mattioli P, Cleeren E, Hadady L, et al (2022) Electric Source Imaging in Presurgical Evaluation of Epilepsy: An Inter-Analyser Agreement Study. 12:

197. Zhang J, Zhang H, Li Y, et al (2021) Arterial spin labeling for presurgical localization of refractory frontal lobe epilepsy in children. Eur J Med Res 26:. https://doi.org/10.1186/S40001-021-00564-0

198. Rentzeperis F, Abdennadher M, Snyder K, et al (2023) Lateralization of interictal temporal lobe hypoperfusion in lesional and non-lesional temporal lobe epilepsy using arterial spin labeling MRI. Epilepsy Res 193:. https://doi.org/10.1016/J.EPLEPSYRES.2023.107163

199. Shang K, Wang J, Fan X, et al (2018) Clinical Value of Hybrid TOF-PET/MR Imaging-Based Multiparametric Imaging in Localizing Seizure Focus in Patients with MRI-Negative Temporal Lobe Epilepsy. AJNR Am J Neuroradiol 39:1791–1798. https://doi.org/10.3174/AJNR.A5814

200. Dangouloff-Ros V, Fillon L, Eisermann M, et al (2023) Preoperative Detection of Subtle Focal Cortical Dysplasia in Children by Combined Arterial Spin Labeling, Voxel-Based Morphometry, Electroencephalography-Synchronized Functional MRI, Resting-State Regional Homogeneity, and 18F-fluorodeoxyglucose Positron Emission Tomography. Neurosurgery 92:820–826. https://doi.org/10.1227/NEU.0000000000002310

201. Zeng JY, Hu XQ, Xu JF, et al (2021) Diagnostic Accuracy of Arterial Spin-Labeling MR Imaging in Detecting the Epileptogenic Zone: Systematic Review and Meta-analysis. AJNR Am J Neuroradiol 42:1052–1060. https://doi.org/10.3174/AJNR.A7061

202. Guo X, Xu S, Wang G, et al (2015) Asymmetry of cerebral blood flow measured with three-dimensional pseudocontinuous arterial spin-labeling mr imaging in temporal lobe epilepsy with and without mesial temporal sclerosis. J Magn Reson Imaging 42:1386–1397. https://doi.org/10.1002/JMRI.24920

203. Coelho VCM, Morita ME, Amorim BJ, et al (2017) Automated Online Quantification Method for 18F-FDG Positron Emission Tomography/CT Improves Detection of the Epileptogenic Zone in Patients with Pharmacoresistant Epilepsy. Front Neurol 8:. https://doi.org/10.3389/FNEUR.2017.00453

204. Rosenow F, Lüders H (2001) Presurgical evaluation of epilepsy. Brain 124:1683–1700. https://doi.org/10.1093/BRAIN/124.9.1683

205. Jahreis I, Bascuñana P, Ross TL, et al (2021) Choice of anesthesia and data analysis method strongly increases sensitivity of 18F-FDG PET imaging during experimental epileptogenesis. PLoS One 16:1–20. https://doi.org/10.1371/journal.pone.0260482